System-Level Reliability Modeling and Evaluation in Power Electronic-based Power Systems

Davoodi, Amirali

DOI (link to publication from Publisher):
10.54337/aau521481678

Publication date:
2022

Document Version
Publisher's PDF, also known as Version of record

SYSTEM-LEVEL RELIABILITY MODELING AND EVALUATION IN POWER ELECTRONIC-BASED POWER SYSTEMS

BY
AMIRALI DAVOODI

DISSERTATION SUBMITTED 2022

AALBORG UNIVERSITY
DENMARK

System-Level Reliability Modeling and Evaluation in Power Electronic-based Power Systems

Ph.D. Dissertation

Amirali Davoodi

Dissertation submitted December 2022

Dissertation submitted: December 2022

PhD supervisor: Prof. Frede Blaabjerg,
Aalborg University

Assistant PhD supervisors: Asst. Prof. Saeed Peyghami,
Aalborg University

Prof. Yongheng Yang,
Zhejiang University

Prof. Tomislav Dragičević,
Technical University of Denmark (DTU)

PhD committee: Associate Professor Amin Hajizadeh
Aalborg University, Denmark

Professor Amirnaser Yazdani
Ryerson University, Canada

Professor Dirk Van Hertem
KU Leuven, Belgium

PhD Series: Faculty of Engineering and Science, Aalborg University

Department: AAU Energy

ISSN (online): 2446-1636
ISBN (online): 978-87-7573-775-8

Published by:
Aalborg University Press
Kroghstræde 3
DK – 9220 Aalborg Ø
Phone: +45 99407140
aauf@forlag.aau.dk
forlag.aau.dk

Printed in Denmark by Stibo Complete, 2023

Biography

Amirali Davoodi

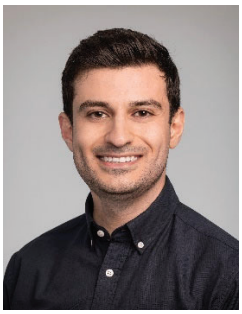

Amirali received his B.Sc. in Electrical Power System Engineering from University of Tehran in 2016. Subsequently, he received his M.Sc. in Power Electronics and Electric Machines from Sharif University of Technology in 2019. From 2019 to 2022, he was employed as a Ph.D. fellow in the Department of Energy at Aalborg University, where he was working on reliability assessment of Power Electronic-based Power Systems, as a member of the REPEPS project, under the Supervision of Prof. Frede Blaabjerg. During his PhD studies, he visited Vestas Wind Systems A/S, where he worked on the reliability modeling of wind turbine components in the Converter and Electrical Department. His main research interests include reliability assessment in power systems, reliability modeling in power electronics, and grid-connected inverters.

Abstract

The main function of the electrical power system is to deliver the demanded power to the end customers in a reliable and economic way. As a result, the reliability is an important requirement in all power systems, since any interruption in the supply of electricity can have large socio-economic consequences. At the same time, the power systems are undergoing a substantial transition, by gradually retiring the conventional synchronous generators and integrating many renewable generation and storage units. Notably, all these units have power electronic converters as a key element, which enables processing power and grid integration. Therefore, the modern power systems will be Power Electronic-based Power Systems (PEPS). On the other hand, there are some reports of noticeable failure rate of power converters in the field. Further, these failure rates increase over time, due to wear-out and aging of components, which aggravates the situation, as predicted in reports by some Transmission System Operators (TSOs). Thus, the large integration of power converters into the grid have raised concerns in terms of the log-term system-level reliability of PEPSs.

To address these concerns, the first step is to be able to assess the PEPS reliability quantitatively. In other words, a method must be developed to enable calculating the system-level reliability of PEPSs. Nevertheless, to achieve this, there are research gaps and challenges that must be investigated and addressed. In this regard, conventional power system reliability assessment methodologies cannot be used directly for PEPSs, due to their oversimplifications and inherent mathematical limitations. For example, they use a purely statistical approach to extract a constant failure rate for modeling the synchronous generator outages, which neglects the aging of units. On the other hand, outage of power electronic converters is a function of their mission profiles, lifetime models, control strategy, and design parameters. The power converter outages can be modeled by considering these factors together with the physics of failure, which results in non-constant failure rates that reflect the power converters aging. However, well-known mathematical methods used for power system reliability assessment (such as Markov method) are unable to be used with these considerations. Therefore, new mathematical methods must be developed to comply with the new consideration introduced in PEPS. Also, various sources of uncertainties in the system, including, generation, mission profiles, and component-to-component variations, must be considered and modeled.

Hence, in this PhD thesis, a comprehensive framework has been proposed to address the above challenges and enable calculating the stem-level reliability of PEPSs with realistic considerations. Further, the thesis gives a good understanding of “power electronic” and “power system” reliability modeling and assessment fields, by highlighting their differences, similarities, assumptions, and limitations. Subsequently, guidelines are proposed to merge the gaps between these field and achieve the system-level framework for PEPSs. The proposed framework is consisting of several blocks, including availability modeling, scenario generation, power system modeling, state enumeration, and index calculation, where the functions and details

of each block have been explained. Moreover, the system-level reliability of several case study PEPSs, have been assessed and analyzed to provide insights and demonstrate the capabilities of the proposed framework.

Notably, the outcome of the PhD project is a model-based framework developed based on a V-shaped approach, where the effect of parameters from the component-level up to the converter-level are reflected on the system-level indices, and contrariwise. Furthermore, the models that are based on physics of failure are mission profile-dependent. Also, the developed methods are computationally efficient, which is critical for analyzing larger system with more power electronic units. Moreover, the framework is developed according to a hybrid "time-based" and "probability-based" approach, by presenting time-dependent PDFs (Probability Density Functions) for reliability indices. The time-dependent term enables muti-timescale analysis of the reliability indices – e.g., investigating the impact of converter aging on the yearly reliability index, or the impact of generation uncertainty on the monthly variation of the reliability indices. The PDFs also represent various sources of uncertainties that exist in the system. Also, the maintenance and change failures are considered in the developed methodologies.

Therefore, the proposed framework provides a tool for system operators to evaluate their system reliability quantitatively. By doing so, they can benchmark the system and ensure whether it meets their long-term goals or if corrective measures must be taken. Also, it will be helpful to system designers, as it enables not only assessing the current status of the system, but also predicting the future performance of the system. Thus, different design scenarios can be evaluated and benchmarked in terms of long-term reliability. Furthermore, the Design for Reliability approach can be realized at the system-level, since a quantitative methodology exists, which enable calculating the proper design margins. In this regards, the system-level reliability indices of several case studies are calculated and analyzed by using the developed method. The impact of power converter aging on the system availability and outage duration and severity are quantified and analyzed. Furthermore, the influence of uncertainty and temporal patterns of mission profiles on the system-level reliability are investigated by providing time-dependent PDFs for the indices. By analyzing the system-level reliability indices, it was shown how the method can be used for benchmarking the system, design, and ensuring the long-term reliability of PEPSs.

Dansk Resumé

El-systemets hovedfunktion er at levere den efterspurgte energi til slutforbrugerne på den mest pålidelige og samtidig mest økonomiske måde. Som følge heraf er pålideligheden et vigtigt element i alle el-systemer, da enhver afbrydelse af el-forsyningen kan have store samfundsøkonomiske konsekvenser. Samtidig gennemgår el-systemerne i dag en væsentlig omstilling, ved gradvist at udfase de konventionelle store kraftværker, som har synkrongeneratorer, med mange vedvarende produktions- og el-lagrings-enheder som gør problemstillingen mere kompleks. Disse produktions-enheder har alle effektelektroniske omformere (imellem energi-kilde og net) som en nøgle-komponent og som muliggør en udnyttelse af processorkraft (intelligens) i dem med henblik på bedre at styre el-nettet. Moderne el-net vil være Power Electronic-based Power Systems (PEPS). Samtidig er der drifts-rapporter om noter-bare fejlrater for effekt-omformerne. Disse fejl-rater stiger over tid på grund af udslidning og ældning af komponenterne i effektomformerne og det vil forværre situationen omkring el-systemets pålidelighed, hvilket også har været forudsagt i rapporter fra nogle af el-transmissionssystem-operatørerne (TSO'er). Den store integration af effektomformere i el-nettet har således givet anledning til bekymring med hensyn pålideligheden af PEPS for fremtiden.

For at imødekomme disse bekymringer er det første skridt at være bedre i stand til at kunne vurdere PEPS-pålideligheden kvantitativt og kvalitativt. For at kunne gøre dette er det nødvendigt at udvikle et værktøj, der gør det muligt at beregne pålideligheden af PEPS på el-systemniveau. Dette er i dag ikke er muligt, idet konventionelle energisystemers pålidelighedsvurderingsmetoder ikke kan overføres direkte til PEPS på grund af oversimplifikationer og model begrænsninger. For eksempel bruges i dag en ren statistisk tilgang til at bestemme fejlraten (som antages konstant) til modellering af synkrongeneratorernes udfald, som negligerer betydningen af ældningen af enhederne. PEPS komponenternes udfald/fejl er en funktion af deres belastninger (missions-profile), komponenternes levetidsmodeller, de benyttede kontrolstrategier og deres design. Effektomformernes udfald kan modelleres ved at inkludere disse faktorer sammen med fysikken bagved fejlene, hvilket resulterer i ikke-konstante fejl-rater på komponenterne og som afspejler bedre effektkonverternes reelle ældning. Endvidere kan de velkendte matematiske metoder, der anvendes til vurdering af energisystemers pålidelighed (såsom Markov-modeller), ikke direkte anvendes ved sådanne karakteristikker. Derfor skal der udvikles nye matematiske metoder til at kunne beregne pålideligheden af fremtidens PEPS. Her skal forskellige kilder til usikkerhederne i systemet også tages i betragtning, herunder effekt-genereringen, belastnings-profilen og komponent-til-komponent variationerne.

Derfor omhandler denne ph.d.-afhandling en ny og detaljeret modelleringsmetode til at imødegå ovenstående udfordringer og muliggøre beregning af PEPS pålidelighed under realistiske forhold. Yderligere giver afhandlingen en god forståelse af effektelektronikkens og el-systemets pålidelighedsmodelleringsmetoder ved at fremhæve deres forskelle, ligheder, antagelser og begrænsninger. Der foreslås nye

metoder til at integrere disse fag-felter og opnå en samlet vurdering af pålideligheden for PEPS på systemniveau. Den foreslåede metode består af flere modelleringsblokke, herunder modellering af tilgængelighed for effektten, generering af scenarier, modellering af el-systemet og indeksberegninger, hvor hver metodes funktioner bliver forklaret i detaljer. Desuden kan pålideligheden på systemniveau af adskillige PEPS også vurderes og analyseres for at give indsigt i og demonstrere mulighederne i den foreslåede modellerings-metode.

Resultatet af ph.d.-projektet et modelbaseret koncept, som er baseret på en V-formet tilgang, hvor effekten af parametrene på komponent-niveau bruges op til omformer-niveau og som endelig afspejles på systemniveau (PEPS), og også modsat rettet i forbindelse med den initiale analyse af PEPS. Desuden er de anvendte modeller baseret på reelle fysiske modeller af fejl og den belastning komponenterne ser over tid. De udviklede metoder er samtidig beregningseffektive, hvilket er afgørende for at kunne analysere større og komplekse systemer med mange effektelektroniske enheder. Desuden er model-strukturen udviklet med en hybrid "tidsbaseret" og "sandsynlighedsbaseret" tilgang ved at anvende tidsafhængige PDF'er (Probability Density Functions) som er pålideligheds-indekser i analyse-apparatet. Det tidsafhængige udtryk muliggør også multi-tidsskala-analyse af pålidelighedsindekserne – for eksempel ved at undersøge påvirkningen af effktomformerens aldring på det årlige beregnede pålidelighedsindeks eller påvirkningen af usikkerheden for effektgenereringen på den månedlige variation af pålidelighedsindeksene. PDF'erne repræsenterer også forskellige kilder til usikkerheder, der findes i systemet. Desuden kan vedligeholdelsen og udbedringen af fejlene også tages i betragtning i de foreslåede metoder.

Derfor giver den foreslåede modellerings-metode et værktøj for el-systemoperatører til at kunne vurdere pålideligheden af deres el-system kvantitativt, når der er mange effektelektroniske enheder tilsluttet el-nettet. Ved at gøre dette kan de benchmarke deres el-system og sikre at de lever op til deres langsigtede mål – hvis ikke kan der træffes beslutninger om at forbedre det. Det vil også være nyttigt for el-systemdesignere, da det ikke kun gør det muligt at vurdere systemets nuværende status, men også kunne forudsige el-systemets fremtidige ydeevne. Dermed kan forskellige design-scenarier for el-systemet evalueres og benchmarkes med hensyn til dets langsigtede pålidelighed. Desuden kan en ”Design for Reliability” tilgang benyttes på systemniveau, da der nu findes en kvantitativ analyse-metode, som gør det muligt at beregne el-systemets pålidelighed langt mere præcis. Reliabilitets indekserne på systemniveau for flere casestudier beregnes og analyseres ved hjælp af den udviklede metode. Effekten af strømkonverterens aldring på systemets tilgængelighed og udfaldsvarighed og alvorlighed kvantificeres og analyseres. Ydermere undersøges indflydelsen af usikkerhed og tidsmæssige mønstre af missionsprofiler på pålideligheden på systemniveau ved at levere tidsafhængige PDF'er til indeksene. Ved at analysere pålidelighedsindekserne på systemniveau blev det vist, hvordan metoden kan bruges til at benchmarke systemet, designe og sikre den langsigtede pålidelighed af PEPS.

Contents

Thesis Details

Thesis title:	System-Level Reliability Modeling and Evaluation in Power Electronic-based Power Systems
Ph.D. student:	Amirali Davoodi
Supervisors:	Prof. Frede Blaabjerg, Aalborg University Asst. Prof. Saeed Peyghami, Aalborg University

The main part of the dissertation is based on the following publications:

Publication in refereed journals:

[J1] **A. Davoodi**, S. Peyghami, Y. Yang, T. Dragicevic, and F. Blaabjerg, "Fast and Accurate Modeling of Power Converter Availability for Adequacy Assessment," in *IEEE Trans. Power Delivery*, vol. 36, no. 6, pp. 3992-3995, Dec. 2021.

Publications in refereed conferences:

[C1] **A. Davoodi**, S. Peyghami, Y. Yang, T. Dragicevic and F. Blaabjerg, "Modelling and Analysis of the Reliability of a PhotoVoltaic (PV) Inverter," in *Proc. IEEE PEDG*, Dubrovnik, Croatia, 2020, pp. 297-303.

[C2] **A. Davoodi**, S. Peyghami, Y. Yang, T. Dragicevic and F. Blaabjerg, "Employing the Generative Adversarial Networks (GAN) for Reliability Assessment of Converters," in *Proc. IEEE ECCE*, Vancouver, Canada, 2021, pp. 3623-3629.

[C3] **A. Davoodi**, Y. Yang, T. Dragicevic and F. Blaabjerg, "System-Level Reliability Analysis of a Repairable Power Electronic-Based Power System Considering Non-Constant Failure Rates," in *Proc. IEEE EPE*, Lyon, France, 2020, pp. 1-10.

This dissertation has been submitted for assessment in partial fulfillment of the Ph.D. degree. Based on the publications shown above, the thesis serves as a summary of those, highlighting the primary outcome of the Ph.D. project. Parts of the results are used directly or indirectly in the extended summary of the thesis. The co-author

statements have been made available to the assessment committee and are also available at the Faculty of Engineering and Science, Aalborg University.

Preface

This dissertation summarizes the outcomes of the Ph.D. project "System-Level Reliability Modeling and Evaluation in Power Electronic-based Power Systems," which was carried out at the Department of Energy, Aalborg University, Denmark. The Ph.D. project was supported by THE VELUX FONDEN under the VILLUM Investigator grant for the Reliable Power Electronic-based Power Systems (REPEPS) project. I would like to thank the above-mentioned institutions for supporting this PhD and the REPEPS project.

I would like to express my sincere gratitude to my supervisor Professor Frede Blaabjerg for his excellent support and guidance throughout my PhD project. His passion and dedication will always inspire me. Furthermore, I would like to extend my deepest appreciation to my co-supervisor Assistant Professor Saeed Peyghami, for his matchless support and the insightful discussions we had throughout my PhD. His bright mind and enthusiasm will always be a source of inspiration for me. I learned a lot from Frede and Saeed, and their priceless recommendations and advice have been essential in completing this work. I would also like to thank Professor Yongheng Yang at Zhejiang University, China, and Professor Tomislav Dragičević, Denmark Technical University (DTU), Denmark for their collaboration in this PhD project.

Moreover, I would like to thank Dr. Lars Helle and Dr. Sungyoung Song, for their collaboration and hosting me during my research visit at Vestas. During my research visit from Vestas, I had so many fruitful discussions with them that gave me invaluable industrial perspective. Also, I received outstanding supervision from them, for which I would like to express my sincere gratitude.

A special thanks to all my colleagues at the Department of Energy, Aalborg University, for all their suggestions, technical discussions, and their advice and help in daily life.

Also, I would like to thank all my friends for their priceless help and support when I was living in Aalborg, and for sharing their happy and sad life moments with me and. Finally, I would like to express my most sincere gratitude to my family members, my father, mother, and my brother for their support, understanding, and encouragement. None of this would have been possible without you.

Amirali Davoodi
November 2022, Aarhus

Part I
Report

Chapter 1
Introduction

1.1. Background

The electrical power system is the largest and most complex system ever created by humankind [1]. It provides us with an immense amount of energy (e.g., 23900 TWh in 2019 [2]), and our economic system, daily life, and a lot of critical activities directly depend on its successful and reliable operation. As a result, it is vital that the electrical power system function reliably all the time forever – i.e., without any interruptions in the supply of electricity.

However, in reality, failures occur in the electrical power systems worldwide, which could lead to large socio-economic consequences. For example, the US Department of Energy (DoE) has estimated the cost of power outages for the US economy around $150 billion annually [3]. In a similar report by European Commission, which covered 28 EU member states, it was estimated that each year, between 600 to 850 GWh of electricity is not supplied to the end customers due to power outages, which results in an economic loss up to €25 billion per year [4]. Likewise, in a study done by the World Bank on low- and middle-income countries, which covers 78% of the world population, it was found that power outages cause an economic loss of around $82 billion per year [5] for these countries. Also, the Swedish Royal Academy of Engineering Sciences estimated the cost of power outages in Sweden in 2015 around SEK1 billion [6]. In [7], the Institute of Energy Economics in Cologne estimated the cost of a blackout in Germany to be around €430 – 750 million per hour. Apart from these overall reports, there are records of significant power outage incidents, which influenced many people and brought about large economic losses. As a recent example, three wind farm operators had to pay £10.5 million as a penalty for not staying connected to the UK grid, which caused a major outage in August 2019 [8]. Also, in 2003, separate blackouts occurred in the US and Italy/Switzerland, which led to an economic loss of $8.2 billion and €1.18 billion, respectively [9], [10].

On the other hand, the power system is undergoing the most significant transition in its history. To achieve the goal of reaching net zero carbon emission by 2050, fifty countries, including the EU member states, have pledged to add 500 GW of solar PhotoVoltaic (PV) and wind to the grid annually by 2030 [11]. In addition, 3 TWh of battery storage capacity must be integrated into the system by 2050 [11]. Furthermore, according to the U.S. Energy Information Administration (EIA), the renewables will account for 49% of world electricity generation by 2050, as shown in Fig. 1.1.

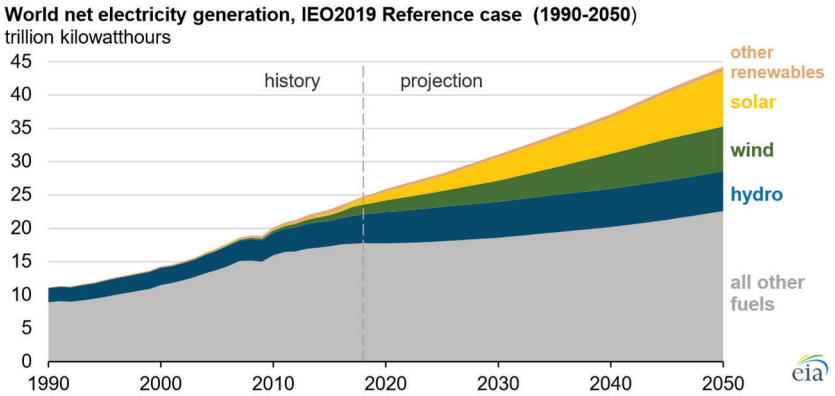

Fig. 1.1. Contribution of different energy resources in the world's net electricity generation: historical data and projections [12].

This large amount of energy needs to be processed through power electronic converters, which highlights the role of power electronics in this historic transition. In addition to power generation and storage, power electronic converters will be used increasingly in the transmission and distribution grids. For example, technologies that use power electronic converters as their core, such as HVDC (High Voltage DC), MVDC (Medium Voltage DC), FACTS (Flexible AC Transmission Systems), SST (Solid State Transformers), active filters, EV (Electric Vehicle) chargers, and motor drives, will be used widely in modern transmission and distribution grids. This ongoing transition has been illustrated in Fig. 1.2, where the configuration of conventional and modern power grids has been compared [13]. From Fig. 1.2, the changes in the electric power grid can be further categorized as follows. The generation resources would be inverter-based, rather than synchronous-machine based. The generation capacity will be variable and uncertain at different timescales. The supply of electricity will become more decentralized compared to the conventional grids. New demand resources will be introduced by intensive electrification in all sectors and integration of energy storage units. Each of these changes can cause challenges for the system reliability and resiliency in terms of resource adequacy, transmission and distribution infrastructure adequacy, grid balancing and flexibility, and grid stability [14]. To transition successfully towards a net zero carbon future, it is important to assess its implications on the system reliability and resiliency. As a result, this PhD thesis will focus on one of these reliability implications (system adequacy) that are caused by power electronic failures, which will be discussed in depth.

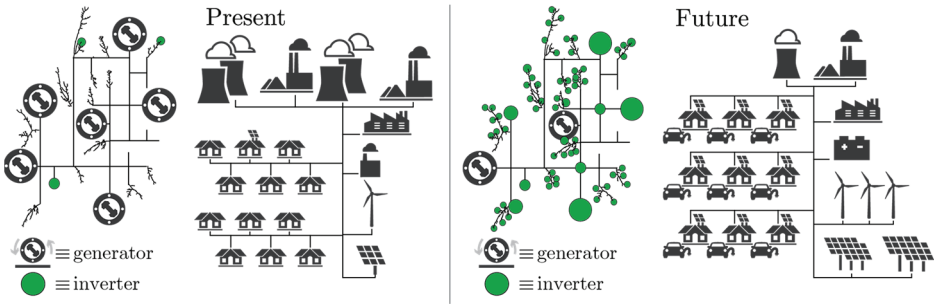

Fig. 1.2. Illustration of the ongoing transition in the electric power grid, showing how moden grids will look like compared to the conventional [13].

1.1.1. Power Electronic-based Power Systems and Challenges

As explained before, the modern power systems will be Power Electronic-based Power Systems (PEPS). However, the abundance of power converters in the modern grid raises some concerns in terms of PEPS reliability, due to the failure-prone nature of components. In other words, the failure of power electronic components and converter aging can cause challenges for the long-term reliability of the system and jeopardize energy security. In this regard, there are studies and reports indicating how power converter failures can be problematic in terms of reliability and economic loss due to downtime and maintenance costs. For example, as stated in a study based on field data in [15], the inverter constituted between 43% to70% of service requests in PV power plants under study. Similarly, in a study by a PV plant operator, it has been shown that inverter failures have resulted in the loss of 2.3 GWh over a 27-month period, which accounted for 36% of total energy losses in the plant [16]. Also, an analysis of 15 PV plants in Spain and Italy revealed that roughly 28% of energy loss in these plants was because to inverter failures [17]. In a field study by Sandia National Laboratory on four PV plants, the inverter failures accounted for between 50% to 89% of all electrical failures [18]. Additionally, in a field study done on 100000 PV systems [19], the inverter was identified as the most common source of hardware failure in PV systems. Similarly, in a recent study on a fleet of 75 Wind Turbines (WTs) in Spain [20], 10% of the downtime happened as a result of converter hardware failures. Also, the power converter was ranked the second in terms of failure rate and downtime in a study by Reliawind on a fleet of 373 WTs [21]. Likewise, after investigating 5800 failure events in a wind farm in China, it was found out that the power converter was the component with the highest failure rate [22]. In a recent study on 1045 offshore WTs in [23], the power converter ranked as the fourth source of failure, with an average failure rate of 1.3 Failures per year per turbine.

These field experiences indicate that the power electronic failures may cause problems for the long-term reliability of the PEPS, if not carefully taken into account. Therefore, it is necessary to come up with models and frameworks to quantify the system-level reliability of the PEPS, particularly considering power electronic failures. These models and frameworks should enable the system designer and

decision-makers to ensure that the PEPS will meet its long-term reliability goals, identify the weakest link of the system, and provide insights on how to improve and maintain a desired level of system reliability. However, there are important challenges that must be dealt with when developing such models and frameworks, which will be discussed here.

Aging and wear-out of power electronic components: First, power electronic components are susceptible to aging, meaning that their failure rate increases with time. Consequently, the system-level reliability of the PEPS will degrade over time if corrective measures are not taken or if a proper margin is not considered in the design phase of the system. In this regard, in a report published by the Danish TSO, Energinet, it has been predicted that the average annual outage duration per customer will increase from 20 minutes in 2020 to 65 minutes in 2030 [24], where the grid aging has been identified as the main reason for this considerable decrease of reliability. In line with this, [25] investigates how the increasing failure rate of power converters due to aging can lead to increased unavailability in the power system over time. As mentioned above, power electronic components are exposed to aging, and many research works have been dedicated to explaining their aging mechanisms. For example, in [26], the aging mechanisms for two of the widely used capacitors in power electronic (i.e., metalized film and electrolytic capacitors) has been investigated, where the effects of electrical, thermal, and mechanical stressors have been expressed in the form of capacitor lifetime models. Similarly, [27] discusses how the aging of power capacitors in DC-link application leads to a drastic increase in the failure rate of the power electronic converters. Likewise, [28] investigates the aging mechanisms of Insulated-Gate Bipolar Transistors (IGBTs) – a widely used component in power electronic converters – due to power cycling, where the results have been verified experimentally. In [29], the effect of thermomechanical stresses on the aging mechanisms of a Gallium Nitride transistor – a cutting-edge semiconductor for power electronic application – has been explored.

Many factors affect converter reliability: Another challenge is that the converters' reliability is a function of many different factors, which makes the system-level modeling more complex, considering that numerous converters exist in a PEPS. A key factor in the reliability of power electronic converters is mission profiles and operational conditions. In other words, the power converter that is being used under severe stress condition is more susceptible to failure, and its reliability is expected to be lower than a converter that is being used under normal stress condition. An example of this can be found in [30], where the effect of mission profiles on the reliability of a PV inverter has been explored. Also, converter-level design parameters, such as switching frequency and DC-link voltage – play a key role in the converter reliability. For instance, [31] studies the effect of switching frequency on the MMC reliability, where an optimal switching frequency is then calculated by comprising between the reliability and total harmonic distortion. In [32], the influence of the DC-link voltage value on the IGBT lifetime in three-phase inverters has been investigated. Additionally, modulation schemes can affect the converter reliability. In this regard, in [33], a new PWM method has been proposed for a multi-level converter, where the

converter reliability improvement has been proved quantitatively. Another important factor that must be considered when calculating the reliability at the system level is the interactions between power converters and the power sharing among them. In this regard, [34], [35] have proposed methods for power sharing among converters in AC and DC microgrids, respectively, to distribute the stress among converters and increase the overall reliability. Thermal management can also influence the reliability of power converters, since the temperature and its cycles are important stressors causing failures in power electronic components over time [36]. In [37], [38], passive and active thermal management methods have been discussed, and their relationship with the converter reliability has been elaborated. A desirable reliability assessment framework must be able to incorporate all the above considerations to produce realistic results, while making simplifications to lower the computational burden.

Uncertainties: Another challenge when moving towards the PEPS is the increased uncertainties, which must be considered when developing a comprehensive reliability framework. For example, mission profiles (such as wind speed or solar irradiance profile) are sources of uncertainty, because they cannot be predicted accurately over long-term periods. In other words, in larger time scales (e.g., several years for power system planning application), it is hard or impossible to predict exactly under what conditions the converters in the PEPS will be working. On the other hand, the mission profiles determine not only the generation capacity of the renewable-based resources but also the wear-out failures of the power electronic converters. Wear-out failures of power converters can be predicted thanks to the lifetime model of components, their design and mission profiles, and the stress-strength analysis [39]. However, it is important to note that these predictions also come with some uncertainties for several reasons - such as lifetime model parameters uncertainty due to lifetime test limitations or component-to-component variations caused in the manufacturing process. Apart from the wear-out failures, power converters can fail because of chance failures – that is, from external factors and overstresses. These occurrences often happen randomly, and they are either impossible or impractical to model physically, which again introduces more uncertainty to the system. Therefore, a good reliability assessment framework must incorporate these uncertainties and provide solutions to handle them and considered in the outcomes.

1.1.2. Reliability Modeling in Power Electronics and Power Systems

There are valuable methods for reliability prediction in power electronics. Similarly, there are well-established methods for reliability assessment in power systems. However, when it comes to the PEPS, these methods cannot be used directly in their current form due to their limitations and deficiencies. Some of these limitations and shortcomings are shown in Fig. 1.3, which illustrates the research gaps that must be bridged in order to assess the PEPS reliability. Also, it is important to note that the experts in the power system reliability and power electronics reliability have different mindsets and speak different “languages,” because their concerns are different, and their definitions and usage of reliability are different. So, first, it is important to understand these differences to be able to translate these two “languages” into each

other. In other words, in order to achieve a reliability assessment framework for the PEPS, it is necessary to bridge the gap between the research on the power electronics reliability and on the power system reliability.

Since reliability is a general term and its meaning might slightly differ in various research areas, it is necessary to discuss its definition and specify what we mean by reliability in this PhD thesis. A widely accepted and general definition of reliability can be quoted as [40]:

"*Reliability is the probability of a device performing its purpose adequately for the period of time intended under the operating conditions encountered.*"

In the power electronics domain, reliability often refers to the probability of the survival of a component or converter until some point in time, under given mission profiles. However, the meaning of reliability in this PhD thesis is more toward system-level – that is, it includes this definition but is not limited to it, which will be further explained hereafter. As shown in Fig 1.4, in power system studies, reliability can be divided into security and adequacy. Security typically deals with the short-term dynamics of the system, such as stability against transients. In other words, security is defined as the ability of a power system to respond to sudden disturbances and abnormal events [41]. Therefore, the security is typically used in the power system operation phase. On the other hand, adequacy deals with the long-term performance of the system and aims to guarantee that enough generation capacity exists at any time to supply the demand [42]. Thus, adequacy is usually associated with the long-term system design and planning phase of the power systems [43]. In most power system research papers, the terms *adequacy* and *reliability* are used interchangeably, which would be the case in this PhD thesis too. The adequacy evaluation is typically performed in all the power system hierarchies – i.e., generation, transmission, and distribution levels. Also, it is often described with probabilistic indices, which account for the frequency and duration of outages and the amount of energy that is expected to be lost, which will be discussed in detail.

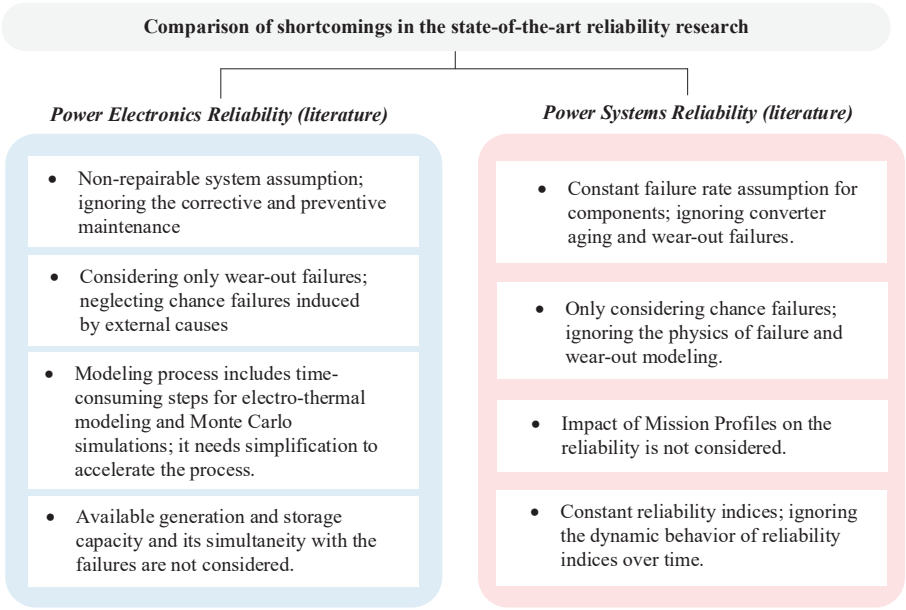

Fig 1.3. Comparison of the assumptions and shortcomings in reliability research of power electronic systems and power systems, i.e., which challenges must be addressed in order to bridge the gap between these technical domains and achieve a unified approach.

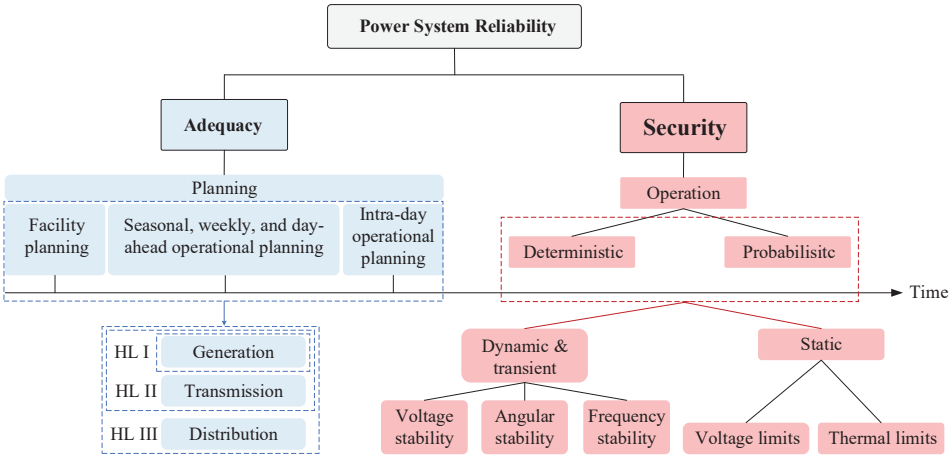

Fig 1.4. Classification of reliability in the planning and operation of conventional power systems (HL x: Hierarchical Level x) [43], where the focus of this PhD project is on adequacy.

There are certain shortcomings in power electronic reliability research, which must be addressed before incorporating them into the PEPS reliability assessment framework.

Mission profiles are important factors to consider when developing a system-level reliability assessment framework. Power electronic converters can be subject to different mission profiles (due to different environmental and operation conditions), which exposes them to different stress levels, leading to a different probability of failures. Therefore, it is necessary to use mission profile-based reliability assessment approaches as described in [39]. This approach aims to investigate the physics of failure, and accordingly develop mathematical models to describe the lifetime of components. Then, by combining these models with the mission profile of converters, the reliability is predicted. Nevertheless, there is another popular but controversial approach for power electronic reliability assessment based on handbooks (such as MIL-HDBK [44], IEC-61709 [45], FIDES [46]). For example, in [47], the reliability of modular multilevel converter has been evaluated using the MIL-HDBK. This approach must be used with extra caution for the following reasons:

- These handbooks are old (e.g., 1995 for MIL-HDBK), and their data might be outdated for the new generation of technologies used in power electronic components.
- Also, the failure rates in these handbooks are the statistical average of field experiences, without considering the application, technology, cause, and physics of failure.
- Moreover, the outcomes of these handbooks are constant failure rates that do not change with time, meaning that they neglect the aging of component.
- Besides, the uncertainties are not considered in the handbooks. So, they do not provide a solid physical interpretation and can be misleading if used for reliability modeling purpose of the PEPS.

Although the model-based and mission profile-based reliability assessment approach provides a realistic and accurate estimation of the converter reliability, they often suffer from a high computational burden, as they use time-consuming steps such as Monte Carlo simulation, rainflow counting algorithm, and detailed electro-thermal models of components [39]. The computation time might be acceptable for one power converter. Nonetheless, when it comes to the PEPS and since the PEPS has several power converters, the computation time might be too high, making these approaches impractical or impossible to be used in their current form. Therefore, in order for these methods to be used for the PEPS, they must be simplified, while keeping an appropriate level of accuracy to make them computationally efficient and accelerate the converter reliability prediction process. Thus, it is vital to find an appropriate level of detail for the models to avoid oversimplification, while reducing the computation time. For example, for electrical modeling and loss calculations, it should be decided whether to use detailed electrical simulations with small timesteps or to use analytical equations. Likewise, for thermal modeling, whether it is necessary to use finite element simulations or use thermal networks and lookup tables are enough.

Another shortcoming is that, typically, repair and replacement are ignored in the power electronics reliability literature. This assumption might be reasonable for mission-based systems such as aerospace applications, where the system has a certain lifetime, and its mission ends at some point. However, the power system is not a mission-based system and is supposed to work all the time forever. In such a system, repair, replacement, and maintenance of subsystems are vital to keep the system running successfully. Since the PEPS has repairable or replaceable subsystems, to calculate its reliability at the system level, measures must be taken to incorporate repair and maintenance (both corrective and preventive) into the existing methods for converter reliability estimation.

Moreover, power electronic reliability research mostly focuses on modeling the failures originating from internal causes such as wear-out failures due to bond wire lift-off [48] or solder layer failure [49]. However, a power electronic converter may also fail due to external causes, i.e., chance failures, such as an overvoltage due to a lightning strike. From a system-level point of view, it is essential to also consider this category of failures in our model. Although it is difficult or cumbersome to develop physical models for all external causes of failure, they can be modeled by using a statistical approach.

From a system-level point of view, apart from the wear-out and chance failures of power converters that can occur at any random time, the available generation capacity must be considered as well when assessing the PEPS reliability. In other words, if at any given time, adequate generation capacity is available, the failures cause unreliability and loss of energy. Similarly, if at any given time, adequate generation capacity is not available, unreliability will be inevitable, even though there is no failure in power converters. Further, unreliability can happen due to the lack of generation capacity and the converter failure occur simultaneously. So, the generation capacity and its simultaneity with failures also influence the overall system reliability. However, in contrast to conventional generators that could be controlled and follow the generation set points, the generation capacity in the PEPS, particularly in PV and wind systems, is directly dependent on climate conditions. This generation uncertainty acts as another source of uncertainty, besides the aforementioned ones. Therefore, it is vital to consider this and model the generation uncertainty and its simultaneity with converter failures.

A typical failure rate description of a power electronic component, also known as the bathtub curve [50], is shown in Fig. 1.5. During the first stage of its life, i.e., the burn-in period, the failure rate decreases due to infant mortalities and early failures. The early failures are usually caused by flaws in the design, production, transportation, and installation [51]. However, it is typically assumed that this type of failure is identified, corrected, and prevented in the final product, thanks to the detective and corrective actions. So, it is justified to neglect this type of failure in the PEPS reliability assessment. Afterward, during the useful lifetime period, the component's failure rate is almost constant over time, which is caused by chance failures. Then, when the wear-out period begins, the failure rate of the component increases, due to the accumulated damage over time and eventually wear-out failures.

In the power system reliability literature, only chance failures are considered, and wear-out failures are neglected. As a result, a constant failure rate is assumed for the subsystems, and the system-level reliability indices are calculated accordingly. This simplification might be acceptable as long as the subsystems are within their useful lifetime period. However, when they enter the wear-out period, the failure rate increases as shown in Fig. 1.5. Therefore, using the common assumption in the power system reliability literature (i.e., constant failure rate) will lead to ignoring the aging of power converters, which can result in considerable errors. Also, the adopted constant failure rate is often derived from statistical analysis of field data, regardless of the application and operational conditions. Therefore, the physics of failure and the effect of mission profiles are not reflected in those numbers, introducing more errors. Moreover, using this approach will result in a time-independent value for the system-level reliability indices. In reality, nevertheless, the system-level indices are not constant and change over time with regard to aging and maintenance. Hence, this approach will ignore the dynamics of the reliability indices, which leads to an overestimation of the indices in the short term or an underestimation of the indices in the long term.

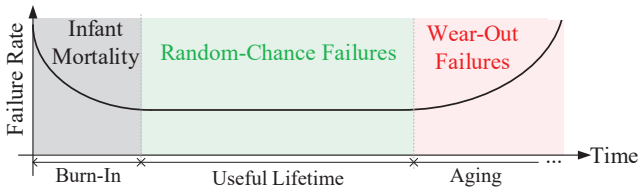

Fig. 1.5. Failure rate of a power electronic component as a function of time (bathtub curve) [52].

So, using non-constant failure rates, reflecting both wear-out and chance failures, is crucial for the PEPS reliability assessment. On the other hand, powerful analytical tools that are conventionally used for power system reliability assessment, e.g., Markov methods [53], only work with constant rates. So, alternative methods, such as Monte Carlo simulation, are to be used. However, this method suffers from a high computational burden and might not be practical when the number of converters in the PEPS increases [25]. Alternatively, approximations such as the method of device of stages [54] can be used to simplify the problem and enable using the Markov methods. Nevertheless, this approach can result in significant errors due to oversimplifications and make it extremely inaccurate to be used for the PEPS reliability assessment. Thus, new methods must be developed to leverage the power of conventional methods and make them compatible with the non-constant failure rates to achieve accurate results with an acceptable computational burden.

1.2. Thesis Motivation and Research Tasks

As discussed above, the reliability of the power system is of great importance, and any failure can have severe consequences. However, with regards to the increasing use of the power electronic converters in the grid, the reliability of such PEPSs is under question due to the failure-prone nature of power electronic components. To benchmark the system and check whether the PEPSs will meet their reliability targets, it is necessary to be able to assess their reliability quantitatively. On the other hand, due to the prevalence of power converters and renewables in the PEPS, new considerations must be taken into account when assessing reliability. For example, non-constant failure rates must be adopted to reflect the converter aging. These failure rates must be modeled based on the physics of failures and mission profiles. Also, various uncertainties, including the generation capacity and chance failures, must not be ignored. Nevertheless, conventional reliability assessment methods cannot be employed either because they are oversimplified and lead to unrealistic results or because of their inherent mathematical limitations. Therefore, this PhD project aims to develop methods and models that can take these considerations into account and finally come up with a comprehensive framework that makes the quantitative reliability assessment of PEPSs possible.

In light of the complexity and the large scale of the PEPS, appropriate simplification of the models is necessary to achieve accurate and realistic results while keeping the framework computationally light. Such a model-based framework for the PEPS reliability assessment can be of help for the system-level designers and decision-makers in many aspects. The first outcome is that benchmarking the system and ensuring that it fulfills the reliability requirements can be done. Furthermore, since the framework is based on physical and statistical models, not only is it possible to assess the current metrics of the system, but also it would be possible to predict the future performance of the system given the mission profiles. Additionally, it would be possible to analyze the impact of converter-level design parameters (e.g., switching frequency and DC-link voltage) on the system-level reliability indices, since the electrical and thermal models of the converters are embedded into the framework. Such a possibility will enable the identification of the weak points in the system and provide insights on how to improve the converter design for better system-level reliability. Also, the outcomes of the framework can be used to schedule the maintenance and replacement of converters to guarantee that the system-level reliability would always remain in an acceptable range, even though the converters degrade over time. Moreover, the framework will act as a design tool for the system-level designers and decision makers to analyze the indices, perform the design for reliability, optimize the system in terms of reliability and other parameters, and select the best option among the available options for system expansion planning. In this regard, the overall activities and research tasks in this PhD project are summarized and shown in Fig. 1.6.

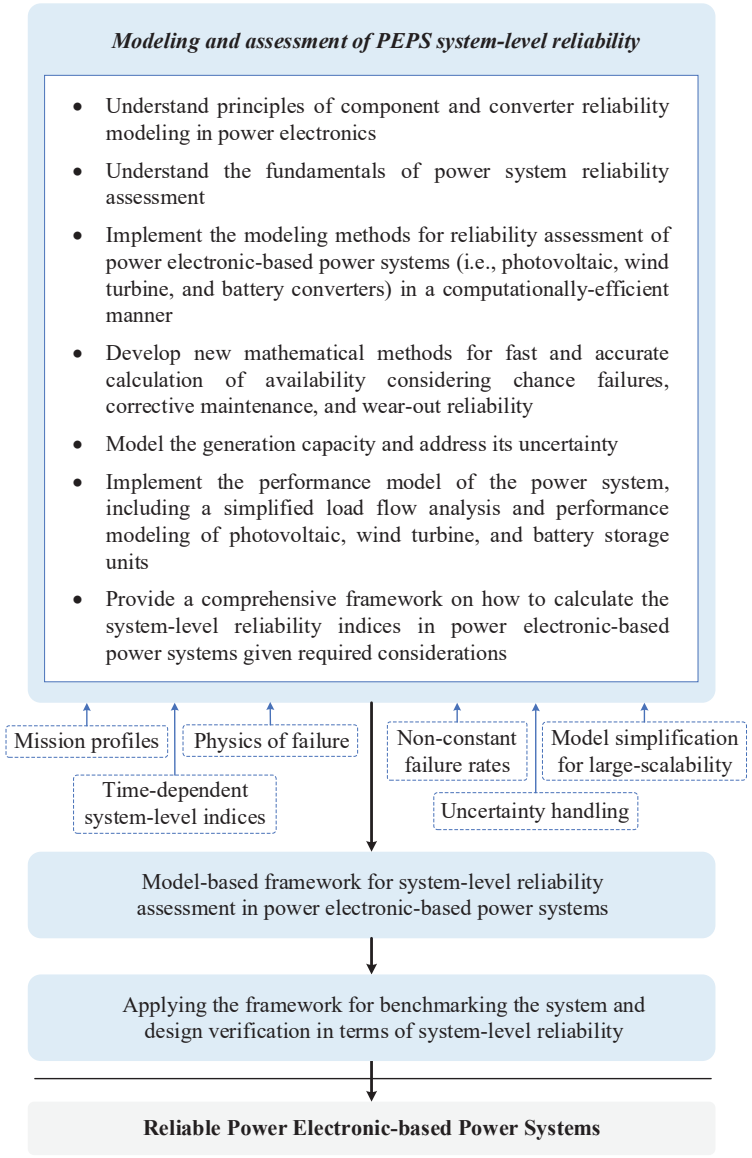

Fig. 1.6. Research tasks and activities of this PhD thesis.

1.2.1. Research Questions and Objectives

The main objective of this PhD study is to develop a comprehensive framework that will make the quantitative reliability assessment possible in power electronic-dominated power grids. So, the main research question of the project can be formulated as follows:

> *How can the system-level reliability indices be calculated for power electronic-dominated power grids, accurately and computationally light?*

To answer this question, several previously discussed research gaps must be addressed, which can be formulated as some sub-questions.

Develop a comprehensive framework for reliability assessment of the PEPS:

To reach a comprehensive framework at the system level, the reliability in lower hierarchies, i.e., component and converter levels, must be modeled meticulously, as demonstrated in Fig. 1.7. To this end, first, it is necessary to realistically predict the PE component's reliability by using physics-based models. To realistically model the component reliability, the stress-strength analysis method must be applied with regards to the physics of failure and mission profiles. On the other hand, typically, the stress-strength analysis method includes several time-consuming steps, e.g., electrical and thermal model of the components, rainflow counting and Monte Carlo simulation. Since a PEPS consists of many converters with numerous components, this process must be done many times to acquire the reliability metrics of all the converters in the PEPS. Therefore, the computation time for component reliability evaluation algorithms is a key factor in making the system-level analysis computationally feasible. As a result, the models and the process must be simplified to reduce the computation time, while oversimplification must be avoided. To this end, the appropriate level of details for the models must be found and justified.

Accordingly, the following sub-questions must be answered.

- What models and methods can be used for accurate modeling of power electronics components reliability?
- What is the right level of detail that must be considered for component reliability modeling to achieve a low computation time, while avoiding oversimplification?

Then, it is necessary to aggregate these component-level models and to build up the converter-level availability and reliability metrics. As discussed before, it is important to adopt non-constant failure rates extracted from models. At the same time, it is necessary to consider the repair and maintenance to obtain the converter availability. Nevertheless, conventional availability modeling methods are unable (or have impractically long computation time) to consider both factors simultaneously. So, new mathematical methods must be developed to overcome this challenge. Accordingly, the following sub-question must be answered.

- What mathematical methods can be helpful to map the component-level reliability into the converter-level reliability?

Provided the model-based reliability, statistics-based chance failure rates, and availability for each converter, they should be combined and translated into the system-level reliability indices. Apart from the failures and repairs, generation

capacity plays a key role here, which in the PEPS case has a considerable uncertainty associated with the intermittent nature of renewables. To consider the available generation capacity at any given time, the power system performance must be modeled by simple implementation of load flow and modeling the performance of PV, WT, and storage units. Also, to avoid over- or underestimating the reliability and study the effect of converter aging, the dynamic behavior of the reliability indices must be calculated rather than using the conventional steady-state values. Accordingly, the following sub-questions must be answered.

- What are the key inputs determining the system-level reliability indices? What are the main considerations in order to achieve realistic results?
- How can the considerable uncertainty of generation capacity in the PEPS be modeled and incorporated into the final indices?
- How can both probabilistic and dynamic behavior of reliability indices be modeled at the same time?
- What is the impact of converter aging, chance failures, and maintenance schemes on the system-level reliability indices?

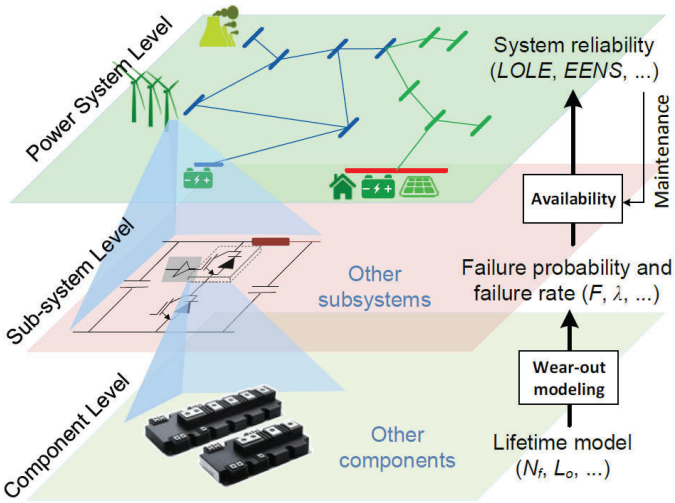

Fig. 1.7. Hierarchies for reliability assessment of power electronic-based power systems [55] (LOLE: Loss Of Load Expectation, EENS: Expected Energy Not Supplied, F: failure probability, λ, failure rate, N_f: number of cycles to failure for semiconductors, L_o: time to failure for capacitors).

Demonstrate the applications of the proposed framework in benchmarking the system and reliability assessment:

Once the above questions have been answered and the comprehensive framework has been reached, it can be used by system planners for expansion planning and system

decision makers to guarantee a reliable system-level design. By using iterative designs and optimization techniques, design for reliability can be realized at a system level. Therefore, system-level designers can benchmark the PEPS and evaluate whether the current design will remain reliable over time or not. Since the framework is model-based, it can reveal the weak points of the system and provide insights on how to mitigate their impact on the overall reliability by using preventive measures, redundant design, or power sharing schemes. Therefore, this question can be further divided into the following sub-questions.

- How can the outcomes of the framework be used to benchmark the system and ensure its long-term system-level reliability?
- How to increase the system-level reliability and maintain it over time to mitigate the effect of converter aging?

To find an answer to the above questions, several considerations must be kept in mind, and many steps must be taken. These considerations and steps are shown in Fig. 1.8, which provides a roadmap to realize an assessment tool for PEPS reliability and use it for its reliability enhancement.

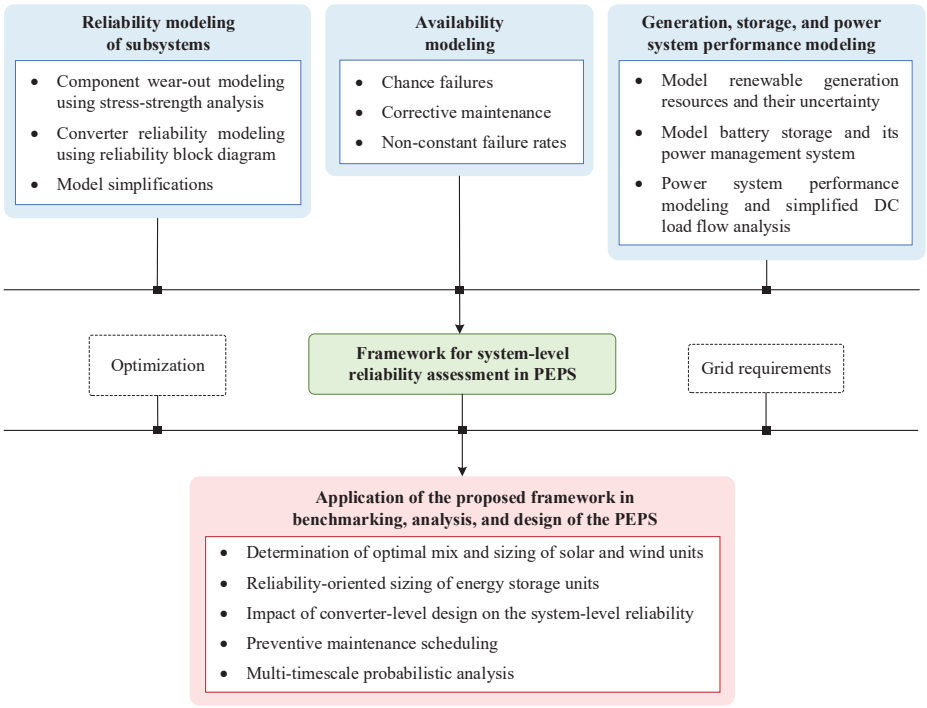

Fig. 1.8. Roadmap and steps that must be taken to achieve a reliability assessment framework and applying it to Power Electronic-based Power Systems (PEPSs).

1.2.2. Project Limitations

Certain assumptions and simplifications have been made during this PhD project that result in certain limitations, which are as follows.

- Only the reliabilities of power semiconductors and capacitors have been modeled in power electronic systems and used for system-level reliability evaluations. This simplification has been done, since these are the reliability-critical components in most power electronic converters and account for a large proportion of failures [56]. Other components of power electronic systems, e.g., PCB, magnetics, connectors, and sensors, can also fail, which can be considered for more accuracy. However, their failure mechanisms have not been investigated properly, and the lack of widely-accepted models is a problem.
- Only thermal-induced stresses have been considered to model component reliability. This has been done because that is the dominant stressor and cause of failure in power semiconductors and capacitors, according to the literature and lifetime models [48]. However, there are other stress factors that are not considered in this study, such as humidity and cosmic rays, which may trigger different failure mechanisms. Also, it should be noted that the respected lifetime models have been adopted from manufacturer data or the literature, and not all of them have been verified by power cycling tests.
- Only the steady state values have been considered to model generation and storage resources, and the dynamics of the controllers have been ignored. This is because adequacy deals with the static values of the generation and demand on very large timescales and investigating the effect of dynamics and transients on the outages lies in the category of stability rather than adequacy.
- Experimental validation has not been done, since the focus of this PhD project is the system-level performance. To verify this experimentally, it requires that a real system (e.g., microgrid) be under operation for an extended period of time (e.g., ten years), where all the data must be gathered. Then, the data over this period must be analyzed in order to calculate the system-level reliability indices and compare them with what has been predicted based on this PhD project.
- DC power flow method has been used to model the performance of the power system to accelerate the overall reliability assessment procedure, since this is a non-iterative and absolutely convergent method. However, the accuracy is lower than that of AC load flow, since only active power has been considered. Also, the electrical models of the lines and their limits have not been considered in the power system performance modeling since the transmission lines have not been the focus of this PhD project, and it has been done to simplify the process.
- Failure of components is assumed to be independent – that is, common-mode failures and cascading failures have not been considered.

- Early failures and infant mortality are assumed to be negligible and have not been considered in this study.

1.3. Thesis Outline

The outcomes of the PhD project are summarized in this thesis based on the published and written papers during the study. The thesis consists of two parts: a report and selected publications. In Fig. 1.9, the structure of the thesis is illustrated, where the relevance of each chapter to selected publications is pointed out. The thesis includes six chapters, where Chapters 2 and 3 address the modeling and assessment task, and Chapter 4 and 5 provide guidelines and examples for evaluation of the PEPSs in terms of system-level reliability based on the models. The rest of the thesis is organized as follows. In Chapter 2, the fundamentals of power system reliability are presented, explaining the system-level indices and conventional methods for calculating them. In Chapter 3, the process for modeling the wear-out of power electronic components, including electro-thermal modeling, rainflow counting, and Monte Carlo simulations, is explained. Also, it is discussed how to translate the component-level wear-out reliability into the converter-level reliability metrics. Then, in Chapter 4, the details of the comprehensive framework for reliability assessment of the PEPS are presented, where all the steps to calculate the system-level reliability in the PEPS are elaborated upon (e.g., availability modeling, generation, storage, and power system performance modeling, convolution of load and generation). Chapter 5 demonstrates the applications of the PEPS reliability assessment framework in benchmarking and design of a system to ensure the long-term reliability, by providing several practical examples. Finally, the conclusions are presented in Chapter 6, where the main contributions are highlighted, and future research possibilities are outlined.

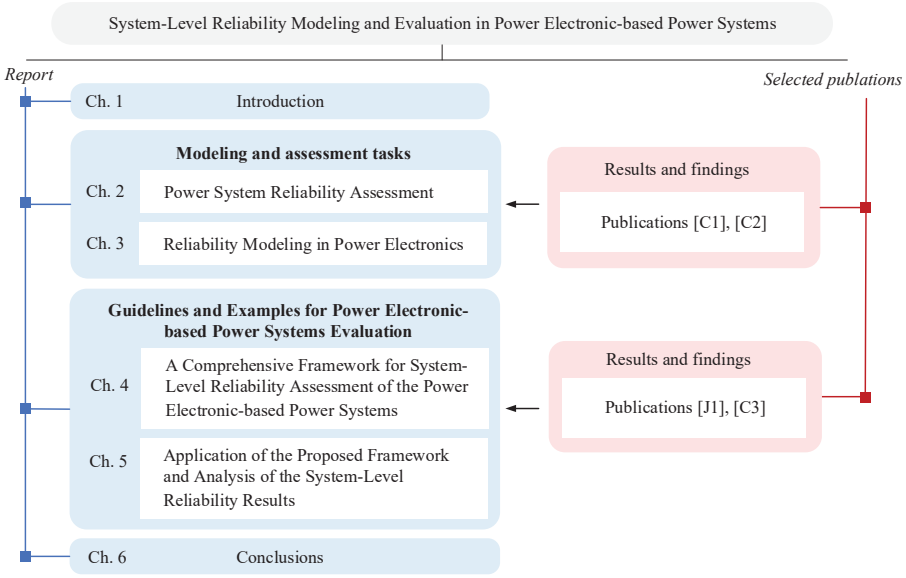

Fig. 1.9. Report structure and demonstration of how selected publications fulfill the specified research tasks.

1.4. List of Publications

The outcomes of the project have been disseminated in various forms, also as journal and conference papers and book chapters. The selected publications are shown in Fig. 1.9, related to the thesis, and the full list can be seen below.

Publication in refereed journals:

[J1] **A. Davoodi**, S. Peyghami, Y. Yang, T. Dragicevic, and F. Blaabjerg, "Fast and Accurate Modeling of Power Converter Availability for Adequacy Assessment," in *IEEE Trans. Power Delivery*, vol. 36, no. 6, pp. 3992-3995, Dec. 2021.

Publications in refereed conferences:

[C1] **A. Davoodi**, S. Peyghami, Y. Yang, T. Dragicevic and F. Blaabjerg, "Modelling and Analysis of the Reliability of a PhotoVoltaic (PV) Inverter," in *Proc. IEEE PEDG*, Dubrovnik, Croatia, 2020, pp. 297-303.

[C2] **A. Davoodi**, S. Peyghami, Y. Yang, T. Dragicevic and F. Blaabjerg, "Employing the Generative Adversarial Networks (GAN) for Reliability

Assessment of Converters," in *Proc. IEEE ECCE*, Vancouver, Canada, 2021, pp. 3623-3629.

[C3] **A. Davoodi**, Y. Yang, T. Dragicevic and F. Blaabjerg, "System-Level Reliability Analysis of a Repairable Power Electronic-Based Power System Considering Non-Constant Failure Rates," in *Proc. IEEE EPE*, Lyon, France, 2020, pp. 1-10.

- **A. Davoodi**, S. Peyghami, Y. Yang, T. Dragicevic and F. Blaabjerg, "A Preventive Maintenance Planning Approach for Wind Converters," in Proc. IEEE eGrid, Aachen, Germany, pp. 1-8.

- **A. Davoodi**, S. Peyghami, Y. Yang, T. Dragicevic and F. Blaabjerg, "A Preventive Maintenance Planning Approach for Wind Converters," in *Proc. IEEE eGrid*, Aachen, Germany, pp. 1-8.

- M. Sandelic, **A. Davoodi**, A. Sangwongwanich, S. Peyghami and F. Blaabjerg, "Multi-Converter System Modelling in Cost for Reliability Studies," in *Proc. IEEE COMPEL*, Cartagena, Colombia, 2021, pp. 1-8.

Book chapter:

- **A. Davoodi**, S. Peyghami, C. Wu, and F. Blaabjerg, " Power Electronics for Smart Grids," in *Reference Module in Materials Science and Materials Engineering*, Elsevier, 2022.

Chapter 2
Power System Reliability Assessment

2.1. Background

To develop a reliability assessment framework for Power Electronic-based Power System (PEPS), first, it is important to take a look at the conventional Power System (PS) methods. By doing so, the shortcomings of these methods will be analyzed, which will pave the way for modifying them and adapting them for PEPS reliability assessment. Hence, this chapter illustrates a big picture of the main research question of the PhD project from a power system point of view. In this regard, important reliability indices will be discussed here, and the methods and assumptions for calculating them will be presented. In other words, the reliability indices in conventional power systems and the details on how to calculate them will be given (in this chapter) based on analytical and numerical methods. These methods include probability convolution methods, Markov method, state enumeration technique, and Monte Carlo simulation, and Capacity Outage Probability Table (COPT). Also, it will be explained that not only the power electronic failures, but also the outage of other units can influence the system reliability. This will be demonstrated by providing an example of the outage modeling of wind turbine circuit breakers.

2.2. Context of Power System Reliability and Its Assumptions

As shown in Fig. 2.1, systems can be categorized as mission-oriented and continuously operated [57]. In the PE reliability literature, the assumption is that the converter or PE systems are mission-oriented and non-repairable, while in PS reliability studies, the system is considered as continuously operated, where repair is a must [55]. In spite of such a fundamental difference, a way must be found to input PE reliability results into the PS reliability studies. This gap can be bridged by adopting the concept of availability, which will be explained further in Chapter 4.

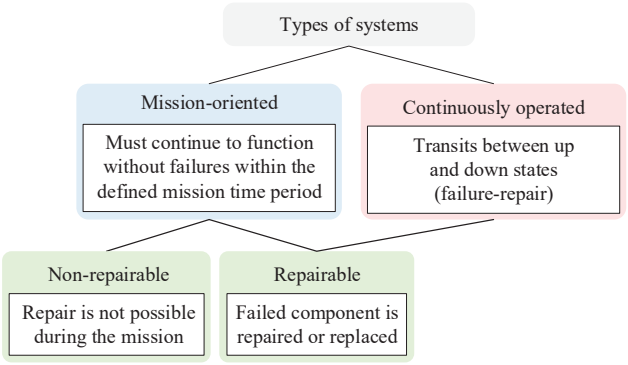

Fig. 2.1. Different types of systems in terms of repairability and operation in power system reliability analysis.

There is another notable difference in the assumptions of PE and PS reliability. In PE reliability, the assumption is that the wear-out of converter and components begins the first moment they are put into operation [58]. In other words, reliability modeling in PE literature revolves around wear-out failure modeling. On the other hand, the assumption in PS is that the wear-out failures are negligible, because the converter operates within its useful lifetime period (before the wear-out phase begins). Therefore, in PS reliability studies, chance failures are considered dominant, while wear-out failures are negligible [53]. When it comes to PEPS, both wear-out and chance failure are equally important and must be modeled, which will be discussed in Chapter 4, where wear-out will be dominant over time.

Power system reliability assessment can be categorized into adequacy and security. Security pertains to system's response to dynamics and transient disturbances and usually deals with smaller time scales. Adequacy is the system's ability to satisfy consumer demand, i.e., having enough generation and storage capacity considering the system constraints, and usually deals with larger time frames. Notably, the focus of this project is on adequacy evaluation. Also, in PS literature, it is common to use "adequacy" and "reliability" interchangeably, which will be the case here too.

From another point of view, power system reliability studies can be classified into qualitative and quantitative. The qualitative approach is according to engineering judgment and based on the experiences of experts. The quantitative approach provides a better way for benchmarking, standardization, and comparison of system reliability. The goal of the quantitative study is to create and calculate indices that can represent the system's risk and reliability. A good index must reflect both the probability and consequence of unwanted events, i.e., the likelihood of the event and its severity.

Since modern power systems are very large, interconnected, and complex, for reliability evaluation purpose, they are divided into separate subsystems and functional areas that can be analyzed separately [59]. These functional areas are shown in Fig. 2.2, where three Hierarchical Levels (HLs) are defined: HL I, HL II, and HL III.

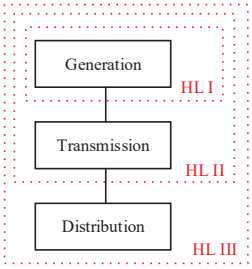

Fig. 2.2. Hierarchical Levels (HLs) in power system reliability assessment.

The first hierarchical level, HL I, represents the generation system. The main goal of reliability studies at HLI is to evaluate the total ability of generation facilities to supply the demand requirement. As a result, when performing reliability assessment in HL I, it is assumed that transmission and distribution equipment are fully reliable and able to transmit and distribute the generated power to the bulk load points. A simple way of reliability assessment in HL I is to develop models for generation capacity and load. Then, the load model and generation capacity model should be convolved to calculate the reliability indices. According to the conventional PS, only the generator's chance failures can influence the generation capacity. In PEPS, however, not only converter chance failures, but also the converter wear-out failures, plus the intermittent nature of renewables, contribute to the generation capacity model. It is worth reminding that the main focus of this PhD project is on the HL I.

The second hierarchical level, HL II, is usually called the composite generation and transmission system. In other words, not only the failures of generators are considered, but also the power line constraints and their failures are taken into account. HL III comprises the entire power system (generation, transmission, and distribution). Due to the size and complexity of PSs, the reliability studies at HL III is only feasible for small systems. As a result, sometimes, the reliability of the distribution system is evaluated alone – that is, the results from HL II are input to the reliability evaluation of the distribution system. However, by so doing, the impact of distribution system reliability on the HL II is neglected.

2.3. Reliability Indices in Power Systems

Reliability indices in PS are categorized as deterministic and probabilistic indices [60]. Deterministic indices, such as Reserve Margin (RM) and Largest Unit (LU), do not consider the stochastic nature of the load and generation, and they are used as a simple and intuitive means of reliability comparison between two systems. Probabilistic indices, on the other hand, consider the stochastic characteristics of the system, including uncertainties in load and generation. As shown in Fig. 2.3, both deterministic and probabilistic indices have different applications in static capacity and operating reserve assessment of the PS.

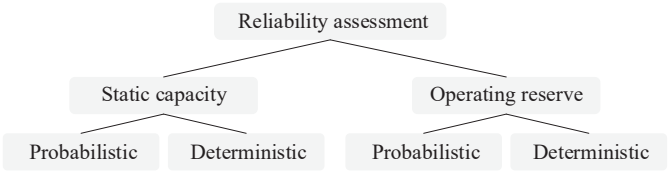

Fig. 2.3. Application of probabilistic and deterministic indices in power system reliability assessment.

For example, deterministic indices can be used for planning generation, operation, and network capacity.

Some of the deterministic indices for reserve capacity determination are as follows:

- Largest Unit (LU): this index indicates that the reserve capacity must be equal to the capacity of the largest or sum of a given number of largest units in the system – also known as (N-1) or (N-x) criteria.
- Fixed capacity margin: this index indicates that the reserve capacity must be a certain fixed value above the peak demand.
- Percentage of system peak demand: this index indicates that the reserve capacity must be equal to a percentage of the system peak load.

However, typically, probabilistic indices are preferable to the deterministic ones for the following reasons. First, the underlying cause of the PS risks and unreliability is its probabilistic behavior. In other words, the stochastic nature of events, which introduces a great deal of uncertainty to the system, plays a key role in the system's reliability. Some of these aspects in the conventional PS are as follows: chance failure of system equipment, load uncertainty, and uncertainty in energy export and import due to a volatile market. Therefore, deterministic indices are unable to represent these events, hence the need for probabilistic criteria. For example, the forced outage rate of generating units depends on their size and type, which cannot be incorporated by considering a fixed percentage reserve. As a result, probabilistic indices are widely used to evaluate the system risk and report its reliability.

The outcomes of PS reliability studies can be described in terms of various indices. The appropriate index must be selected for the study, depending on the hierarchical level and the purpose and application of the study. LOLP, LOLE, and EENS are some of the main reliability indices at HL I and HL II. LOLP, or the Loss Of Load Probability, indicates the probability that the load shedding happens in the system. LOLE, or the Loss Of Load Expectation, indicates the expected amount of time when an outage or load shedding event is experienced annually. This index is usually reported in the form of a unit of time per year. Typically, certain targets for LOLE are defined by the policymakers to ensure that the customers experience a standard level of reliability. For example, for Denmark, the target LOLE is equal to 35 [minutes/yr] [24]. For some European countries, the value of LOLE targets varies from 4 to 8 [hours/yr] [55]. For the US, the target LOLE revolves around 0.1 [days/yr] [61]. EENS, or Expected Energy Not Supplied, indicates the amount of energy that is expected to be lost annually. This index is especially desirable for economic studies

and evaluating the cost of unreliability in the system, as it can be monetized by using the value of the lost energy. It is also worth mentioning that these indices can be reported either as the delivery point or system indices. Delivery point indices are calculated based on what is seen from a specific load point of view, while for system indices, one value is calculated for the entire system, representing all the load points' unreliability. In this PhD project, all the calculated indices are system indices. Furthermore, as mentioned before, an ideal reliability index must reflect both probability and consequence of unreliability events. Therefore, here, the focus will be on calculating LOLE and EENS as they hold this characteristic. Also, in HL III and for distribution systems, many different reliability indices (e.g., SAIFI, SAIDI, CAIDI, average outage time [62]) exist, which will not be explained here as they are not the focus of this project.

The basic steps to calculate the reliability in HL I are shown in Fig. 2.4.

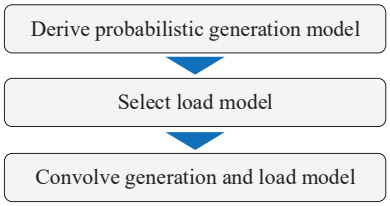

Fig. 2.4. Fundamental steps to calculate the power system reliability indices in HL I.

For the conventional power system, only the chance failures of generators are assumed to influence and contribute to the generation model at HL I. The generation capacity and load can be modeled probabilistically or by using time series. The above principle has been illustrated in Fig. 2.5, for a simple system, where one load and one generating unit exists, and the generation and load are modeled by individual PDFs.

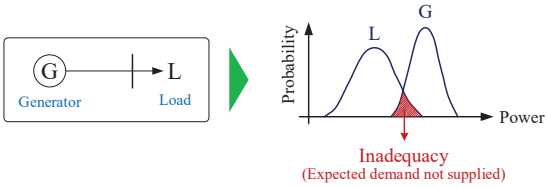

Fig. 2.5. Probabilistic modeling of Load (L) and Generation (G) and convolving them to calculate the reliability indices.

When more generating units and load points exist in the system, they can be merged to form one equivalent generation unit and one equivalent load, as shown in Fig. 2.6. Then, by convolving the equivalent load and generation model, the reliability indices can be calculated [41].

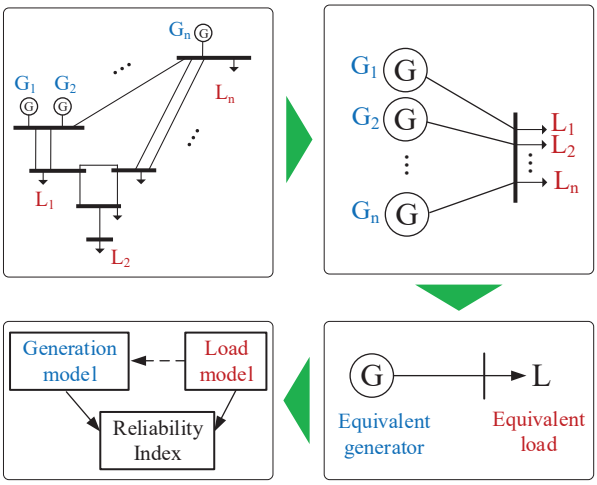

Fig. 2.6. Developing equivalent load and generation model of the power system to obtain system-level reliability indices (G: Generation, L: Load).

Instead of a probabilistic approach (which was illustrated in Fig 2.5), a time series approach can also be adopted to model the load and generation, if such data are available.

So far, the principles of calculating reliability indices in PS have been discussed. Now the mathematical details will be explained. The overall procedure to calculate the reliability indices in PS is shown in Fig. 2.7.

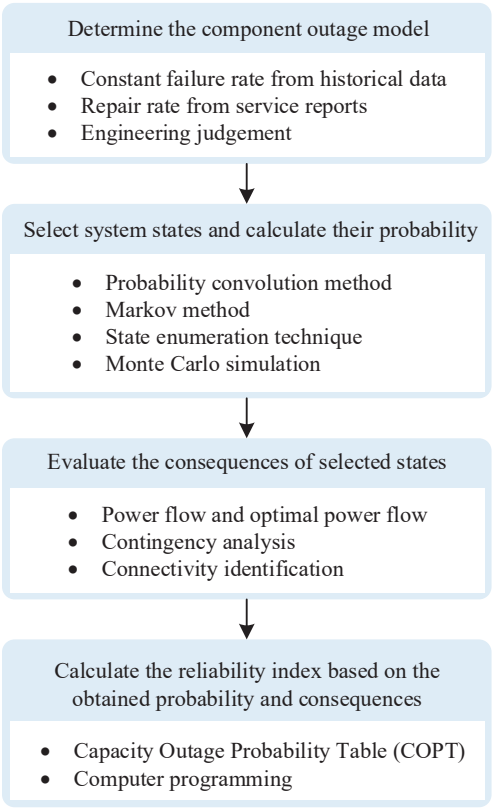

Fig. 2.7. The steps to calculate the reliability indices for a power system.

2.4. Outage Models and Calculating State Probabilities

Since the generation model in conventional PS is a function of generator failures, it is necessary to know the outage models of these units. The presumption in power system studies is that the units are working within their useful lifetime period (as shown in Fig. 2.8), where chance failures are dominant, and wear-out failures are ignored. As a result of this assumption, a constant failure rate, λ, is used to model generator outages. These constant failure rates are often extracted based on historical statistics and field failure reports, although in some cases, the engineering judgment is used to estimate them (e.g., when historical data is not available). Also, it is assumed that the generating unit is restored to its initial condition after each failure, with a repair rate of μ. This repair rate depends on the type of failure, distance, the number of the maintenance crew, and their experience, as well as available spare units.

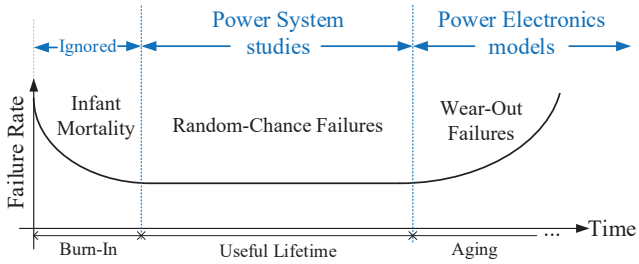

Fig. 2.8. Comparison of the assumptions for the operating range of the units in power system versus power electronic reliability studies.

The methods for calculating the state probabilities can be categorized into analytical and numerical methods. Both analytical and numerical methods have merits and shortcomings. Analytical methods aim to model the system by using mathematical equations and find the state probabilities by solving them. Probability Convolution Method (PCM), State Enumeration Technique (SET), and Markov approach are among the analytical methods. Typically, when the number of severe events is small, or operating conditions are not too complex, SET and Markov approach are more efficient. For a single-generator single-load system, PCM is applicable. Also, if the failure probabilities of the units are relatively small, the SET is preferable. On the other hand, numerical methods aim to model the random behavior of the system through simulation, based on physical and statistical relationships. The most common numerical method is the Monte Carlo Simulation (MCS), which can be useful when the system has complex operating conditions or the number of severe events is large, although it will have a high computation time.

2.5. Probability Convolution Method

This method is straightforward and applicable to calculate both EENS and LOLE for systems with one equivalent generation unit and one equivalent load. To realize this method, the following steps must be taken:

- Find the probability distribution of generation capacity
- Find the probability distribution of the load
- Convolve two distributions

If G and L are random variables, respectively representing generating unit and load with the following discrete PDFs [41]:

$$P(G = G_j) = p_j \qquad (j = 1,...,n) \tag{2.1}$$

$$P(L = L_i) = p_i \qquad (i = 1,...,m) \tag{2.2}$$

The EENS and LOLE can be calculated as

$$EENS = \sum_{j=1}^{n}\sum_{i=1}^{m} \max(0, L_i - G_j).p_i.p_j.T \tag{2.3}$$

$$LOLE = \sum_{j=1}^{n} \sum_{i=1}^{m} \frac{\max(0, L_i - G_j)}{L_i - G_j} . p_i . p_j . T \tag{2.4}$$

where T is the time length of study, typically one year or 8760 hours.

2.6. Markov Method

For systems with a few generating units, where finding an equivalent generating unit is not simple, the Markov method can be helpful. Markov method is also called the state-space approach since it is based on a state-space diagram, which provides a graphical way to illustrate various states and the transitions among them. For a system with four generating units, the state space diagram in the Markov approach is shown in Fig. 2.9.

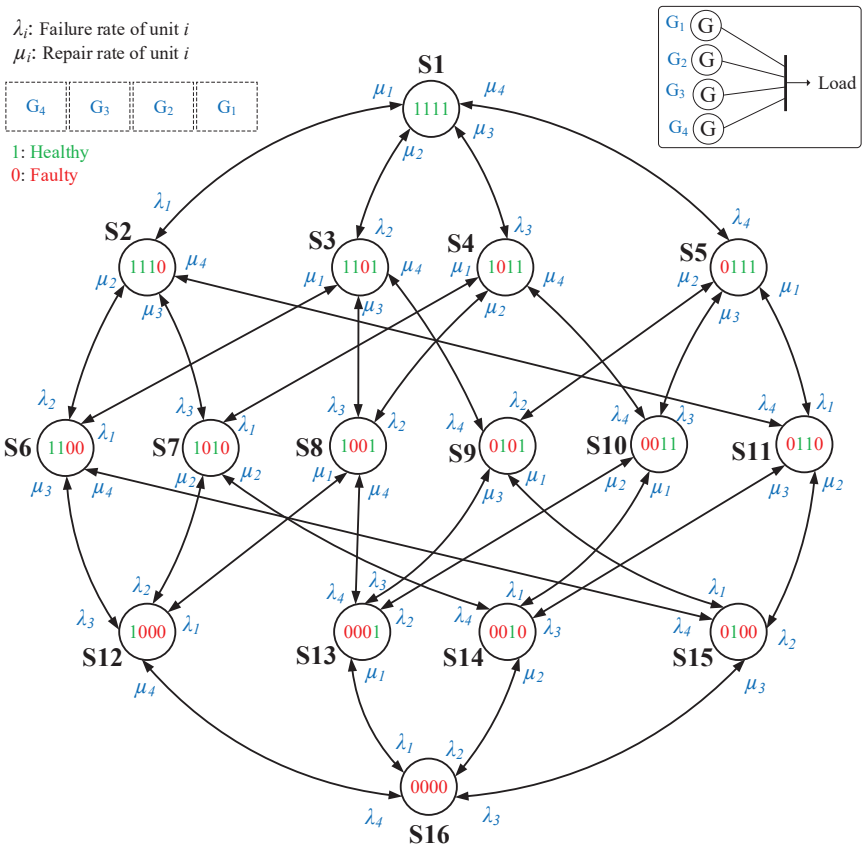

Fig. 2.9. State-space representation of a power system with four generating units (S: State, G: Generator).

For a system with N generating units, the number of states in the state space diagram will be 2^N. Therefore, for systems with a large number of generators (large N), the Markov method is not practical. It should also be pointed out that the Markov method will provide us with the probability of each state, while the consequence of each state must be known by analyzing the system by using power flow or other methods shown in Fig. 2.7.

After drawing the state-space diagram, a differential equation can be written in terms of failure and repair rates for each state. By considering the initial conditions and solving the set of differential equations for all states (also known as Chapman-Kolmogorov equations), the probability distribution of residing in each of the states can be calculated. A typical state and its neighboring states are shown in Fig. 2.10, where the possible transitions among them due to failures (λ) and repairs (μ) are depicted.

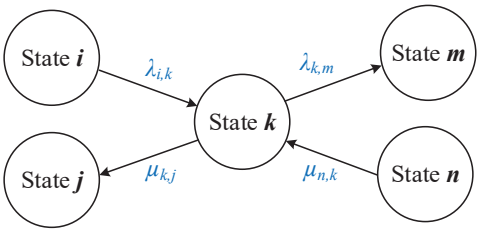

Fig. 2.10. A certain state in the state-space representation of the power systems, used to write the Markov equations accordingly.

From Fig. 2.10 and Chapman-Kolmogorov equations, the time derivative of $P_k(t)$, which is the probability of residing in state k, can be written as [63]:

$$\frac{dP_k}{dt} = \sum_i \lambda_{i,k} P_i + \sum_n \mu_{n,k} P_n - (\sum_j \mu_{k,j} + \sum_n \lambda_{k,n}) P_k \tag{2.5}$$

When the above equation is written for all states, a set of differential equations can be solved given the initial conditions for $P_k(t)$. As a result, $P_k(t)$,the probability of residing in each state k will be revealed.

2.7. State Enumeration Technique

In this technique, the availability, A_i, and unavailability, U_i, of unit i is approximated by:

$$A_i = \frac{\mu_i}{\mu_i + \lambda_i} \tag{2.6}$$

$$U_i = \frac{\lambda_i}{\mu_i + \lambda_i} \tag{2.7}$$

where μ_i and λ_i are the repair rate and chance failure rate for unit i.

It is worth mentioning that this approach is only valid when constant failure rates are used, as it is the case for conventional PS. When non-constant failure rates are to be used, as it is the case in PEPSs, this approximation is not valid, and new approaches must be used to model the availability. A solution has been proposed for this problem in [J1], where the details will be discussed in Chapter 4.

For a system with N generating units, the probability of the occurrence of state S, in which N_d units are down (failed) can be written as [53]:

$$P(S) = \prod_{i=1}^{N_d} U_i . \prod_{i=1}^{N-N_d} A_i \tag{2.8}$$

where U_i and A_i can be calculated from (2.6) and (2.7). It should be noted that a major drawback of this method is that it only presents the steady-state values of probabilities. In other words, the time-dependent behavior of the probability cannot be calculated by using this, while it could be studied by using the Markov method.

2.8. Monte Carlo Simulation in Power System Reliability Analysis

As explained before, when the number of states increases or complex operating conditions exist, numerical methods, e.g., the MCS, can be employed. Although the principle of this MCS is similar to what is used for PE reliability modeling, its purpose and implementation details are substantially different. This method is very versatile and allows for modeling aging and reliability in repairable, non-constant failure rates, and complex systems. However, this versatility comes at the cost of increased computation time. The flowchart to implement the MCS for a system with two generating units is shown in Fig. 2.11.

Given that the PDF of time to repair and time to failure are known, two random numbers are generated for each unit at each iteration of MCS. These random numbers are then plugged into the inverse of these PDFs, resulting in a random value for time to failure (*ttf*) and time to repair (*ttr*). As shown in Fig. 2.12, the unit is up during the *ttf* and down during the *ttr*. This process is continued so that the unit status is known for the entire study period, T. With a similar approach, the status (up or down) of all units is sampled for the given study time frame. This process is repeated as long as certain stopping criteria are not met. Once the stopping criteria are met, the outcomes of different iterations are averaged, where the probability of occurrence of any state can be calculated based on the simulated results.

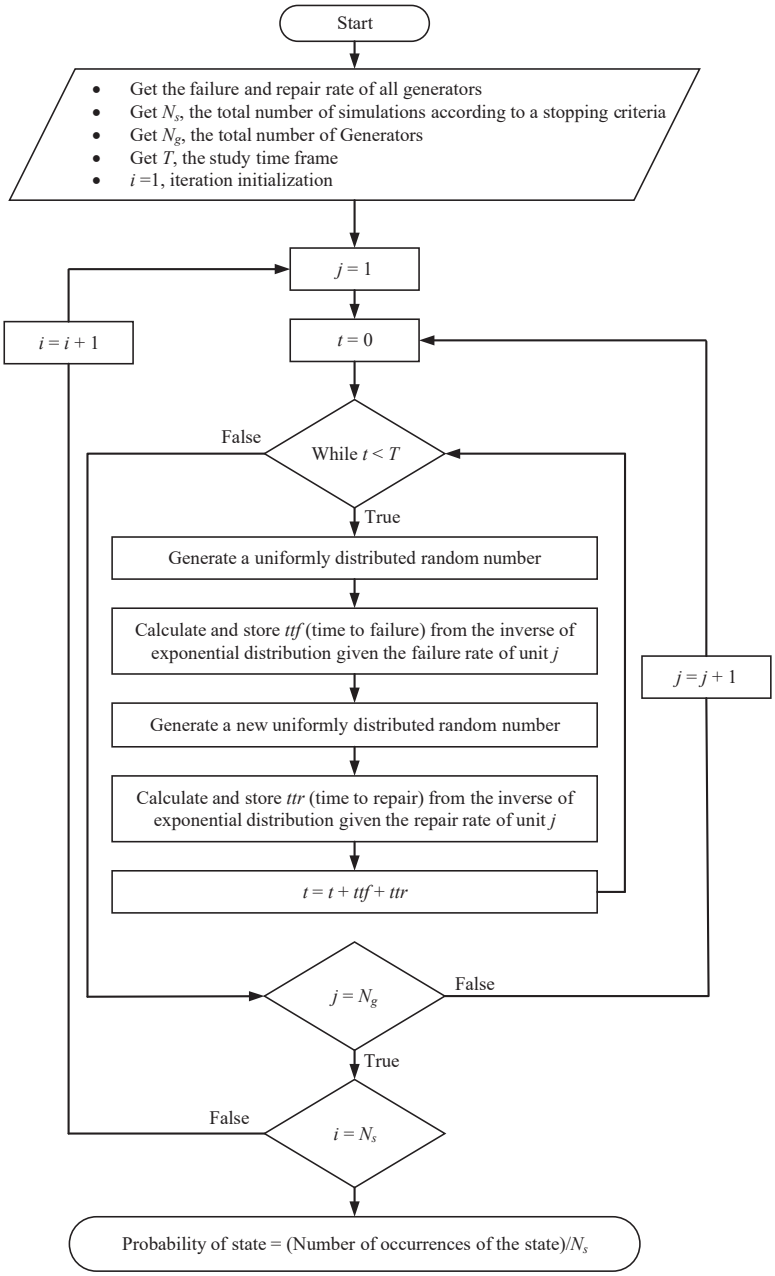

Fig. 2.11. Flowchart to implement the Monte Carlo simulation for power system reliability assessment.

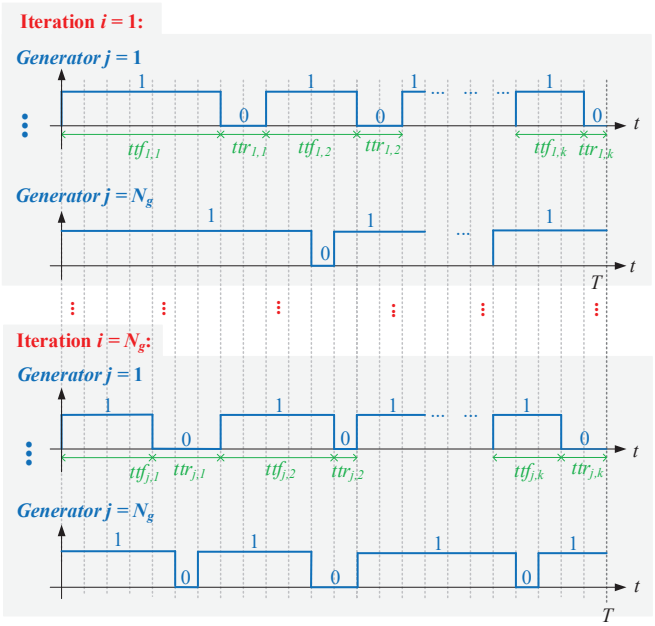

Fig. 2.12. Graphical representation of the Monte Carlo simulation for calculating the state probabilities and power system reliability assessment.

2.9. Capacity Outage Probability Table (COPT)

COPT characterizes the power system by providing a probabilistic model of its generating units. In COPT, all the available generating capacity states that the system can experience are listed, where their respective probabilities of occurrence are also provided. The probability of these states can be calculated by using one of the analytical or numerical methods explained above. A simplified demonstration of COPT can be seen in Table 2.1, where individual probabilities, p_j, and they can be calculated by one of the methods explained above, and available capacity, G_j, can be calculated by power flow analysis or contingency analysis.

Table 2.1. General form of the Capacity Outage Probability Table (COPT)

j	**Available capacity (G_k)**	**Capacity outage**	**Individual probability (p_k)**	**Cumulative probability**
1	G_1	0	p_1	$\sum_{k=1}^{N_{COPT}} p_k$
2	G_2	G_1-G_2	p_2	$\sum_{k=2}^{N_{COPT}} p_k$
…	…	…	…	…
N_{COPT}	G_{Ncopt}	G_1- G_{Ncopt}	p_{Ncopt}	p_{Ncopt}

The concept of COPT is the same for both small and large systems. For systems with few generating units, writing the COPT is possible manually. However, for larger systems, the concept of COPT must be realized through computer programming.

Since the COPT presents a probabilistic model of generating capacity, the reliability indices can be calculated if the load model is known too. In this regard, various load models can be used for power system studies, such as the constant load model, hourly load model, daily peak load model, Load Duration Curve (LDC), and Daily Peak Load Variation Curve (DPLVC). The hourly load model and daily peak load model describe the load chronologically, which are suitable when time series of generating capacity is available. Therefore, they are usually used to evaluate the past performance of the system rather than predicting its long-term future performance. An example of the hourly load model for the RBTS (Roy Billinton Test System) is shown in Fig. 2.13.

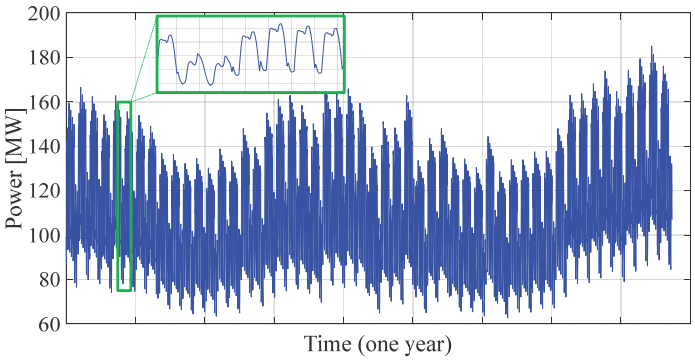

Fig. 2.13. Hourly load model, time series of the load model used in Roy Billinton Test System (RBTS).

If a constant load model is used, the LOLE and EENS can be calculated as:

$$LOLE = \sum_{j=1}^{N_{COPT}} \frac{\max(0, L - G_j)}{L - G_j} . p_j . T \tag{2.9}$$

$$EENS = \sum_{j=1}^{N_{COPT}} \max(0, L - G_j) . p_j . T \tag{2.10}$$

where j is the number of rows in COPT, T is the time length of the study, p_j and G_j are the individual probability and the available capacity at row j of COPT, respectively, and L is the constant load value.

If an LDC or DPLVC is used to model the load, the indices can be calculated similarly. The difference between LDC and DPLVC is that the LDC uses hourly peak load (or peak load in smaller time frames), while DPLVDC uses daily peak loads. Then, as shown in Fig. 2.14, these load levels are sorted in descending order, and the amount of time that load level has occurred is calculated, which can be translated into

the probability of the occurrence of the load level, where the probability of each load level can be calculated from $p_i = T_i / T$.

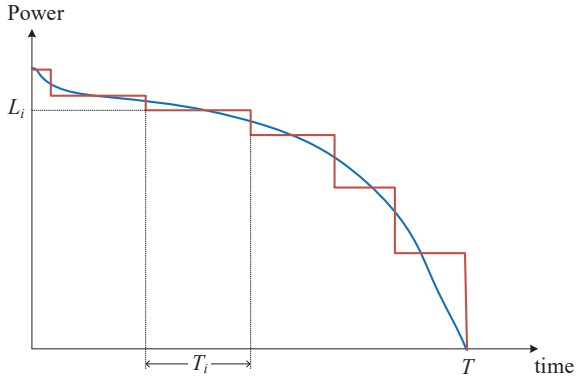

Fig. 2.14. Simplified graphical illustration of the Load Duration Curve (LDC).

The LDC for the RBTS is shown in Fig. 2.15, where it is obtained by translating the hourly load model (shown in Fig. 2.13) to an LDC.

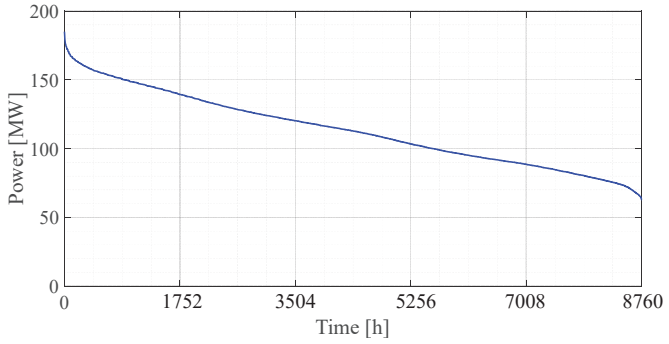

Fig. 2.15. Load Duration Curve (LDC) of the load model used in Roy Billinton Test System (RBTS).

If an LDC is used to model the load, the reliability indices can be calculated as:

$$l_{ij} = \begin{cases} 0 & L_i \le G_j \\ 1 & L_i > G_j \end{cases} \tag{2.11}$$

$$LOLE = \sum_{j=1}^{N_{COPT}} \sum_{i=1}^{N_{LDC}} p_i . p_j . l_{ij} . T \tag{2.12}$$

$$EENS = \sum_{j=1}^{N_{COPT}} \sum_{i=1}^{N_{LDC}} p_i . p_j . \max(0, L_i - G_j) . T \tag{2.13}$$

where L_i is the i^{th} load level in the LDC, p_i is the probability of the i^{th} load level, N_{LDC} is the number of load levels, N_{COPT} is the number of rows in COPT, p_j is the individual probability in the j^{th} row of LDC, G_j is the available capacity in the j^{th} row of COPT, and T is the study time frame.

2.10. Impact of Non-Power Electronic Failures on Power System Reliability

Another major difference between PS and PE reliability studies is that in PS, many components play a role – not only generators or power converters. Since the physical failure models provide better insight and accuracy, they are preferred over statistical models. If the physical models for the outage of a specific component exist, they will be incorporated into the calculations. However, such models do not exist for all PS components, in spite of their considerable role in the system reliability. For example, Wind Turbines (WTs) are used in large quantities in PEPSs. One of the key factors in their reliability is the converter failures, which has been studied extensively. However, other WT components also influence its reliability, such as its internal Circuit Breaker (CB) [64]. CB has a relatively large failure rate and has a noticeable impact on the WT reliability, and therefore, the system-level reliability. However, a mission profile-based and physical model-based method to assess its reliability is missing. Since, at the system level, the objective is to include the model-based reliability for as many components as possible, developing such a methodology to assess the WTCB can be of interest.

The application of CB in WT structure is shown in Fig. 2.16. Also, the steps to model its reliability are shown in Fig. 2.17, where the CB's main stressor must be found first. So, various stressors, such as the number of activations, current, temperature, humidity, and harmonics, were analyzed [65]–[67]. As a result, the number of activations and current were identified as the main stressors that determine the mechanical and electrical endurance of the CB [64]. Considering this, the lifetime model of the CB can be described in terms of its endurance curve, as shown in Fig. 2.18.

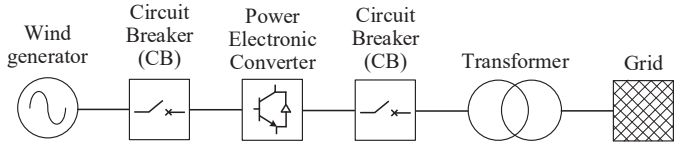

Fig. 2.16. Application of the circuit breaker in the PMSG-based wind turbine with full-scale power converter.

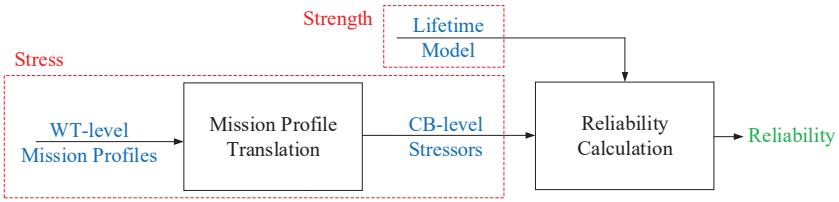

Fig. 2.17. Procedure to develop a reliability model for the circuit breaker based on physics of failure.

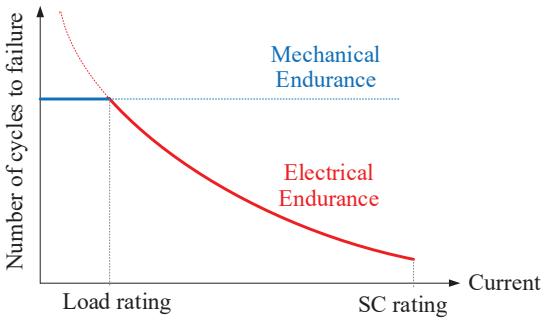

Fig. 2.18. Endurance curve of the circuit breaker: representing mechanical and electrical endurance.

For the CB in WT application, the electrical endurance exceeds the mechanical endurance. Accordingly, the lifetime model of the CB can be written as:

$$f_m = \beta \frac{N_f^{(\beta-1)}}{\alpha^{\beta}} \exp[-(\frac{N_f}{\alpha})^{\beta}] \tag{2.14}$$

where α and β are the Weibull scale and shape parameters from the endurance test, and N_f is the number of cycles to failure.

Next, the mission profiles must be identified, and models must be developed to translate them into the CB stressor. From analyzing the CB performance, it was shown that the wind speed, requested reactive power, and safety alarms are the main contributing factors to the CB activations. Thus, models were developed to translate these mission profiles into the number of activations. By employing an approach similar to the stress-strength analysis in PE literature, a method was developed to model CB reliability in the WT. The schematics of the developed method are illustrated in Fig. 2.19, where the overall block diagram can be seen.

The reliability of a case study was evaluated by using the developed approach. The mission profiles used for this case study are shown in Fig. 2.20, and other parameters are presented in Table. 2.2.

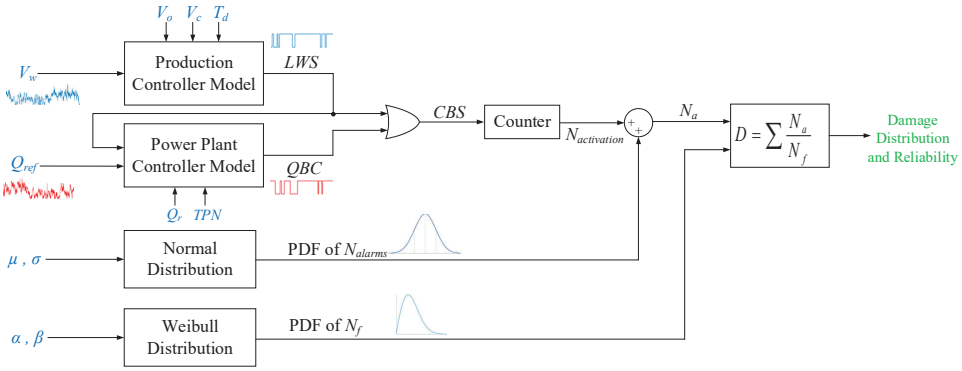

Fig. 2.19. Block diagram of the proposed reliability modeling method for wind turbine circuit breaker (V_w: wind speed, Q_{ref}: grid reactive power set-point, D: Damage, N_f: number of cycles to failure, α and β: scale and shape parameter of the Weibull for lifetime model, μ and σ: mean and standard deviation of N_{alarms} (the annual number of alarms)).

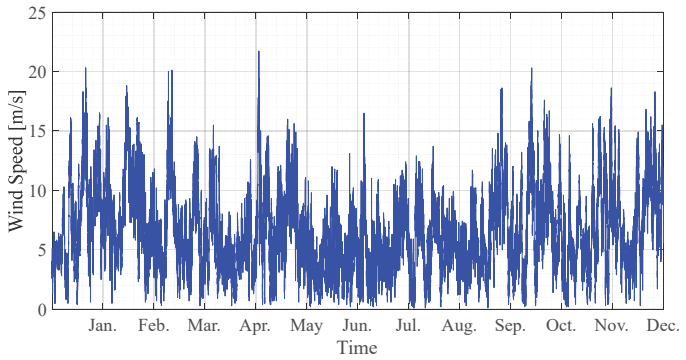

(a)

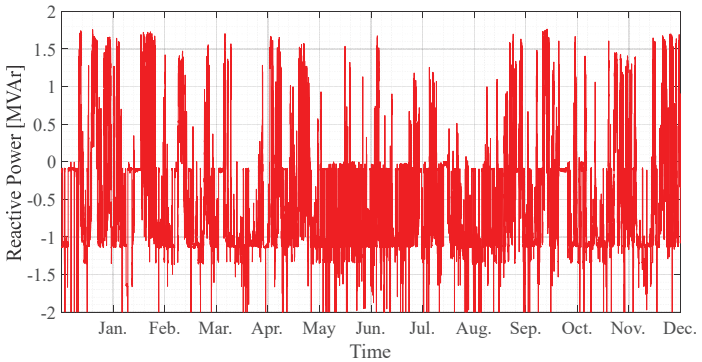

(b)

Fig. 2.20. Wind turbine-level mission profiles (MP1): (a) yearly profile of wind speed and (b) yearly profile of reactive power requested by the grid.

Table 2.2. Parameters used for the case study wind turbine

Parameter	Value
V_o [m/s]	3
V_c [m/s]	3.5
T_d [minutes]	120
Q_r [kVAr]	330
TPN	7
Number of turbines in park	7

Given the above mission profiles and parameters, the damage distribution for the CB under study was extracted, as shown in Fig. 2.21. Accordingly, its reliability was calculated, which is shown in Fig. 2.22.

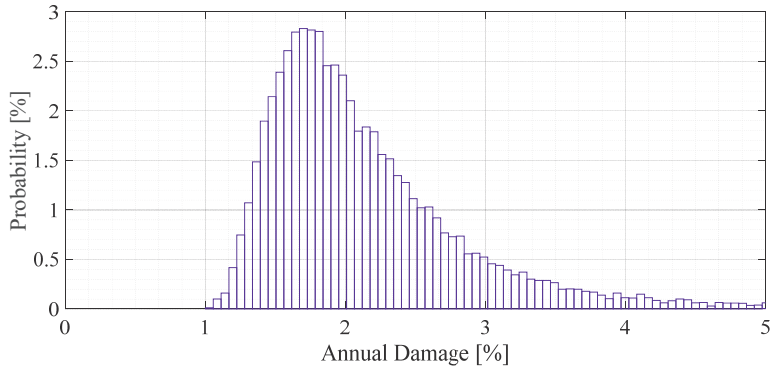

Fig. 2.21. Distribution of the accumulated damage to the circuit breaker.

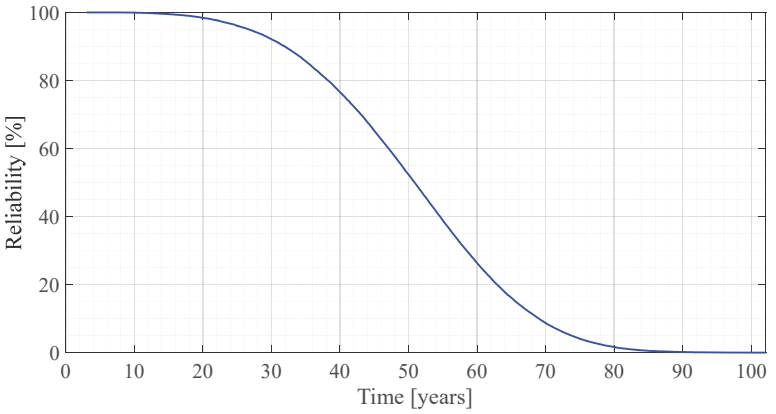

Fig. 2.22. Reliability of the circuit breaker as a function of time.

The main advantage of the developed method is that it is mission profile-based. For example, a new set of mission profiles was considered for the same case study. When the reliability of the case study was evaluated with respect to the new MPs, new results were obtained for the reliability, as shown in Fig. 2.23. Therefore, the developed method provides a tool to study the effect of MPs on the CB reliability and compare the performance of the CB under different MPs.

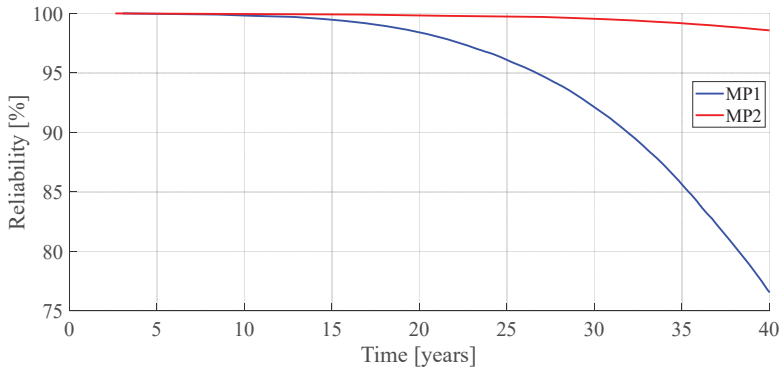

Fig. 2.23. Comparison of the reliability curves under two different mission profiles.

Another advantage of the developed method is that it is model-based. For example, several parameters play a role in the CB control strategy, all of which are modeled here. T_d is one of the control parameters, which is modeled in the production controller unit, as shown in Fig. 2.19. By using the developed method, one can investigate how the variation of this parameter affects the number of activations, which is the main CB stressor. In this regard, a $N_{activations}$-T_d curve is obtained by performing a sensitivity analysis, which shows that the CB stress decreases as T_d increases, as shown in Fig. 2.24. Also, to study the effect of T_d on the CB reliability, three cases were defined, i.e., T_d = 120 [minutes], T_d = 180 [minutes], and T_d = 240 [minutes]. The reliability of the CB in these three cases was calculated and compared with each other, as shown in Fig. 2.25. As Fig. 2.25 suggests, increasing T_d leads to an increase in reliability too. However, increasing T_d also causes other problems, such as stressing the converter. Furthermore, the developed method enables the quantitative evaluation of the CB reliability given specific model parameters. For example, for t = 30 [years], the unreliability of the CB in the above three cases of T_d were obtained $U(t)$= 7.8%, $U(t)$ = 3.1% and $U(t)$ = 1.7%, respectively.

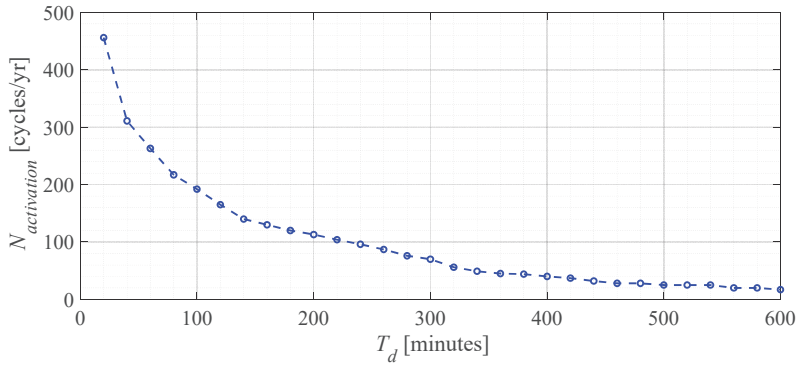

Fig. 2.24. $N_{activations}$-T_d curve, showing the variation of $N_{activations}$ (number of circuit breaker activations as T_d (one of the control parameters) varies.

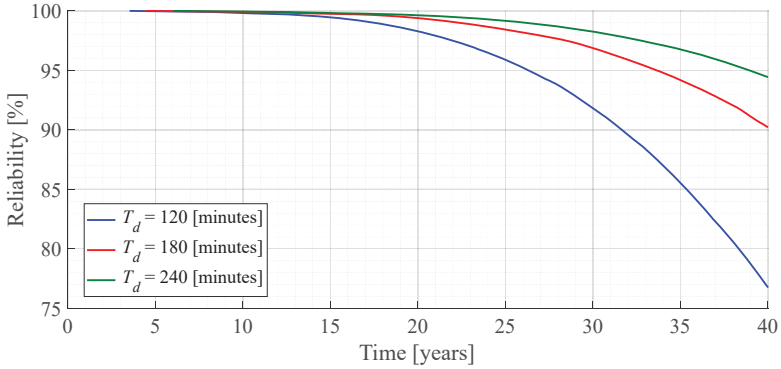

Fig. 2.25. Comparing the reliability of the circuit breaker under three different values for T_d to investigate the effect of control parameters on its reliability.

2.11. Summary

In this chapter, the reliability assessment of conventional power systems was studied, where all the steps and methods to implement them were discussed. Particularly, analytical and numerical methods for calculating state probabilities, such as the probability convolution method, Markov method, state enumeration technique, and Monte Carlo simulation were explained in detail. Moreover, different load models as well as the mathematical equations to calculate the reliability indices in conventional power systems by using the above methods were presented. Also, since in the PS, the outage model of all components matters, the developed reliability model for a wind turbine CB was demonstrated as an example. As a result, in this chapter, a larger picture of the PEPS reliability assessment was illustrated from a PS perspective.

Chapter 3
Reliability Modeling in Power Electronics

3.1. Background

The key to the PEPS reliability assessment is to bridge the gap between the Power Electronics (PE) reliability models and Power System (PS) reliability assessment methods. In the previous chapter, a basic understanding of the PS reliability assessment, including the concepts and methodologies, was provided. Since the power electronic converters are the backbone of the PEPSs, it is imperative to know the proper way of reliability modeling of their components and implement them in a computationally efficient way. As a result, this chapter will cover the modeling of reliability for power electronic converters. This includes efficient implementation of several steps, such as electro-thermal modeling, damage calculation using lifetime models, Monte Carlo simulation for variation analysis, and reliability block diagram technique. The implementation details of these methods will also be presented in this chapter by a case study of a PhotoVoltaic (PV) system. Also, the uncertainty of mission profiles and a proposed solution to model that will be discussed.

3.2. Wear-Out Failure Modeling

Despite many flaws, using reliability handbooks is still one of the popular methods for reliability modeling in power electronics, due to their simplicity and straightforwardness. Among these handbooks MIL-HDBK-217F [44] has been widely used. However, there are serious flaws in using this handbook, namely, outdated data, ignoring the physics of failure in components, and ignoring the application and operating conditions. Similar to this handbook, some companies have provided their own reliability guidelines, e.g., Siemens SN29500, RDF-2000, and Telcordia SR-322 [39]. Despite the improvements they provide (such as being application-based and incorporating newer technologies), they share the rest of the shortcomings with MIL-HDBK-217F. To improve these, International Electrotechnical Commission published IEC TR-62380 [68], which considers Mission Profiles (MPs). Nevertheless, this handbook was substituted with IEC 61709 [45] to update the data and incorporate modeling of failure mechanisms. Since the failure mechanisms in these handbooks are not modeled physically and still are based on statistics, FIDES [46] was published to address this challenge and incorporate the physics of failure into reliability modeling. In spite of these efforts, the final outcomes of FIDES and the other handbooks are constant failure rates, which means that the aging of power converters will not be considered. In other words, it is assumed that the components do not enter a wear-out phase, while the wear-out modeling is a main concern for the reliability modeling of PE for PEPS application [43]. For the above reasons, in this PhD project, the reliability modeling based on handbooks was not

used. Instead, mission-profile-based and model-based reliability evaluation method, also known as stress-strength analysis, was adopted. The procedure for stress-strength analysis and modeling the reliability from component-level up to converter-level is shown in Fig. 3.1. It is worth mentioning that the focus of this method is on the wear-out failure modeling of components, while the chance failure modeling was presented in the Chapter 2.

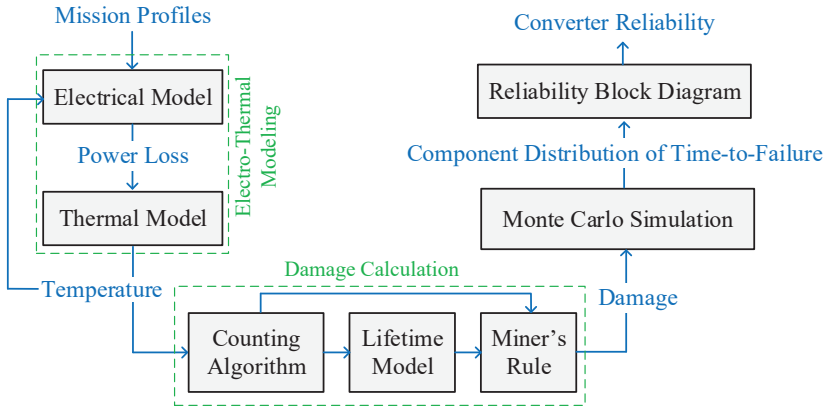

Fig. 3.1. Basic reliability modeling process of power electronic converters [C1].

3.3. Electro-Thermal Modeling

The stress-strength analysis begins with electro-thermal modeling, also known as mission profile translation. There are various stressors, such as temperature, humidity, and voltage, which trigger different failure mechanisms in PE components and influence their lifetime. Among these stressors, temperature and its swings are the main ones for the reliability-critical components – i.e., power semiconductors and capacitors. Hence, in this PhD project, only the thermal-induced stresses have been modeled and explained. Therefore, to calculate the reliability of a component, first, its temperature must be known. So, the process of electro-thermal modeling aims to translate the mission profiles into the temperature of the reliability-critical components by means of thermal and electrical models. Mission profiles are the operating conditions to which the PE converter is subjected, which determine the temperature of the reliability critical components. For a PhotoVoltaic (PV) converter, typically, a yearly profile of solar irradiance and ambient temperature is considered. For a wind converter, typically, yearly profiles of wind speed and ambient temperature are considered.

Often, this step is done by performing computer simulations of the converter system in the electrical and thermal domains. Nevertheless, this approach will make the electro-thermal modeling and the entire reliability modeling process time-consuming [69]. Considering that many converters must be modeled in a PEPS, this approach may result in unrealistically large computation times at the system level. To

accelerate the electro-thermal modeling, detailed analytical models can be adopted. In this regard, in [C1], the details of reliability modeling of a PV inverter at the converter level have been presented, where an analytical approach has been adopted for electro-thermal modeling. In this case, first, the PV panels must be modeled in order to know the input power and voltage to the inverter. The power and voltage characteristics of a PV panel for several solar irradiance levels are shown in Fig. 3.2 [70]. The assumption is that the maximum power will be extracted from the panel at any solar irradiance level by using the Maximum Power Point Tracking (MPPT) algorithm. One approach to model this is to simulate the panel in the computer environment. However, apart from being time-consuming, this is not a model-based approach, and the process needs to be repeated whenever a new panel is used. Instead, the single-diode model of the panel (shown in Fig. 3.3) has been used, which enables fast analytical translation of solar irradiance to output power and voltage with a few parameters that are available in the PV panel datasheet. These analytical expressions have been presented in [C1].

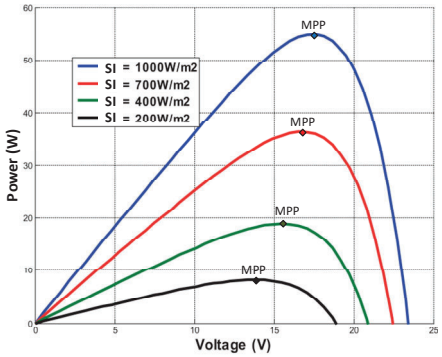

Fig. 3.2. An example of Power-Voltage characteristic curve of a PV panel at different solar irradiance levels at a fixed ambient temperature (SI: Solar Irradiance, MPP: Maximum Power Point) [70].

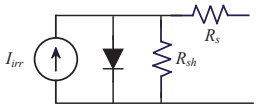

Fig. 3.3. Electrical equivalent of a PV cell according to the single-diode model [C1].

Similarly, for a wind power converter, the wind speed must be translated into the converter input power. To do so, the turbine power curve must be utilized, which relates the output power of the generator to the wind speed. The turbine power curve is provided to the wind turbine operator by the manufacturer. An example of the turbine power curve for a two-Megawatt wind turbine is shown in Fig 3.4 [52].

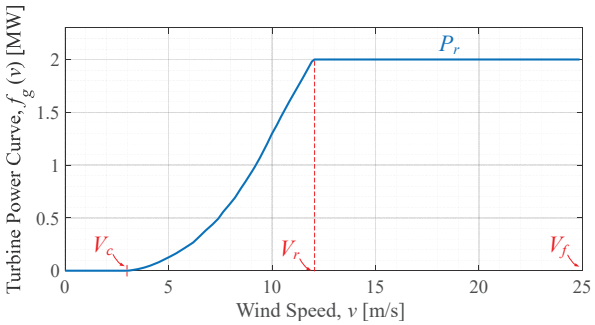

Fig. 3.4. Turbine power curve for a two-Megawatt wind turbine (V_c: cut-in speed, V_r: rated speed, V_f: cut-out speed) [52].

Notably, the turbine power curve is characterized by four parameters. V_c is the cut-in speed, the speed at which the blades start rotating and the power production begins. V_r is the rated turbine speed. When the turbine reaches V_r, it produces the rated power P_r. For the speeds above V_r and below V_f, the turbine power remains constant and equal to P_r. V_f is called cut-out speed, where the turbine blades are faded out at the wind to prevent the stress on the rotor due to high wind speed. If the turbine power curve is not available from the manufacturer, the following equation can be used to describe it [71].

$$P(v)=\begin{cases}0 & v<V_c \text{ or } v>V_f \\ P_r\cdot\dfrac{v^2-V_c^2}{V_r^2-V_c^2} & V_c\le v<V_r \\ P_r & V_r\le v<V_f\end{cases} \tag{3.1}$$

where v is the wind speed, V_c, V_r, V_f, and P_r are cut-in, rate, cut-out speeds, and P_r is the rated power of the turbine.

The temperatures of semiconductors and capacitors are driven by their power losses and ambient temperature. Ambient temperature is available from the yearly mission profiles. For a typical three-phase voltage source inverter shown in Fig 3.5, the conduction (P_C) and switching losses (P_S) of IGBTs can be calculated from [72]:

$$P_C=\left(\frac{1}{2\pi}+\frac{m\cos\varphi}{8}\right)V_{CE0}I_1+\left(\frac{1}{8}+\frac{m\cos\varphi}{3\pi}\right)r_{CE}I_1^2 \tag{3.2}$$

$$P_S=f_{sw}(E_{on}+E_{off})\frac{I_1}{\pi I_{ref}}\left(\frac{V_{DC}}{V_{ref}}\right)^{K_V}(1+\alpha_{E_{SW}}(T_j-T_{ref})) \tag{3.3}$$

where m is the modulation index, φ is power factor angle, f_{sw} is the switching frequency, I_1 is the fundamental harmonic of inverter output current, α_{Esw}, is the switching losses temperature coefficient, V_{ref}, I_{ref}, and T_{ref} are the reference values for voltage, current, and temperature in the datasheet of IGBT , and E_{on} and E_{off} are turn-on and turn-off energy losses per pulse.

As can be seen in (3.2) and (3.3), to calculate the losses, the m and cosφ must be known. To know them, the grid and output filter must also be modeled. Grid and filter models are shown in Fig. 3.6, where the detailed equations are presented in [C1].

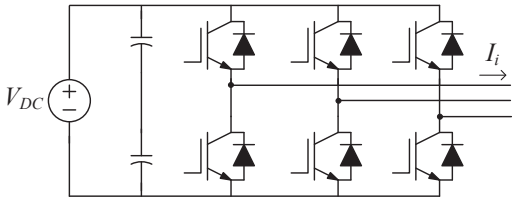

Fig. 3.5. Circuit diagram of an IGBT-based three phase voltage source inverter.

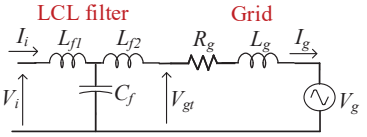

Fig. 3.6. Equivalent circuit of the grid and LCL filter [C1].

Once the losses are calculated, they must be translated into the temperature. To do so, two approaches are possible: simulation with the Finite Element Method (FEM) and thermal equivalent circuits. The former is more accurate but time-consuming. Therefore, the latter approach has been used, which is fast and provides acceptable accuracy. To realize the analytical modeling for the semiconductor, a Foster network has been used, as shown in Fig. 3.7, where in this case, n = 5.

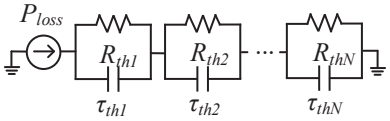

Fig. 3.7. N-th order Foster network (equivalent thermal circuit) for thermal modeling of IGBTs [C1].

As shown in Fig. 3.8, the IGBT temperature fluctuation has two components, T_{jm} variations, or slow variations due to solar irradiance and ambient temperature changes, and ΔT_{jm}, line-frequency variations. The detailed equations to calculate both of these components given the above Foster network have been presented in [C1]. Similarly, the DC-link capacitor temperature is driven by its ESR (Equivalent Series Resistant) losses, which is a function of the current. The capacitor currents can be formulated as [73]:

$$I_{C,rms} = I_1 \sqrt{m[\frac{\sqrt{3}}{4\pi} + \cos^2\varphi(\frac{\sqrt{3}}{\pi} - \frac{9}{16}m)]} \tag{3.4}$$

where m is the modulation index, φ is the power factor angle, and I_1 is the fundamental harmonic of inverter output current. Accordingly, the hotspot temperature of the

capacitor can be calculated. Also, in [C1], the dependency of ESR on the frequency, as illustrated in Fig. 3.9, has been considered.

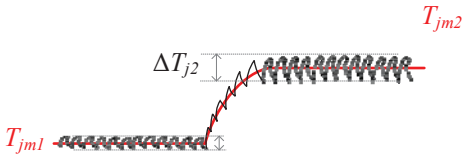

Fig. 3.8. The junction temperature of an IGBT consisting of slow variations in T_{jm} and line-frequency variations, ΔT_j [C1].

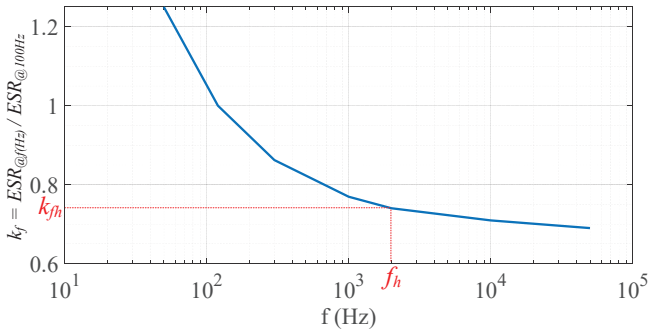

Fig. 3.9. Dependency of capacitor ESR on the frequency [C1].

The above modeling has been implemented in [C1], where, for a case study PV inverter, the mission profiles have been translated into T_j and ΔT_j for IGBTs, and T_h for capacitors. Fig. 3.10 shows the case study system, and the detailed parameters can be found in Table 3.1 and Table 3.2 and [C1].

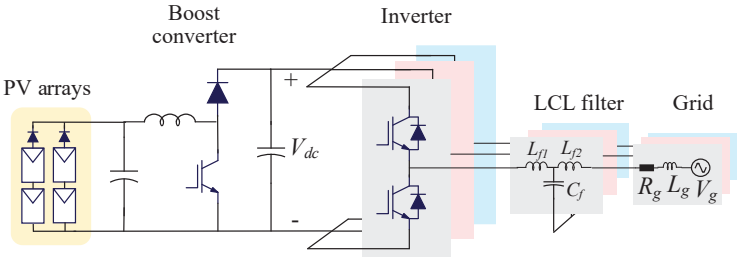

Fig. 3.10. Schematics of a PV system for a case study, including PV arrays, boost converter, PV inverter, LCL filter, and grid model [C1].

Table 3.1. Inverter parameters for the case study in Fig. 3.10 [C1]

Parameter	Value
V_{dc}	800 (V)
f_{sw}	2500 (Hz)
L_{f1}	3.5 (mH)
L_{f2}	0.5 (mH)
C_f	22 (μF)

Table 3.2. Grid parameters for the case study [C1]

Parameter	Value
V_g	230 (V)
f_g	50 (Hz)
R_g	0.5 (Ω)
L_g	1 (mH)

The used mission profiles are shown in Fig. 3.11, which includes the yearly profiles of solar irradiance and ambient temperature in Aalborg, with a time resolution of five minutes.

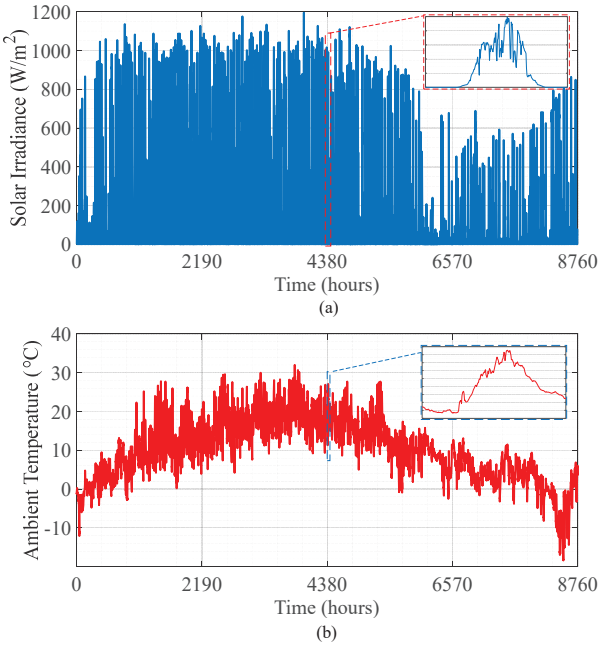

Fig. 3.11. Mission profile of Aalborg used in this case study: (a) solar irradiance and (b) ambient temperature [C1].

By using the above analytical modeling method, the T_j, ΔT_j, and T_h have been calculated and shown in Fig. 3.12.

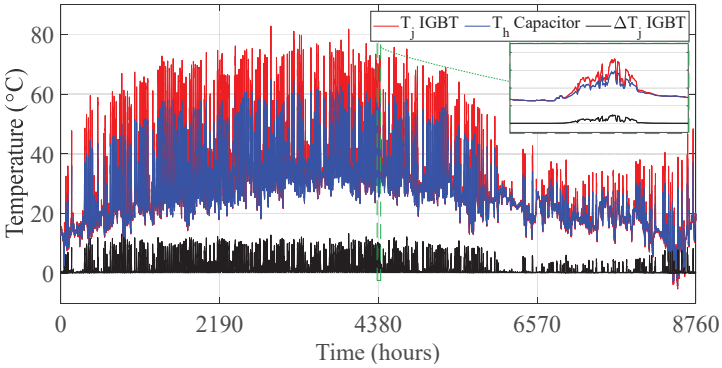

Fig. 3.12. IGBT and capacitor temperature profiles: T_j (red) and ΔT_j (black) for IGBT, and T_h (blue) for capacitors using the mission profiles in Fig. 3.11 [C1].

Apart from the analytical modeling, a detailed simulation model has also been implemented in PLECS. To verify the accuracy of the analytical results, they are compared to simulation results, as shown in Fig. 3.13 and Fig. 3.14.

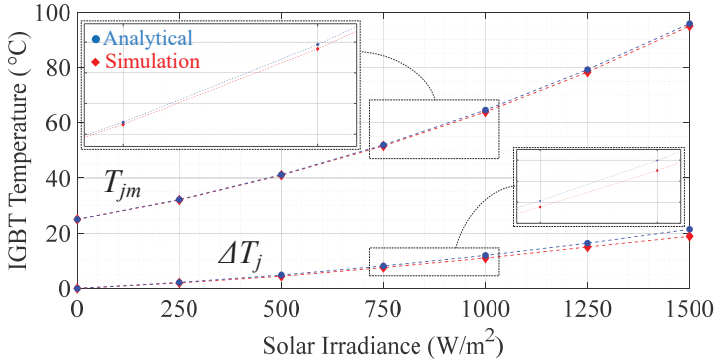

Fig. 3.13. Comparison of analytical and simulation modeling results: IGBT junction temperature for different irradiations [C1].

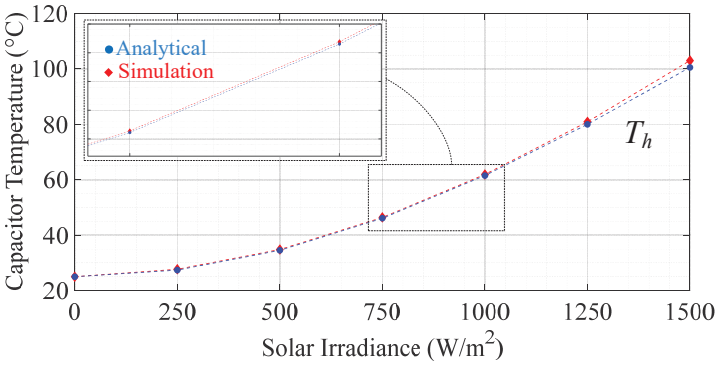

Fig. 3.14. Comparison of analytical and simulation modeling results: capacitor hotspot temperature for different irradiations [C1].

As Fig. 3.13 and Fig. 3.14 show, there is a good match between the detailed simulation results and the results derived from analytical models. It should be noted that at the design phase of the converter and before prototyping, only detailed simulation models exist for analysis. However, the analytical models outperform the simulation models in terms of computational efficiency, since they provide a comparable accuracy with shorter computation times.

3.4. Damage Calculation Using Lifetime Models

Lifetime models: From Fig. 3.1, when the electro-thermal modeling is finished, the damage calculation using lifetime models must be done. Lifetime models are mathematical expressions based on the physics of failure describing the lifetime of a component in terms of time or number of cycles to failure. For semiconductors, the lifetime model is in terms of the number of cycles to failure, N_f, and can be described as

$$N_f = A\Delta T_j^{\beta_1} \exp\left(\frac{\beta_2}{T_{j\max}+273}\right)\left(\frac{t_{on}}{1.5}\right)^{\beta_3} \tag{3.5}$$

where ΔT_j and T_{jmax} are the range and maximum of the junction temperature in the cycle, respectively, and t_{on} is the on-time of the cycle. A, β_1, β_2, and β_3 are lifetime parameters that can be obtained from the curves provided by the manufacturer or from accelerated tests. An example of such curves is shown in Fig. 3.15 [74], which shows the number of cycles to failures for the IGBT used in this case study in terms of its junction temperature fluctuations.

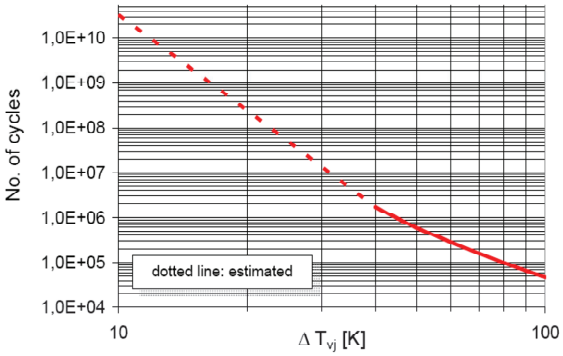

Fig. 3.15. Number of cycles to failure versus the junction temperature of an IGBT, obtained from power cycling test [74].

For capacitors, the lifetime model is in terms of time to failure at a given temperature (T_h) and voltage (V), and can be described as

$$L = L_{ref}.2^{\frac{T_{h,ref}-T_h}{n_1}}.(\frac{V}{V_{ref}})^{-n_2} \quad (3.6)$$

where $T_{h,ref}$ is the reference hotspot temperature, L_{ref} is the rated lifetime of the capacitor under the reference hotspot temperature, V_{ref} is the reference voltage, and n_1 and n_2 are parameters provided by the manufacturer. The lifetime model parameters for the IGBT and capacitors used for this study are presented in Table 3.3 and Table 3.4.

Table 3.3. Parameters of the lifetime model for the IGBTs [C1]

Lifetime parameter	**Value**
A	8.3255^{14}
β_1	-7.01
β_2	2553
β_3	-0.3

Table 3.4. Parameters of the lifetime model for capacitors [C1]

Lifetime parameter	**Value**
L_{ref}	7000 (hours)
T_{ref}	105 C
n_1	10
n_2	2.5

Damage calculation: Accumulated damage, D, indicates the proportion of the device lifetime that is consumed annually under a certain mission profile. When a rainflow counting algorithm is used on the IGBT junction temperature profile, it classifies the profile into k different cycles and provides a ΔT_j, T_{jm} and t_{on} associated with each. It also counts the number of times that the cycle is repeated (n). Since the line frequency

is fixed, the temperature variations and the number of cycles are known for the line-frequency fluctuations. According to Miner's rule, the accumulated damage to the IGBT can be written as:

$$D_{IGBT} = \sum_{i=1}^{K} \frac{n_i}{N_{fi}} \tag{3.7}$$

where N_{fi} is the number of cycles to failure from the lifetime model, n_i is the number of occurrences of each cycle obtained from the rainflow counting algorithm.

For the capacitor, T_h profiled is categorized into M temperature levels by using a histogram, where for each temperature level i, t_i is the time period of its occurrence. According to the Miner's rule, the accumulated damage to the capacitors can be calculated from:

$$D_{cap} = \sum_{i=1}^{M} \frac{t_i}{L_i} \tag{3.8}$$

where L_i is the capacitor time to failure at temperature level i (derived from the lifetime model of the capacitor), and t_i comes from the histogram as explained.

3.5. Monte Carlo Simulation (MCS) and Converter-Level Reliability

The above calculated damage is a constant value, and therefore it is also known as static damage. However, there are different sources of uncertainties during the calculation procedure, which must be considered. Some of these sources of uncertainty are as follows; lifetime model parameters uncertainties due to a limited number of samples during the accelerated lifetime test, component-to-component variations due to manufacturing processes, and smaller errors in the electro-thermal models. To handle these uncertainties, a type of Monte Carlo simulation is adopted as shown in Fig. 3.16. In the above calculations, a static value was considered for all input parameters, and a static damage was resulted. By using the MCS, however, a Probability Density Function (PDF) can be obtained for each input parameter, where random samples of them will be taken to find the PDF of the output parameter. Therefore, a PDF will be obtained for the accumulated damage, rather than a static value.

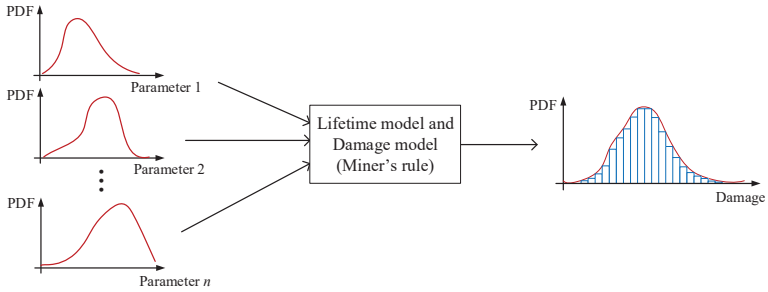

Fig. 3.16. Schematic of the Monte Carlo simulation used to calculate the damage distribution for a power electronic component.

For the above-mentioned case study, the PDF of the damage for IGBT and capacitors are calculated by using the MCS, as shown in Fig. 3.17 and Fig. 3.18.

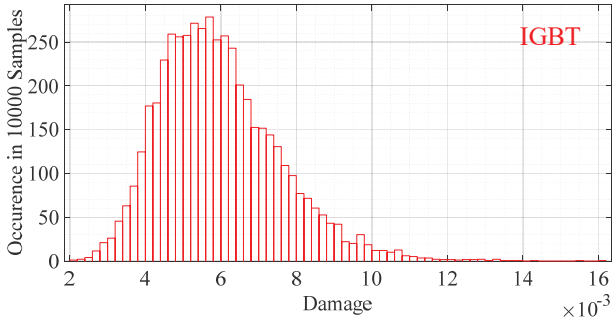

Fig. 3.17. Distribution of Damage to IGBTs [C1].

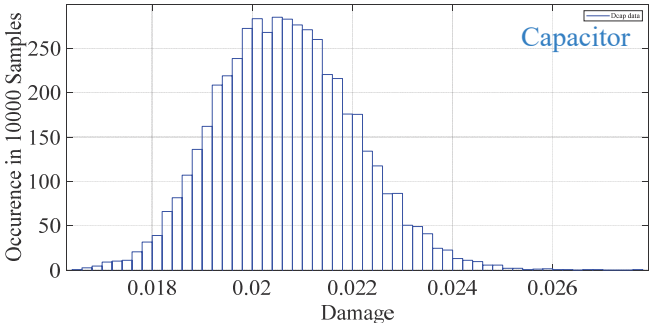

Fig. 3.18. Distribution of Damage to the capacitor [C1].

Next, the time to failure, *ttf*, of each component must be calculated, which can be done by using $ttf = 1/D$. Since the PDF of D is known from the MCS, the PDF of *ttf*,

f(t), can also be calculated easily. By knowing f(t), the reliability of the component can be found from:

$$R(t) = 1 - \int_0^t f(\tau) d\tau \tag{3.9}$$

Then, the component-level reliabilities must be translated into the converter-level reliability by using the Reliability Block Diagram (RBD) [75] approach. Typically, the entire converter stops working when only one of its reliability-critical components fails. In RBD, this means that all reliability-critical components are in series, as shown in Fig. 3.19. It should be noted that this diagram could be different for other systems.

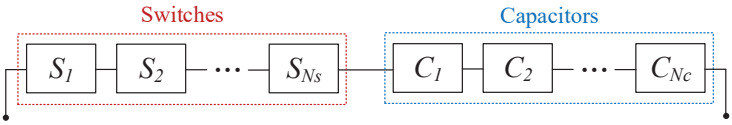

Fig. 3.19. Representation of the converter structure by using the Reliability Block Diagram (RBD) approach.

Therefore, for a converter with N_S switches and N_C capacitors, the converter-level reliability can be calculated according to

$$R_{inv}(t) = R_S^{N_S}(t).R_C^{N_C}(t) \tag{3.10}$$

where R_C and R_S are the capacitor and switch reliability. Accordingly, the converter-level reliability for the case study is calculated and shown in Fig 3.20.

By applying distribution fitting methods to the converter reliability curve, it can be approximated with a Weibull distribution with shape and scale parameters of β and η. By knowing β and η, $MTTF$ and B_X lifetime can also be calculated for the converter from the following equations.

$$B_X = \eta \sqrt[\beta]{\ln\left(\frac{1}{1 - X/100}\right)} \tag{3.11}$$

$$MTTF = \eta \Gamma\left(1 + \frac{1}{\beta}\right) \tag{3.12}$$

$MTTF$ is the average time to failure and B_X lifetime is the lifetime at which more than X% of the population has failed. In this regard, β, η, $MTTF$, and B_{10} for the above case study are as presented in Table 3.5.

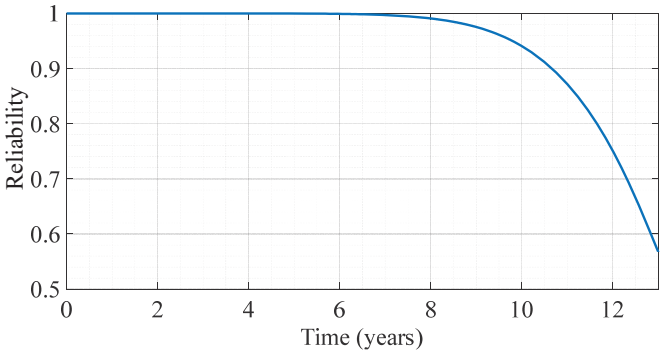

Fig. 3.20. Reliability of the complete inverter over time [C1].

Table 3.5. Calculated reliability metrics for the case study inverter [C1]

Reliability metric	**Value**
(β , η)	(8.5 , 13.9)
B_1	8.1 years
B_{10}	10.7 years
MTTF	13.14 years

Since all the above procedures are model-based, the execution time would be fast. Furthermore, these parameters have a physical meaning. Therefore, if any parameter changes in the future, such as DC-link voltage, switching frequency, PV panel parameters, or grid impedance, the new results can be obtained simply by changing the corresponding parameter in the model. For example, the impact of switching frequency on the B_{10} lifetime of the case study inverter is shown in Fig. 3.21 by performing a sensitivity analysis.

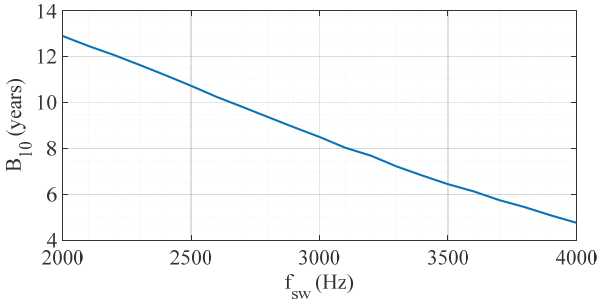

Fig. 3.21. Impact of the switching frequency on the converter B_{10} lifetime.

3.6. Mission Profile Uncertainty

As discussed in Chapter 1, a key challenge that must be dealt with in this project is modeling the uncertainties. By using the MCS, some sources of uncertainty were considered that could be statistically modeled, such as component-to-component

variation, tolerance of values, and model errors. However, variation of mission profile from year to year is another source of uncertainty, which can introduce large errors and cannot be modeled with the MCS. For example, Fig. 3.22 shows the solar irradiance profile for three different years for Las Vegas, NV [76]. As it can be seen from Fig. 3.22, the variations can be substantial, even at the same period of the year, resulting in different stress levels in different years.

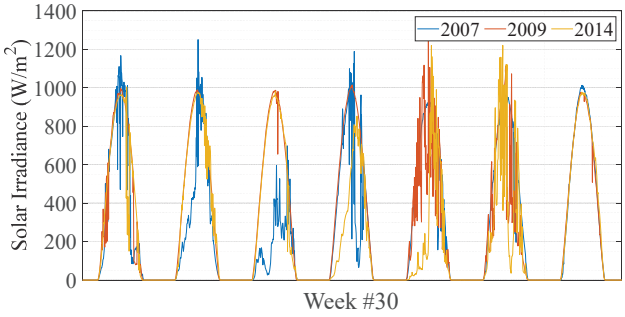

Fig. 3.22. Comparison of solar irradiance profiles of years 2007, 2009, and 2014 at week #30 [76].

Given the above MPs shown in Fig 3.22, the reliability of the case study is calculated and shown in Fig. 3.23, considering only the IGBT failures. As it can be seen from Fig. 3.23, the calculated reliability is greatly dependent on the selected MP year. This is reasonable because some years induce a higher stress on the components and consume more lifetime, and vice versa.

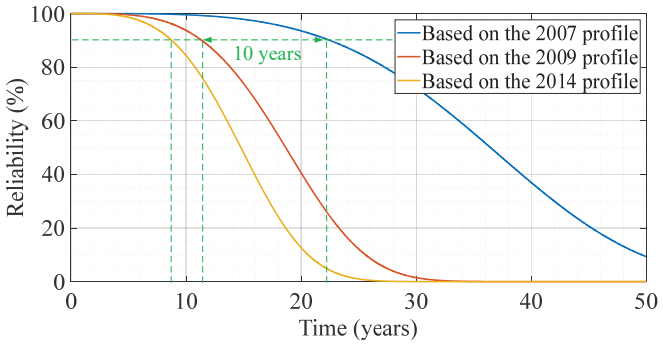

Fig. 3.23. Comparison of the converter reliability by using three different mission profiles – 2007, 2009, and 2014 [C2].

To overcome this challenge, the Generative Adversarial Networks (GANs) [77], [78] can be used to do the scenario generation for the MPs. In other words, the GAN can be trained based on existing MPs to generate a larger number of scenarios representing all the MPs that the inverter might experience in the future. The structure

of the GAN is shown in Fig 3.24, while all the mathematical details on how to train and utilize it for scenario generation have been explained in section III of [C2].

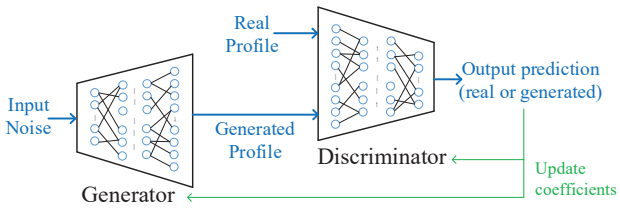

Fig. 3.24. Overall structure of the Generative Adversarial Networks (GAN) and its training process used for mission profile generation [C2].

By implementing the GAN using Python, it was trained based on real MPs. Accordingly, 150 years of MP were generated. One of these generated profiles is shown in Fig. 3.25.

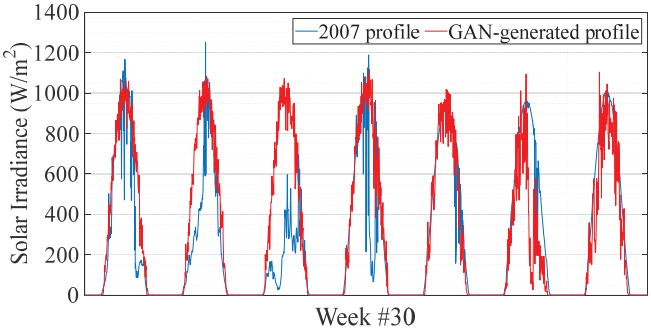

Fig. 3.25. Comparison of the real and GAN-generated solar irradiance profiles at week #30 [C2].

These GAN-generated profiles were compared with realistic profiles in terms of their Cumulative Distribution Function (CDF), monthly average, and Power Spectral Density (PSD). The results of this comparison are shown in Fig. 3.26 to Fig. 3.28.

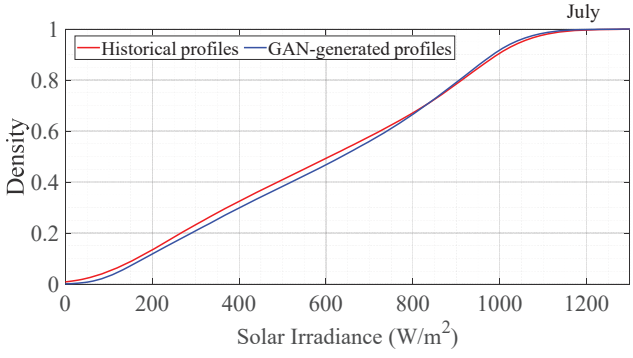

(a)

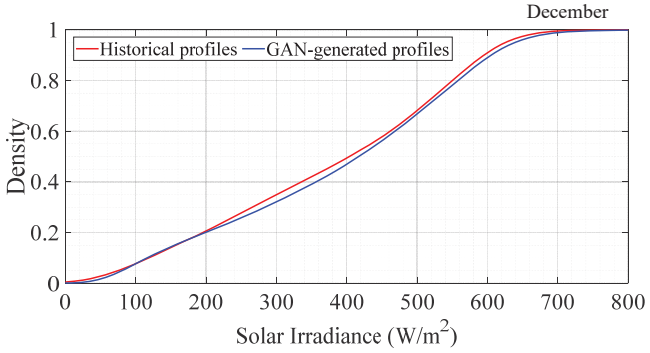

(b)

Fig. 3.26. Comparison of the historical and GAN-generated profiles in term of the CDF (Cumulative Distribution Function) of the daytime solar irradiance: (a) July and (b) December [C2].

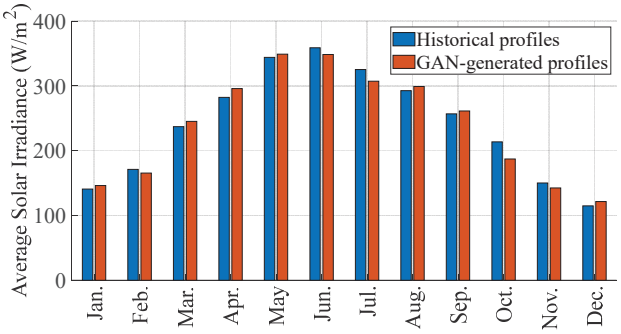

Fig. 3.27. Comparison of the historical and GAN-generated profiles in terms of average solar irradiance in different months [C2].

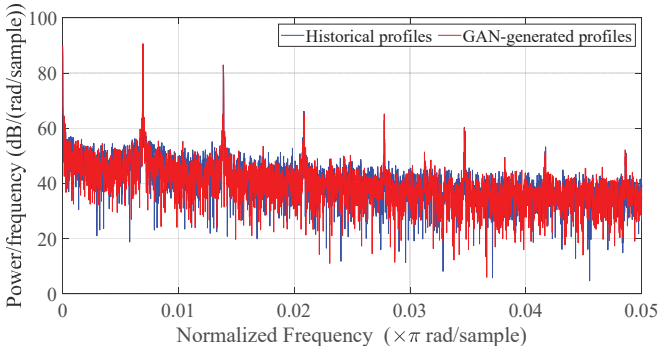

Fig. 3.28. Comparison of the historical and GAN-generated profiles in terms of PSD (Power Spectral Density) of the daytime solar irradiance [C2].

From Fig. 3.26 to Fig. 3.28, it can be seen that the GAN-generated profiles approximately hold the same statistical and temporal properties of the real profile. However, they are not identical neither to each other, nor to the real profile, which is suitable for emulating MPs. Finally, to study whether the GAN-generated profiles can help in reducing the errors due to mission profile uncertainty, three cases were considered. The reliability of the above-mentioned case study was evaluated by using the stress-strength analysis and compared to each other. As shown in Fig. 3.29, Case I (blue curve in Fig. 3.29) is where only the MP of the year 2007 was considered, Case II (red curve in Fig. 3.29) is where 14 years of MP from 2007-2020 were considered, and Case III (yellow curve in Fig. 3.29) is where 150 GAN-generated scenarios were considered.

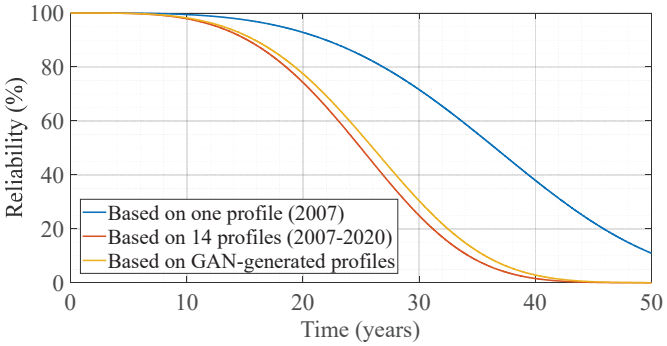

Fig. 3.29. Comparison of the inverter reliability based on GAN-generated profiles and historical profiles [C2].

As it can be seen from Fig. 3.29, by using the GAN-generated profiles, the estimated reliability matches the average of many years of MPs (comparing Case III and Case II). However, if only one year of MP was selected (which is typically the case in the literature), the reliability prediction will have a large error (compare Case I and Case II). In other words, by using the GAN, many scenarios are generated based on a limited number of real profiles, which reduces the sensitivity of the reliability estimation on the selected year of MP, and thereby reducing the errors. Therefore, when limited real data is available for MPs, using the GAN can help increase the reliability estimation accuracy by mitigating the effect of the mission profile uncertainty.

3.7. Summary

In this chapter, the methods for modeling power electronics reliability were presented, and their implementation details were discussed. In this regard, first, the details of reliability modeling of a PV inverter were presented, where all steps, including electrothermal modeling, lifetime models, damage calculation, Monte Carlo simulation, and RBD, were elaborated upon. Next, the mission profile uncertainty issue was discussed, where it was proposed to use GAN for MP scenario generation

and model its uncertainty. It was shown that by using this approach, the sensitivity of the estimated reliability to the mission profile is reduced.

Chapter 4
A Comprehensive Framework for System-Level Reliability Assessment of Power Electronic-based Power Systems

4.1. Background

In reliability assessment of Power Electronic-based Power System (PEPS), certain concerns must be addressed to avoid large errors and achieve realistic results. First, the mission profiles, converter wear-out models, and the physics of failures must be considered. These concerns were discussed in Chapter 3 by explaining the PE reliability modeling methods. The outcome of these methods are non-constant failure rates, neglecting the repair and chance failures. On the other hand, while PS reliability assessment methods (as explained in chapter 2) consider repair and chance failures, they are unable to incorporate non-constant failure rates. This chapter aims to bridge the gap between Chapter 2 and 3 to propose a reliability assessment method for the PEPSs. In this regard, a new availability modeling method for power converters in the PEPS will be discussed in this chapter. Another factor that significantly influences the PEPS reliability is the generation uncertainty. Due to the strong temporal patterns in PhotoVoltaic (PV) generation units, and since storage units are highly dependent on the dynamics of the power flow in the system, purely probabilistic methods cannot be used to model generation uncertainty. As a result, scenario generation based on Generative Adversarial Networks (GANs) is adopted and will be explained here. By doing so, both temporal and probabilistic aspects of generation capacity will be considered through emulating the mission profiles that mimic the future experience of the system. Also, to model the consequence of outage of units, the power system performance models for PV, Wind Turbine (WT), and Battery (BT) units must be considered, which will also be discussed in this chapter. Finally, it will be explained how to aggregate the data from the above models to calculate the reliability indices for a PEPS.

4.2. Description of the Methodology

A simplified schematic of a PEPS is shown in Fig. 4.1. As discussed in Chapter 1, due to the abundance of power electronics and renewables in such as system, new considerations must be taken into account when assessing its reliability. As a result, existing approaches might not be directly usable for PEPS reliability assessment, and hence we need to develop new methods or modify the existing ones. Therefore, a comprehensive framework is developed here and will be elaborated in this part, which enables the system-level reliability assessment of PEPSs. As shown in Fig. 4.2, the proposed framework for the PEPS reliability assessment has several blocks, each of them aims to address one of the discussed considerations. The main blocks of the

framework are as follows: Converter availability modeling, power system model, scenario generation, state enumeration, and index calculation.

Converter availability model: One of the main considerations in the PEPS reliability assessment is to model and study the impact of power electronic failures and converter aging on the system-level reliability. In this block, such consideration will be addressed by adopting the wear-out models, which are developed based on mission profiles and physics of failure. To make it comprehensive, the effect of externally-caused failures is taken into account by incorporating chance failures into the model. Furthermore, the repair and corrective maintenance of the units are modeled.

Power system model: In order to model the reliability, the consequence of each failure in the system in terms of lost energy and downtime must be known. Conventional generation units in Power Systems (PSs) could follow a certain setpoint as long as it was within their active and reactive power capability limits. As a result, it was simple to model the consequence of failure in that generating unit, as its output power would have become zero in that case. However, as it can be seen in Fig. 4.1, in a PEPS, the generating units are renewable-based, which are dependent on climate conditions and need to be modeled efficiently in the system. Moreover, storage units are a key contributor to the system reliability, whose output power and the State-Of-Charge (SOC) depend on the load-generation balance, which require accurate and efficient modeling. Therefore, this block aims to provide efficient models of the generation and storage units in the PEPS to enable calculating the available power to the load at any time.

Generative Adversarial Networks for scenario generation: Apart from power electronics failure, generation uncertainty can be an important cause of unreliability in the system. For example, when storage units are empty, and no wind and sunlight are available, the customers can experience outages even though no power electronic failures have happened. Since PV (because of its temporal patterns) and BT (because energy is a function of time and not only the power) are used in the PEPS, the dynamics of the generation are of great importance, and this problem cannot be modeled with purely probabilistic approaches such as Markov method. Therefore, Generative Adversarial Networks (GANs) are used to generate realistic mission profile scenarios, which emulates the wind and solar resources and enables modeling the generation uncertainty.

State enumeration and index calculation: The fundamental principle of calculating reliability indices in any PSs is to know the probability and the consequence of unreliability events. In this regard, this block provides a systematic way to consider all the unreliability events that are caused by the failures or the lack of generation and storage power. In other words, it ensures that no unreliability event is ignored. Furthermore, not only the probabilistic but also the time-dependent behavior of reliability indices can be studied, thanks to providing time-varying PDFs for any index, rather than a static value.

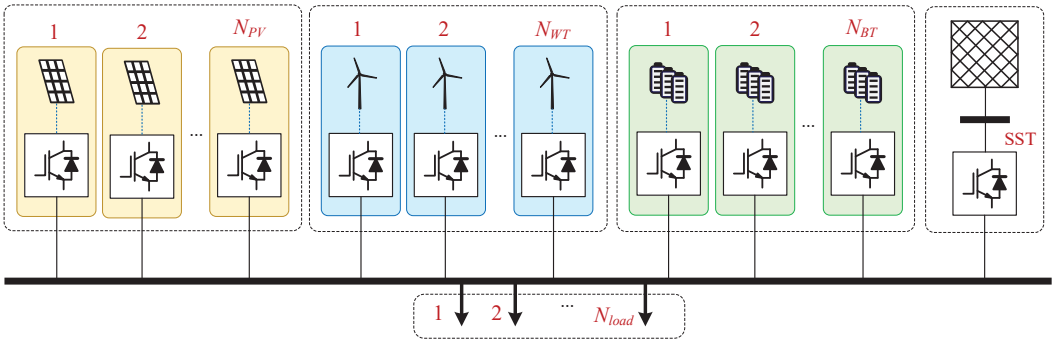

Fig. 4.1. Representation of a power electronic-based power system (generation-demand model, SST: Solid-State Transformer, N_{PV}, N_{WT}, and N_{BT}: number of photovoltaic, wind turbine, and battery units, respectively).

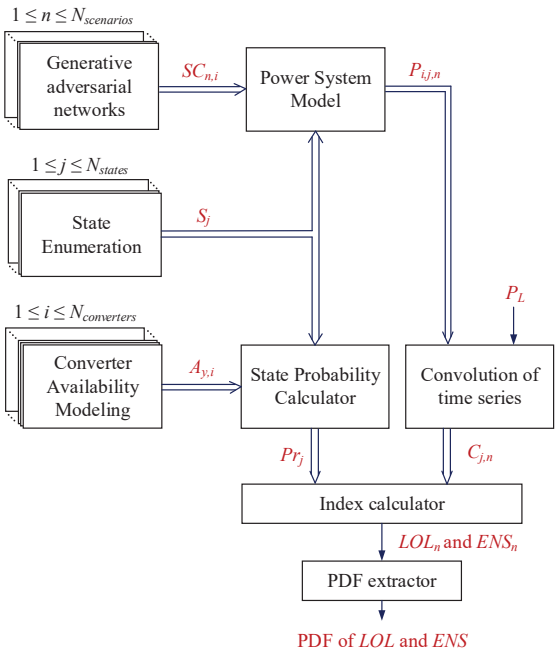

Fig. 4.2. Block diagram of the proposed framework for system-level reliability assessment of power electronic-based power systems ($SC_{n,i}$: n^{th} scenario (yearly profile of wind speed or solar irradiance) for the i^{th} converter, S_j: bit array for system state j, $A_{y,i}$: availability of the i^{th} converter at age y, $P_{i,j,n}$: the output power of the i^{th} converter at state j for scenario n, P_L: aggregated load profile, Pr_j: probability of the occurrence of the system state j, $C_{j,n}$: consequence of state j in scenario n, PDF: Probability Density Function).

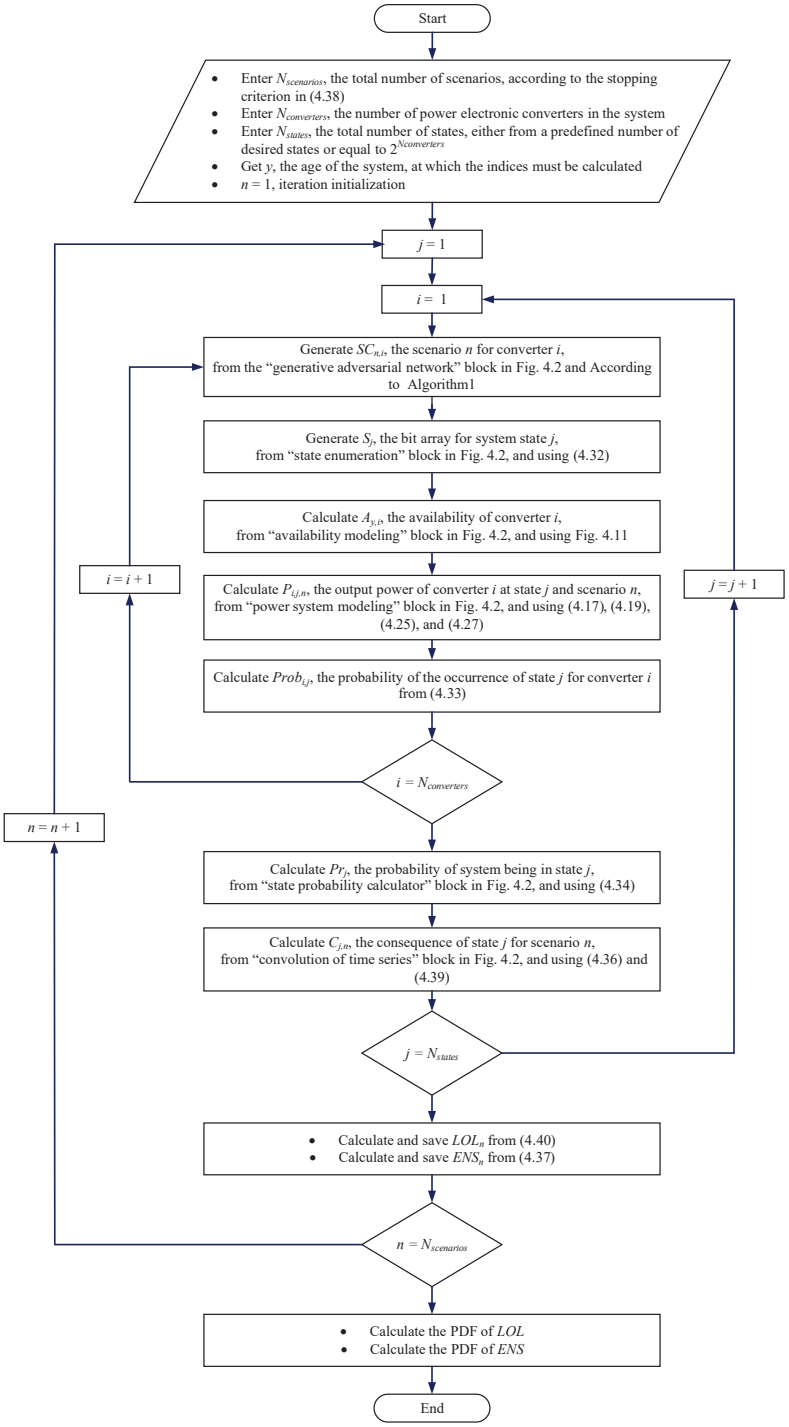

Fig. 4.3. Flowchart of the proposed framework for system-level reliability assessment of the Power Electronic-based Power Systems (PEPSs).

To calculate reliability indices, the probability and consequence of each failure event must be known. In this regard, the probability of system states is calculated in the "converter availability modeling" block and the "state probability calculator" block. Also, the consequence of the failure event is evaluated by using the "GANs" block (i.e., scenario generation block) and the "power system model" block. Then, in the "index calculation" block, the probability and consequences for all states generated by "state enumeration" block are combined to acquire the *LOL* (Loss Of Load) and *ENS* (Energy Not Supplied).

The flowchart of the developed framework can be seen in Fig. 4.3. First, a scenario, $SC_{1,i}$, is generated for converter i, by using the GAN, which include a yearly profile of solar irradiance or wind speed. Next, the "state enumeration" block generates the first state to be evaluated, S_1. According to S_1 and based on the availability results at the desired age of y from the "converter availability modeling" block, the state probability is calculated in "state probability calculator" block. Then, S_1 and generated scenarios are input to the "power system model" block. Accordingly, this block calculates the available generation capacity from the PV and WT units, and available power and the SOC of battery storage units, for the given scenario at S_1. Next, the "state enumeration" block will generate the next desirable state, S_2, where the probability and consequences of this state will be evaluated in a similar manner. This process will be repeated for all possible (or desirable) system states, N_{states} (generated by "state enumeration" block), where the probability and severity of all states will be evaluated. With respect to the probability and severity of all states, the *ENS* and *LOL* will be calculated for the first scenario for all converters, $SC_{1,i}$, $1 \leq i \leq N_{converters}$, in the "index calculation" block. Then, a new scenario will be generated by the GAN, $SC_{2,i}$, $1 \leq i \leq N_{converters}$, where a value of *ENS* and *LOL* will be calculated for it by repeating the same process explained for $SC_{1,i}$. Totally, $N_{scenarios}$ scenarios will be generated, where a value of *LOL* and *ENS* will be calculated for each according to Fig. 4.3. $N_{scenarios}$ can be determined by defining a stopping criterion, which will be explained later. Based on the frequency of the occurrence of the obtained *LOL*s and *ENS*s, a Probability Density Function (PDF) can be extracted for each, which shows the probability distribution of the reliability index at age y. This PDF can further be fitted with a Normal distribution, where it can be represented by two parameters, $N(\mu , \sigma)$. For different ages of y, $N(\mu , \sigma)$ will change accordingly, which can be calculated by using the above framework. As a result, by using the above model-based framework, the effect of power electronic failures, component aging, generation uncertainty, and penetration of renewables on the system-level reliability can be studied quantitatively.

4.3. Availability Modeling

As Fig. 4.4 shows, outages in a PEPS can happen due to wear-out failures and chance failures. It is assumed that the early failures and infant mortality are negligible compared to wear-out and chance failures. Wear-out failures happen because of accumulated damage inside the Power Electronic (PE) component over time [39]. For

example, failure of Insulated-Gate Bipolar Transistors (IGBTs) due to bond-wire lift off can be categorized as wear-out failures. The process of modeling these types of failures for power electronic converters considering the physics of failure and was explained previously in chapter 3. Typically, wear-out failures are reported in the form of Weibull distributions, where the reliability can be found according to

$$R(t) = \mathrm{e}^{-(\frac{t}{\eta})^{\beta}} \tag{4.1}$$

where β and η are shape and scale parameters from the Stress-Strength Analysis (SSA) explained in Chapter 3.

On the other hand, chance failures have their root-causes outside the PE components, such as external overstresses. For example, the catastrophic failure of a power converter due to overvoltage, overcurrent, human error, or lightning can be categorized due to chance failures. Since many factors influence these types of failures, it is impossible to develop comprehensive physical models that can consider all of them. Alternatively, chance failures are modeled statistically with a constant failure rate of λ, which is extracted from filed failure data. In the PS literature, exponential distribution is used to describe chance failures, whose reliability can be written as:

$$R(t) = \mathrm{e}^{-\lambda t} \tag{4.2}$$

where λ is the constant failure rate due to chance failures.

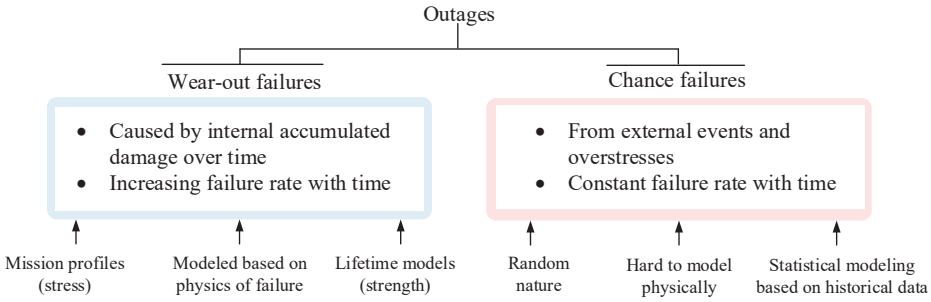

Fig. 4.4. Classification of root-causes of outages in a power electronic-based power system.

The failure rate of Weibull distribution is increasing over time, while the failure rate of chance failures is constant over time. Therefore, the overall failure rate of a power converter will be as shown in Fig. 4.5, and it can be written as:

$$\lambda_A(t) = \lambda + \frac{\beta}{\eta}(\frac{t}{\eta})^{\beta-1} \tag{4.3}$$

where $\lambda_A(t)$ is the actual failure rate of the power converter, λ is the constant failure rate due to chance failures, and β and η are shape and scale parameter from the SSA.

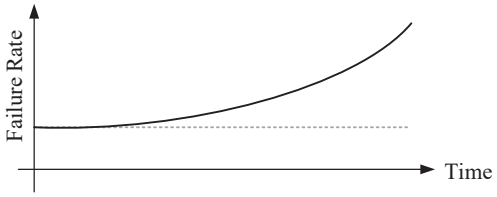

Fig. 4.5. Actual failure rate of the converters in a power electronic-based power system, considering that wear-out and chance failures are dominant.

On the other hand, unlike in the PE literature, all power converters must be modeled as repairable units in a PEPS (since a PS is a continuously-operated system). The state-space diagram of a repairable and a non-repairable system is shown and compared with each other in Fig. 4.6.

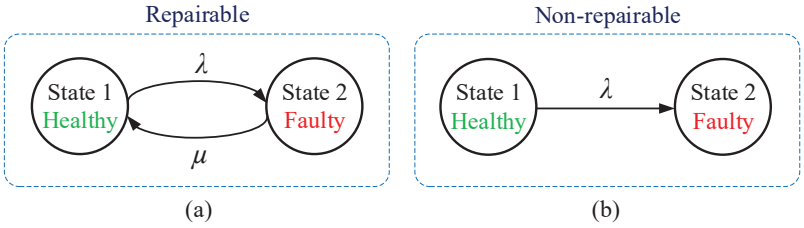

Fig. 4.6. State-space diagram of (a) a repairable unit compared to (b) a non-repairable system, where λ is the failure rate and μ is the repair rate of the unit.

As Fig. 4.6 shows, in a repairable system, when the system goes to the down state with a rate of λ, it can also return to the up state with the rate of μ. For such systems, the concept of availability (which is similar but not identical to reliability) is defined, which characterizes the probability of finding the system in the up state. In conventional power systems, the availability of a unit can be found by using the Markov method, according to the state-space diagram shown in Fig. 4.6 (a). Often, in the PS reliability studies, the dynamics of the availability is ignored and the steady-state value of the availability is used, which can be written as:

$$A = \frac{\mu}{\mu + \lambda} \tag{4.4}$$

where A is the constant (steady-state) availability of the unit, and μ as well as λ are the unit's repair rate and failure rate, respectively.

However, this method and other alternative availability calculation methods in PS are valid only for constant failure rates. In other words, if they are used with a non-constant failure rate, as it is the case in PEPS, they will lead to wrong results. To solve this problem, other methods such as, Monte Carlo Simulation (MCS) [75], Semi-Markov Approach (SMA) [79], Method of Device of Stages (MDS) [57], and

PieceWise Approach (PWA) [80] can be used. However, these methods have certain limitations, which makes them unsuitable for availability modeling in PEPS. For example, PWA and MDS have some approximations and simplifications of the real problems, which can sometimes result in noticeable errors. Similarly, SMA and MCS suffer from a significant computational burden [25], [75]. These methods and their performance have been discussed in [J1], where more details in terms of accuracy and computational burden are presented.

Therefore, in this PhD project, a new method is proposed to calculate an Equivalent Failure Rate (EFR). This EFR can then be used with conventional PS methods such as Markov to calculate the transient and steady-state availability, as illustrated in Fig. 4.7.

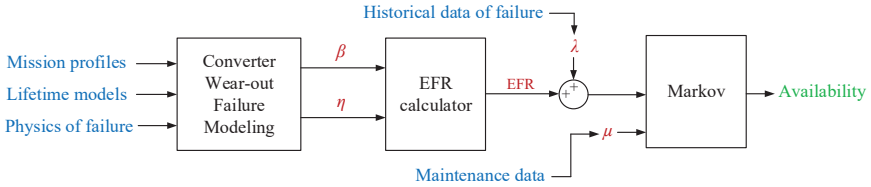

Fig. 4.7. Block diagram of the proposed availability modeling method for power converters (EFR: Equivalent Failure Rate, β: shape parameter of the Weibull distribution from the stress-strength wear-out modeling, η: scale parameter of the Weibull distribution from the stress-strength wear-out modeling, λ: chance failure rate, μ: repair rate).

Concept of Equivalent Failure Rate (EFR):
The time-dependent term of the failure rate is shown in Fig. 4.8, given that no failures happen before t.

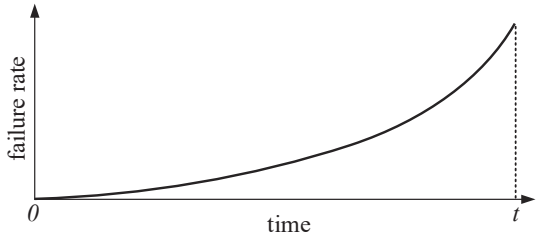

Fig. 4.8. Wear-out failure rate, provided that no failure has happened before t.

where it can be written according to the time-dependent term of (4.3). If, before t, only one failure had happened at the random time of τ ($\tau < t$), and the converter is restored to the initial conditions immediately after that, the failure rate will be as shown in Fig. 4.9.

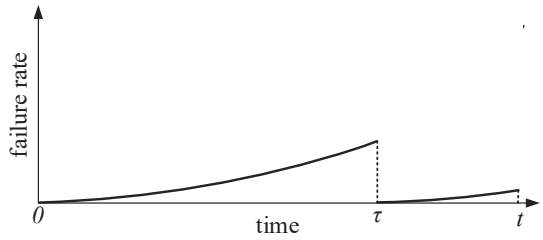

Fig. 4.9. Wear-out failure rate, provided that only one failure has happened before t, and the converter has been repaired.

As $0 \le \tau < t$, the EFR at t can be written as [C3]:

$$\lambda_{eq}(t) = f_W(t) + (f_W * f_W)(t) \tag{4.5}$$

$$(f_W * f_W)(t) = \int_0^t f_W(\tau) f_W(t-\tau) d\tau \tag{4.6}$$

$$f_W(t) = \frac{\beta}{t}\left(\frac{t}{\eta}\right)^{\beta} \mathrm{e}^{-\left(\frac{t}{\eta}\right)^{\beta}} \tag{4.7}$$

where β and η are shape and scale parameter of Weibull distribution.
In theory, an infinite number of failures and repairs could have happened before t at different instants of time as shown in Fig. 4.10.

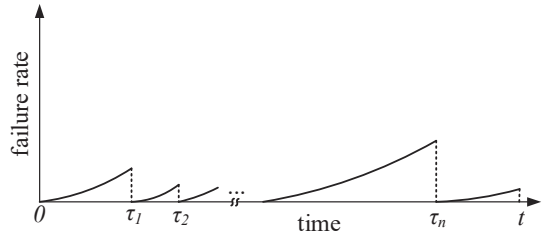

Fig. 4.10. Wear-out failure rate, provided that n failures have happened before t (and the converter has been repaired every time), where n can be infinite in theory.

Therefore, the EFR, $\lambda_{eq}(t)$ in this case can be written as:

$$\lambda_{eq}(t) = f_W(t) + f_W(t) * f_W(t) + f_W(t) * f_W(t) * f_W(t) + \ldots \tag{4.8}$$

$$\lambda_{eq}(t) = \sum_{n=1}^{\infty} f_W(t)^{*n} \tag{4.9}$$

where (*) denotes the convolution operator as (4.6) and $f_W(t)$ is the PDF of the Weibull distribution as (4.7). Since (4.9) does not have a closed-form solution, a different approach will be used to find the EFR usable for availability calculation, which is explained in detail in [J1].

The actual failure rate of a PE system was shown in Fig. 4.5 and (4.3). Accordingly, the PDF of the time-to-failure can be calculated as:

$$f(t) = \lambda(t).\exp(-\int_0^t \lambda(\tau)d\tau) \tag{4.10}$$

where $\lambda(.)$ can be calculated from (4.3).

From [J1], the EFR can be calculated from:

$$\Lambda(t) = 1 + \int_0^t \Lambda(\tau) f(t-\tau) d\tau \tag{4.11}$$

$$\lambda_{eq}(t) = \frac{d\Lambda(t)}{dt} \tag{4.12}$$

where $f(.)$ can be obtained from eq (4.10).

Then, this EFR can be used in Markov method, according to the Fig. 4.7, and the time-dependent availability $A(t)$ can be written as:

$$\frac{dA(t)}{dt} = \mu - (\mu + \lambda_{eq}(t))A(t) \tag{4.13}$$

where μ is the repair rate and $\lambda_{eq}(t)$ is the EFR. μ, the repair rate which is typically extracted from service and maintenance reports and is a function of accessibility, maintenance crews experience, and available spare units. To find A, availability, these equations (4.11)-(4.13) can be solved numerically according to Fig. 4.11.

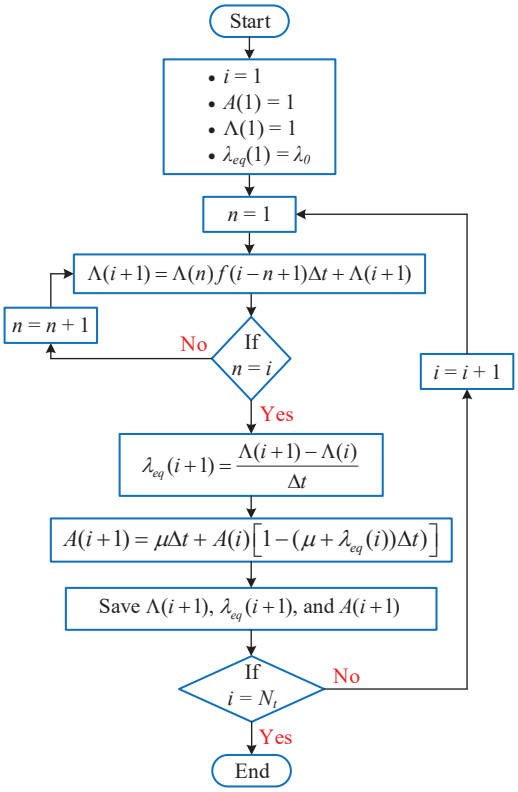

Fig. 4.11. Flowchart of the proposed availability modeling method for power electronic converters [J1].

In Fig. 4.11, T_s is the study time horizon, Δt is the time step, N_t is the number of steps such that $\Delta t = T_s / N_t$. Also, $t(i) = i\Delta t$, where $i \in \mathbb{Z}^+$ and $1 \leq i < N_t$. The assumption is further that the converter starts at the healthy state, and hence $A(1) = 1$.

4.4. Power System Modeling

A substantial part of reliability assessment is to calculate the consequence of failure events. To do so, the available generation and storage power in the system must be known at any given time, with respect to the healthy or faulty status of the units. As shown in Fig. 4.1, the generation capacity in PEPS is determined by PV and WT units, which are dependent on the solar irradiance and wind speed. The output power of these units must be modeled with regards to the failures and the respective mission profiles. Also, the available power and the SOC of the BT units must be modeled, which is determined by the load-generation balance in the system. It is worth mentioning that, in Fig. 4.1, to make the system fully power electronic-based, an SST

(Solid-State Transformer) is used, which is responsible for exporting and importing power from neighboring grid in case of excess and shortage of the power. Since the focus of this project is on the reliability assessment in hierarchical level I, the line limits are ignored, and a DC power flow has been considered. Therefore, the main objective of the Power System Modeling (PSM) block is to provide the power flow in the system by translating the mission profiles into the available power by the generation, storage, and transmission facilities, given their faulty or healthy status. Therefore, without losing generality, the modeling of PV, WT, BT, and SST, as common building blocks of modern PEPSs will be discussed here. It should be noted that the above modeling must be done such that it minimizes the computation time, while presenting sufficient accuracy. The overall schematic of the PSM block is shown in Fig. 4.12.

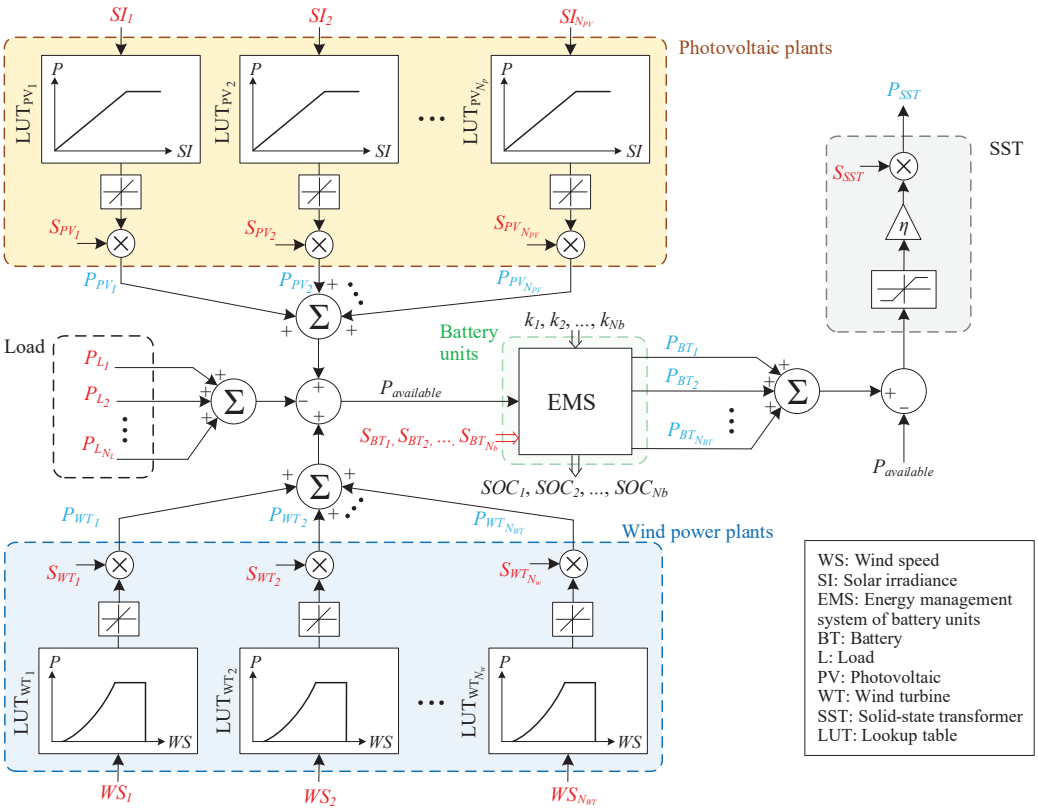

Fig. 4.12. Overall representation of the power system modeling block in Fig. 4.2.

Photovoltaic units (PV):
PV units are one of the main sources of power generation in modern PEPS. Therefore, the appropriate modeling of these units is crucial to translate the Solar Irradiance (SI) to output power, given the converter health status.
Typically, a PV unit model is comprised of PV panels, PE interface, filter, and the grid. Many topologies and structures might be used in different parts of a PE unit. However, it is essential to achieve a general solution for modeling the PV units to satisfy the above-mentioned goal of the PSM efficiently. There are various methods, e.g., single-diode equivalent circuit, to interpret the relationship between the production of a panel a solar irradiance [81]. Also, often, it is assumed that the PV unit operates at the maximum power point. Given this assumption, it can be approximated that the output power of the PV panels changes linearly with SI. Moreover, For a PV system, R_s, the sizing ratio can be defined as the ratio of the PV panels rated power at the standard test condition, $P_{PV,rated}$, to the PE interface rated power $P_{PE,rated}$ according to [82]

$$R_s = \frac{P_{PV,\,rated}}{P_{PE,\,rated}}. \tag{4.14}$$

Typically, since the cost of PV panels per unit of power is lower than that of the PE interface, and therefore $R_s \geq 1$, that is, the rate power of panels is larger than that of the PE interface. In this situation, the rated power of the PV unit is limited by the rate power of the PE interface. Considering the linear relationship of the output power with SI and the limit from the PE interface, the PV unit production can be characterized as shown in Fig. 4.13. In Fig. 4.13, at the beginning, as the SI increases, the production increases approximately linearly. The increase continues until the rated power limit of the unit, P_r, is reached, where typically $P_r = P_{PE,rated}$.

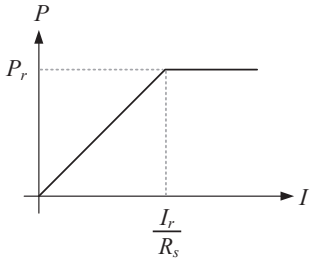

Fig. 4.13. Output power (P) of the photovoltaic units as a function of solar irradiance (I), where P_r is the rated power of the unit, I_r is solar irradiance at standard test condition in the panel datasheet, and R_s is the sizing ratio of panels to the power converter.

The above characteristics can be presented with the following formula

$$P(I) = \begin{cases} G.I \ , \ I \le \dfrac{P_r}{G} \\ P_r \ , \ I > \dfrac{P_r}{G} \end{cases} \tag{4.15}$$

where P is the output power of the unit, and I is the solar irradiance, and P_r is the rated power of the unit. Also, G can be obtained from the PV panel and PE interface datasheet or more accurately from the simulation or experimental modeling. Otherwise, it can be calculated form the following equation

$$G = R_S \frac{P_r}{I_r} \tag{4.16}$$

where I_r is the solar irradiance at the standard test condition (typically 1000 [W/m^2]), and the R_s is known from (4.14).

Subsequently, at the j^{th} state, the output power of the i^{th} converter unit (if it is a PV unit) can be obtained from

$$P_{i,j,n} = S_j(i) \times P(I_{n,i}) \tag{4.17}$$

where $S_j(i)$ is the i^{th} bit of the system state bit array, S_j (which comes from the state enumeration block in Fig 4.2), $I_{n,i}$ is the solar irradiance (based on the n^{th} scenario for the i^{th} converter from the GAN block in Fig. 4.2, i.e., $SC_{n,i}$) and $P(.)$ can be calculated from (4.15) and (4.16).

Wind turbine units (WT):

In a modern PEPS, a large proportion of generated power can come from the WT units. Therefore, to evaluate the system-level reliability accurately, it is vital to model the WT units properly. The PSM for WT aims to translate the Wind speed (WS) to the output power of the WT, given the health status of the converter.

Also, it should be noted that there are countless variations of WT in terms of generator, converter, and their structure as reviewed in [83]. Hence, the appropriate PSM must be comprehensive to be applicable to all of them, accurate enough, and computationally efficient. To do so, the turbine power curve, can be used, which shows the relationship between the WS and output power, as it was explained in Chapter 3. A general form of the turbine power curve can be seen in Fig. 4.14. If not available from the manufacturer, the turbine power curve can be approximated with [71]

$$P(V) = \begin{cases} 0 & V < V_c \text{ or } V > V_f \\ P_r . \dfrac{V^2 - V_c^2}{V_r^2 - V_c^2} & V_c \le V < V_r \\ P_r & V_r \le V < V_f \end{cases} \tag{4.18}$$

where P is the WT output power, V is the wind speed, and V_c, V_r, V_f, and P_r are cut-in, rated, cut-out speeds of the turbine.

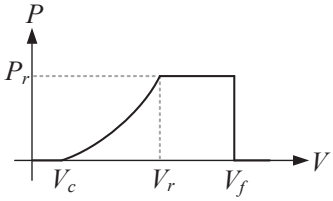

Fig. 4.14. Output power (P) of the wind turbine units as a function of wind speed (V), where P_r is the rated power of the unit, and V_c, V_r, and V_f are cut-in, rated, and cut-out speeds of the turbine.

Subsequently, at the j^{th} state (from state enumeration) the output power of the i^{th} unit can be obtained from

$$P_{i,j,n} = S_j(i) \times P(V_{n,i}) \tag{4.19}$$

where $S_j(i)$ is the i^{th} bit of the system state bit array, S_j (which comes from the state enumeration block in Fig 4.2), $V_{n,i}$ is the wind speed (based on the n^{th} scenario for the i^{th} converter from the GAN block in Fig. 4.2, i.e., $SC_{n,i}$) and $P(.)$ can be calculated from (4.18).

Battery energy storage units (BT):

Due to the intermittent nature of renewable energies, energy storage units have a pivotal role in modern PEPS. Among various types of energy storage units, BTs are widely used and have a promising future. The objective of the PSM for the BT is to obtain the output power and the SOC of the battery units and their converters given the available input power and the converter state of health considering the battery and converter limits.

The overall process for modeling the BT in the PSM (i.e., to calculate the output power and SOC of battery units given their healthy and faulty condition) is illustrated in Fig. 4.15. The power sharing among several battery units can be considered according to Fig. 4.15 (b), where k_i are the droop gains for power sharing among BTs and $\sum k_i = 1$. By doing so, in normal condition, when the converters of all battery units are healthy, the power is shared according to the k_i coefficients. However, in case of failures, which is the focus of this paper, the battery units with a healthy converter can take over the amount of power which was not consumed or provided by the failed ones. Also, the Battery Unit Model (BUM) block in Fig. 4.15 (b) is the model for one battery unit, which is shown in Fig. 4.15 (a).

BUM: Battery Unit Model

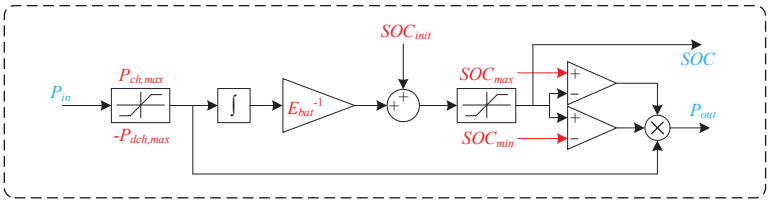

(a)

EMS: Energy Management System

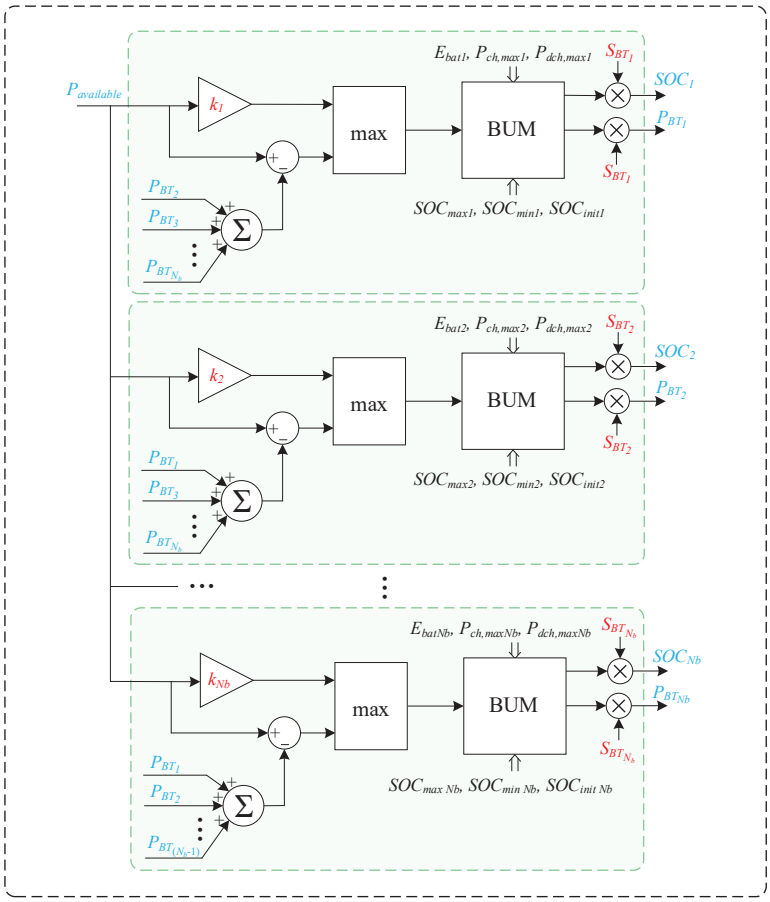

(b)

Fig. 4.15. (a) Overall block diagram for modeling the output power and State Of Charge (SOC) of a battery unit, (b) Schematic of the energy management system to model the power sharing among batteries.

Now, the mathematical equations behind the above models will be discussed. The available power to the storage units at state j for scenario n is given from:

$$P_{available,j,n} = \sum_{i=1}^{N_{PV}} P_{i,j,n,PV} + \sum_{i=1}^{N_{WT}} P_{i,j,n,WT} - \sum_{i=1}^{N_{Load}} P_{i,load} \tag{4.20}$$

where N_{PV}, N_{WT}, and N_{Load} are the number of PV and WT units and load points, respectively. $P_{i,Load}$ is the demanded power at the i^{th} load point from the load mission profiles. Also, $P_{i,j,n,PV}$ and $P_{i,j,n,WT}$ are the output power of the PV and WT converter units, which can be obtained from (4.17) and (4.19), respectively.

$$P_{in,i,j,n} = \max(|\, P_{available,j,n} - \sum_{\substack{c=1 \\ c\neq i}}^{N_{BT}} P_{in,c} \,|, |\, P_{in,d} \frac{k_i}{k_d} \,|) \quad , \quad 1 \le i \le N_{BT} \quad , \quad d \neq i,\ 1 \le d \le N_{BT} \tag{4.21}$$

$$\sum_{i=1}^{N_{BT}} k_i = 1 \tag{4.22}$$

where k_i is the power sharing droop gain for BT unit i, N_{BT} is the number of BT units, and $P_{available,j,n}$ can be calculated from (4.20).

Various battery technologies have different maximum values for charging and discharging current. At the system level, this can be taken into account by the following equations

$$P_{bat,i,j,n} = \begin{cases} -P_{dch,\max} & P_{in} < -P_{dch,\max} \\ P_{in,i,j,n} & -P_{dch,\max} \le P_{in,i,j,n} \le P_{ch,\max} \\ P_{ch,\max} & P_{in} > P_{ch,\max} \end{cases} \tag{4.23}$$

where $P_{in,i,j,n}$ is given from (4.21) and (4.22), $P_{ch,max}$ is the maximum charging power of the battery, and $P_{dch,max}$ is the maximum discharging power of the battery.

From the Coulomb counting, the battery SOC can be calculated by

$$SOC_{i,j,n}(t+dt) = SOC_{i,j,n}(t) + \frac{P_{i,j,n}(t)}{E_{bat}} dt \tag{4.24}$$

where E_{bat} is the battery capacity, $SOC(t)$ is the battery unit's state of charge at instant t, and dt is the time step of the mission profile. Furthermore, $P_{i,j,n}$ is the effective output power of the BT unit, which can be obtained from

$$P_{i,j,n} = S_j(i) \times \mathrm{sgn}(P_{available,j,n}) \times \begin{cases} P_{bat,i,j,n} & SOC_{\min} < SOC(t) < SOC_{\max} \\ \dfrac{P_{bat,i,j,n} - |P_{bat,i,j,n}|}{2} & SOC(t) \ge SOC_{\max} \\ \dfrac{P_{bat,i,j,n} + |P_{bat,i,j,n}|}{2} & SOC(t) \le SOC_{\min} \end{cases} \tag{4.25}$$

Where SOC_{max} and SOC_{min} are the maximum and minimum allowed SOC for the BT unit, respectively. Such limits are use for the battery units to extend their lifetime by decreasing the depth of discharge (DOD). Also, $P_{available,,j,n}$ and $P_{bat,i,j,n}$ were explained before and can be calculated from (4.20) and (4.23), respectively. $S_j(i)$ is the i^{th} bit of the system state bit array, S_j (which comes from the state enumeration block in Fig 4.2). $SOC(t)$ is the current state-of-charge of the BT unit, which can be calculated from (4.24) and sgn(.) is the sign function.

Solid-state transformer (SST):

The generation and storage units at the LV (Low Voltage) are connected to the upper MV (Medium Voltage) network through a transformer. In a full power electronic-based grid, an SST can be used to link the LV and MV networks. In this case, to determine the reliability, the exchanged power through the SST must be known. It should be noted that the power through the SST is bidirectional. In other words, not only can the existing LV network receive power from the MV network, but it can also send the excess amount of power to it.

In this case, the exchanged power through SST at instant t can be obtained from

$$P_{sst,j,n}(t) = \sum_{i=1}^{N_{Load}} P_{load,i}(t) - \sum_{i=1}^{N_{PV}} P_{PV,i,j,n}(t) - \sum_{i=1}^{N_{WT}} P_{WT,i,j,n}(t) + \sum_{i=1}^{N_{BT}} P_{BT,i,j,n}(t) \qquad (4.26)$$

$$P_{i,j,n} = \min(\left|P_{i,j,n}\right|, P_{r,SST}).\mathrm{sgn}(P_{i,j,n}) \qquad (4.27)$$

where $P_{load,i}(t)$ is the load demand at instant t at the i^{th} load point from the mission profiles. $P_{PV,i,j,n}(t)$, $P_{WT,i,j,n}(t)$, and $P_{BT,i,j,n}(t)$ are, respectively, the output power of the i^{th} PV, WT, and BT unit at instant t for scenario n at state j, which can be calculated from (4.17), (4.19), and (4.25). Also, N_{PV}, N_{WT}, N_{BT}, and N_{Load} are the number of PV, WT, and BT units as well as load points, respectively.

4.5. Scenario Generation

As explained before, the basic principle of reliability assessment in power system is to check whether enough generation capacity exist to meet the load demand or not. One factor that could influence the generation capacity in PEPSs is the failure of units, which was discussed before. In conventional generation units, this was the main factor determining the generation capacity as the units could follow any generation set points as long as it was within their operational limits. On the other hand, in the PEPS, another factor that determines the generation capacity is the intermittent nature of renewable resources. For example, in a PEPS without storage units, when no wind and sunlight are available, the customer will experience outages, even though no power electronic failure has happened. Thus, it is vital to model generation capacity in the PEPS.

Since the renewable resources have a stochastic nature, one approach to model them is to use probabilistic methods such as Markov method or Monte Carlo simulation. However, by using probabilistic methods, the dynamic behavior of generation capacity is ignored. In contrast, the generation capacity of PV units follows strong diurnal and seasonal patterns. Hence, the generating capacity of PV units

cannot be modeled by using purely probabilistic approaches as those patterns are important but will be neglected. Moreover, BT units work based on the energy, which is a product of time and power. As a result, in modeling BT units not only the power flow itself, but also the dynamics of the power flow must be considered. In other words, the chronology of the power balance between load and generation determines the BT unit's output power and SOC. Therefore, the BT unit cannot be modeled with purely probabilistic approaches. Also, the coincidence factor between load and generation will be ignored by using purely probabilistic approaches and ignoring the dynamics of the generation capacity. In other words, the load and generation might have the same probabilistic model, while the timing of load and generation determines whether the unreliability happens or not.

To address the above challenges, time series methods can be used to model the generation capacity. In addition to the time-dependent nature, the renewable resources also have a stochastic nature. Therefore, the generation capacity varies from year to year. So, an uncertainty is associated with the generation capacity, which must be modeled by considering many years of mission profiles. Typically, there are few years of mission profiles available, which cannot represent enough diversity to model the generation uncertainty. In this case, realistic scenarios can be generated based on these few mission profiles to regenerate enough diversity to model the uncertainty of generation capacity. To do the scenario generation, the GANs are used in this project, since it is model-free, and due to its superior performance over the popular Autoregressive Moving Average (ARMA) [84]. It should be noted that ARMA is prone to overfitting and misidentification of temporal patterns [78]. Also, it requires a large number of historical data to achieve an acceptable diversity in generated scenarios by ARMA, which is not available in all cases. As it was shown in chapter 2, The generated mission profile scenarios by GAN had the same statistical and temporal properties of the real profiles. In other words, the GAN is used to generate scenarios because it models not only the stochastic nature of the generation capacity but also its dynamic behavior.

By using the GAN, mission profile scenarios can be generated for both load and generation. Nevertheless, in this thesis, it has been used only to model the generation capacity. Since, in the PEPS, the main mission profiles are solar irradiance and wind speed, the GAN is used to generated yearly profiles of these parameters. As Fig. 4.16 shows, real mission profiles are used to train the GAN first, which will take some time. Once the training is done, the trained GAN can be used to generate new mission profiles fast. The process of generating new mission profiles can be continued as long as a certain stopping criterion is not met (which will be discussed later). By doing so, the generated mission profiles will cover most of the possible scenarios that will happen in the future, and thereby emulating the generation capacity and its uncertainty. For each scenario, the performance of the system can be evaluated in terms of reliability indices according to the Fig. 4.2 and Fig. 4.3.

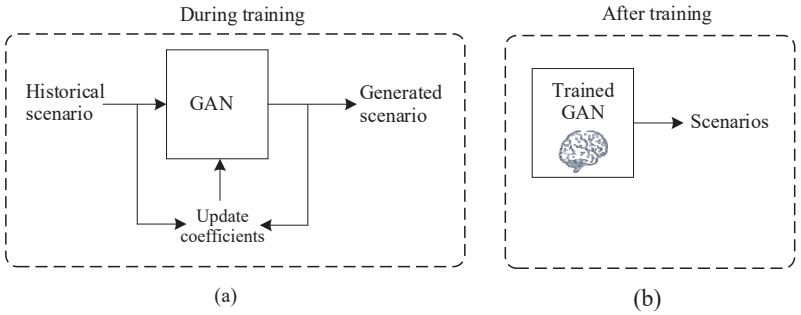

Fig. 4.16. Simplified illustration of how the GAN (Generative Adversarial Networks) is used for scenario generation in the proposed framework.

The architecture of the GAN was presented in Fig. 3.24 in Chapter 3. Further, in Chapter 3, the generated profiles were shown, where they were also compared with real profiles in terms of the Cumulative Density Function (CDF), Power Spectral Density (PSD), and monthly average values. It was shown that the generated scenarios have the same visual, temporal, and probabilistic characteristics of the historical profiles and capture their intrinsic properties. Now, the usage of GAN for scenario generation for the PEPS will be explained here in details.

GAN is a data-driven approach and does not require a physical model to generate scenarios. As it was shown in Fig 3.24 in Chapter 3, the GAN incorporates two Deep Neural Networks (DNNs) in its structure – the generator and the discriminator. The generator is in charge of reproducing the complex and nonlinear relationships existing in the historical data. The discriminator, on the other hand, tries to classify the historical and generated data. The operation of the GAN is based on a game between the generator and the discriminator, where the former aims to generate realistic scenarios which cannot be distinguished from historical scenarios by the discriminator. Accordingly, at every training epoch, the coefficients of two DNNs are updated. Notably, it will be a minmax two-player game, where, according to the game theory, at its Nash equilibrium point, the generator is the winner of the game [78]. In other words, at that point, the generator can reproduce the distribution of the real data and capture all its temporal and probabilistic properties, such that the discriminator cannot differentiate between the generated and real data. At each training epoch, according to the output of the discriminator, the loss functions are defined and used to update the coefficients of both the generator and the discriminator.

Now, the problem and the objectives of using GAN for scenario generation will be formulated, the loss functions are defined, and the training procedure will be explained. Assume that the real data is a time series indexed as $t = 1, 2, \ldots, T$ – i.e., x^t such that $t \in T$ denotes each point in the time series. In addition, it is assumed that the real data are distributed according to the P_X distribution, which is unknown and to be reconstructed. Moreover, z represents the input noise vector following a Gaussian distribution P_Z such that $Z \sim P_Z$. The objective of the scenario generation part is to

train the GAN such that any random sample z from P_Z to follow P_X at the output of the generator. Consider that $G(\,.\,;\theta^{(G)})$ represents the generator function, G, with the coefficients of $\theta^{(G)}$, and similarly, Similarly, $D(\,.\,;\theta^{(D)})$ represents the discriminator function, D, with the coefficients of $\theta^{(D)}$. The output of the generator, that is $G(\,z\,;\theta^{(G)})$ can be considered as a new random variable with the P_G distribution, provided that Z is a random variable with P_Z distribution. The output of the discriminator, p_{real}, can be written as

$$p_{real} = D(x;\theta^{(D)}) \tag{4.28}$$

where x can be sampled from P_{data} or P_Z. Notably, p_{real} indicates how much the inputs of the discriminator (historical and generated samples) follow the P_X distribution.

In the GAN, two DNNs should be trained at the same time. To do so, the loss functions for the Generator and the Discriminator, L_G and L_D, should be formulated. In addition, a game value function $V(G, D)$ should be defined. The loss function for the generator can be formulated as [77]

$$L_G = -\mathrm{E}_Z[D(G(Z))] \tag{4.29}$$

where Z is the random noise input, $G(.)$ is the generator function, $D(.)$ is the discriminator function, and E[.] is the operator of expected value. Moreover, in order for the discriminator to distinguish Px from P_G, E[$D(X)$]-E[$D(G(Z))$] must be maximized. Therefore, the loss function for the discriminator can be formulated as [77]

$$L_D = -\mathrm{E}_X[D(X)] + \mathrm{E}_Z[D(G(Z))] \tag{4.30}$$

where X is the historical data, Z is the random noise input, $G(.)$ is the generator function, $D(.)$ is the discriminator function, and E[.] is the operator of expected value. Then, a minmax two-player game can be set between the generator and the discriminator by combining the aforementioned loss functions and forming a game value function $V(G, D)$ according to [78]

$$\min_{\theta^{(G)}} \max_{\theta^{(D)}} V(G,D) = \mathrm{E}_X[D(X)] - \mathrm{E}_Z[D(G(Z))]\cdot \tag{4.31}$$

When starting the training process, since the generated samples poorly follow the P_X, L_D has a small value, while the values for L_G and $V(G, D)$ are large. As the training process goes on, L_D increases and L_G decreases until the optimal solution for the coefficients of two DNNs are found, when the generated data will not be differentiated form historical data. It should be noted that typical training methods can be used to train both generator and the discriminator DNNs. The algorithm to train the DNNs and update their coefficients based on the gradient descent method with the *RMSProp*, which is presented in Algorithm 4.1 as follows [77], [78], [85].

Algorithm 4.1. Gradient descent training of the GAN for scenario generation [77], [78], [85]

Input: batch size m, number of discriminator iterations for each generator iteration n_{discri}, learning rate α, clipping parameter, c, $\theta^{(G)}$ initial coefficients of generator, $\theta^{(D)}$ initial coefficients of discriminator.

While $\theta^{(D)}$ has not converged do

For $t = 0, \ldots, n_{discri}$ **do**

Sample a batch from historical data:

$$\left\{x^{(i)}\right\}_{i=1}^{m} \; from \; P_X$$

Sample a batch from the input noise:

$$\left\{z^{(i)}\right\}_{i=1}^{m} \; from \; P_Z$$

Update the discriminator coefficients using the gradient descent method:

$$g_{\theta^{(D)}} \leftarrow \nabla_{\theta^{(D)}} \frac{1}{m}\left[\sum_{i=1}^{m} D(G(z^{(i)})) - \sum_{i=1}^{m} D(x^{(i)})\right]$$

$$\theta^{(D)} \leftarrow \theta^{(D)} - \alpha.RMSProp(\theta^{(D)}, g_{\theta^{(D)}})$$

$$\theta^{(D)} \leftarrow clip(w, -c, c)$$

End for

Update the generator coefficients using the gradient descent method:

$$g_{\theta^{(G)}} \leftarrow \nabla_{\theta^{(G)}} \frac{1}{m}\sum_{i=1}^{m} D(G(z^{(i)}))$$

$$\theta^{(G)} \leftarrow \theta^{(G)} - \alpha.RMSProp(\theta^{(G)}, g_{\theta^{(G)}})$$

End while

4.6. State Enumeration and Index Calculation

In this part, the state enumeration and how to calculate the reliability indices based on the above information will be discussed.

State enumeration:

The system can be in various states depending on whether the converters are the faulty or healthy status. In this case, considering that the overall number of power converters in the system is $N_{converters} = N_{PV} + N_{WT} + N_{BT} + N_{SST}$, the number of possible states are

$N_{states} = 2^{Nconverters}$. To calculate reliability indices the probability and consequence of each state must be known. To accelerate the process, it is possible to define a subset of all states as the desired states to be considered for the study, e.g., the states that maximum two failures have occurred in the system simultaneously. To ensure that all the possible states or all the desired states are covered, a new state enumeration technique is proposed here based on binary coding. In other words, it is a systematic way to make sure no state is overlooked, which can also be implemented by computer programming. As shown in Fig. 4.17, in the proposed approach, at the state j, the system is represented by a bit array, S_j, where each of the bits represent the status of each converter. In other words, in a system with $N_{converters}$ converters, at the state j, S_j is a bit array with the length of $N_{converters}$, and each of the bits can be either 0 or 1. In other words, $S_j(i) = 1$, when the i^{th} converter is up, $S_j(i) = 0$, when the i^{th} converter is down, where $0 \le i \le (N_{converters} - 1)$. Therefore, the S_j can be given from

$$S_j = \mathrm{DBC}(j-1) \quad , \quad 1 \le j \le N_{states} \tag{4.32}$$

where DBC is the Decimal to Binary Converter, and $N_{states} = 2^{Nconverters}$ if no desired states is defined.

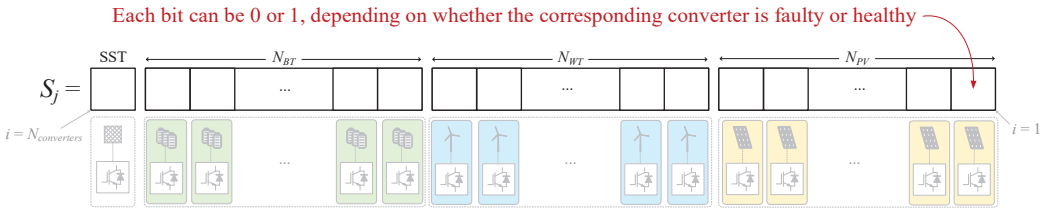

Fig. 4.17. Bit array representation of the system states, proposed for performing a systematic state enumeration.

Index calculation:

For each state j, the probability of the state Pr_j can be calculated from

$$Prob_j(i) = S_j(i).A_{y,i} + [1 - S_j(i)][1 - A_{y,i}] \tag{4.33}$$

$$Pr_j = \sum_{i=1}^{N_{converters}} Prob_j(i) \tag{4.34}$$

where $A_{y,i}$ is the availability of the i^{th} converter at age y, calculated from the "converter availability modeling" block in Fig. 4.2. $S_j(i)$ is the i^{th} bit of the system state bit array, S_j (which comes from the "state enumeration" block in Fig 4.2). Also, $N_{converters} = N_{PV} + N_{WT} + N_{BT} + N_{SST}$ is the number of power converters in the system.

Therefore, the probability of state j can be obtained from (4.33) and (4.34). The consequence of the state j for scenario n can be defined depending on the reliability index that is to be calculated. In this chapter, the consequence for the widely used indices of *LOLE* and *EENS* will be introduced. It is worth noting that other indices such as *EIR*, *EDNS*, *LOLP* can be calculated from *LOLE* and *EENS* [53]. Similarly, the consequence for other indices can be defined simply based on the same principles.

Notably, in the literatures *LOLE* and *EENS* are constant values. However, the outcomes of the proposed framework will be *LOL* and *ENS*, which are PDFs and not just constant values. It should be noted that the conventional indices can also be calculated based on the outcomes of the proposed framework, as the *LOLE* is the expected value of the PDF of *LOL*, and *EENS* is the expected value of the PDF of *ENS*.

EENS indicates the amount of load energy which is expected not to be supplied annually and is reported in terms of unit of energy per year. Therefore, to calculate the *ENS* and *EENS*, the amount of energy not served to the load must be defined and calculated as the consequence of each state j for each scenario n. To do so, the output power of converter must be known. In other words, once a scenario is generated by the GAN, i.e. $SC_{n,i}$ in Fig. 4.2, it must be input to the PSM – that is the scenario must be translated to the output power of converters based on (4.17), (4.19), (4.25), and (4.27). Accordingly, $C_{ENS,j,n}(t)$, the consequence of state j for scenario n at instant t, in terms of Energy Not Supplied (ENS), can be expressed as

$$DNS_{j,n}(t) = \sum_{i=1}^{N_{Load}} P_{load,i}(t) - \sum_{i=1}^{N_{PV}} P_{PV,i,j,n}(t) - \sum_{i=1}^{N_{WT}} P_{WT,i,j,n}(t) + \sum_{i=1}^{N_{BT}} P_{BT,i,j,n}(t) - P_{SST,j,n}(t) \tag{4.35}$$

$$C_{ENS,j,n}(t) = \frac{DNS_{j,n}(t) + \left| DNS_{j,n}(t) \right|}{2} \tag{4.36}$$

where $DNS_{j,n}(t)$ is the Demand Not Supplied at the state j for scenario n in instant t. $P_{load,i}(t)$ is the load demand at instant t at the i^{th} load point from the mission profiles. $P_{PV,i,j,n}(t)$, $P_{WT,i,j,n}(t)$, $P_{BT,i,j,n}(t)$, and $P_{SST,j,n}(t)$ are, respectively, the output power of the i^{th} PV, WT, BT, and SST unit at instant t for scenario n at state j, which can be calculated from (4.17), (4.19), (4.25) and (4.27). Also, N_{PV}, N_{WT}, N_{BT}, and N_{Load} are the number of PV, WT, and BT units as well as load points, respectively.

Since all the terms in the right side of (4.35) and (4.36) are time series, the consequence of state j, $C_{ENS,j}(t)$, will also be a time series. As a result, the ENS_n (the *ENS* for the n^{th} scenario) can be obtained by convolving the probability and consequence of each state as

$$ENS_n = \sum_{j=1}^{N_{states}} \int_{1-year} Pr_j . C_{ENS,j,n}(t).dt \tag{4.37}$$

where Pr_j is the probability at state j from (4.34) $C_{ENS,j,n}(t)$ is the consequence of state j for scenario n at instant t, in terms of energy not supplied from (4.36). N_{states} is the number of desirable states. As shown in Fig. 4.2 and Fig. 4.3, when the ENS_n for a given scenario n is obtained, the process must be repeated by generating new scenarios, and calculating their corresponding values for *ENS*. This process is repeated as long as the required number of scenarios $N_{scenarios}$ is not reached. Notably, $N_{scenarios}$ can be determined based on the following stopping criterion [86].

$$\sqrt{N_{scenario}} \geq \frac{\sigma}{\mu\theta} \Phi^{-1}(1-\frac{\delta}{2}) \tag{4.38}$$

where σ and μ are the standard deviation and mean of the obtained outputs, respectively. θ and δ are relative error and confidence interval that are required for the results, and Φ^{-1} is the inverse CDF of normal distribution. So, from (4.38), $N_{scenarios}$ can be calculated. When ENS_n was calculated for $1 \leq n \leq N_{scenarios}$, a PDF can be obtained for the ENS, which will be the final output of the proposed framework as the PDF of a reliability index.

LOLE is another well-known system-level reliability index, which is used to benchmark the system performance and check whether it meets the standards. It indicates the aggregated time that the load will experience the outage and is reported in terms of [h/yr] or [days/yr]. Considering the meaning of *LOLE* and *LOL*, the consequence of state j for scenario n at instant t (in terms of outage duration) can be formulated as

$$C_{LOL,j,n}(t) = \begin{cases} 1 & , C_{ENS,j,n}(t) > 0 \\ 0 & , C_{ENS,j,n}(t) \leq 0 \end{cases} \tag{4.39}$$

where $C_{ENS,j,n}(t)$, was explained in (4.36). As a result, the LOL_n, the LOL for the scenario n, can be obtained by convolving the probability and consequence of each state as

$$LOL_n = \sum_{j=1}^{N_{states}} \int_{1-year} Pr_j . C_{LOL,j,n}(t).dt \tag{4.40}$$

where Pr_j is the probability at state j from (4.34) $C_{LOL,j,n}(t)$ is the consequence of state j for scenario n at instant t, in terms of outage duration from (4.39). Also, N_{states} is the number of desirable states.

By performing the above steps, the value of LOL_n for scenario n can be obtained. Other indices can be calculated by adopting the same approach only by changing the definition of the consequence in (4.36) and (4.39). This process is repeated as long as the required number of scenarios $N_{scenarios}$ is not reached – that is as long as the stopping criteria, (4.38), is not met.

Therefore, once the stopping criteria is met, LOL_n and ENS_n will be available for $1 \leq n \leq N_{scenarios}$. Accordingly, a PDF can be extracted for *LOL* and *ENS*, demonstrating their distribution.

This is one of the main advantages of the proposed frameworks over the existing approaches. By using the proposed framework, one can obtain the probability distribution of *ENS* and *LOL*, which incorporates both generation uncertainty and converter outages. In contrast, existing approaches only provide a constant number as *EENS* or *LOLE* (and not a distribution), which typically neglects not only the power electronic failures but also generation uncertainty. It is worth mentioning that the PDFs obtained from the proposed framework can also be easily translated into the static values of the *EENS* and *LOLE* by calculating the first moment of the PDFs of *ENS* and *LOL* according to

$$EENS = \mathrm{E}[ENS] = \int_0^\infty x f_{ENS}(x)dx \tag{4.41}$$

$$LOLE = \mathrm{E}[LOL] = \int_0^\infty x f_{LOL}(x)dx \tag{4.42}$$

where E[.] denotes the expected value operator, and $f_{ENS}(x)$ and $f_{LOL}(x)$ are the PDF of *ENS* and *LOL* extracted as the outcomes of the proposed framework. Therefore, not only the conventional indices can be calculated but also other insights regarding the uncertainty of the indices can be gained, which will be discussed in the next chapters.

4.7. Summary

In this chapter, the implementation details of the proposed framework for reliability assessment of PEPS were explained. An overall block diagram was presented, where the interconnection between the blocks and the role of each block was highlighted. These blocks are as follows: converter availability model, power system performance model, scenario generation, state enumeration, and index calculation. In the converter availability modeling block, the proposed method for calculating the availability of power converts in PEPS was presented, in addition to its mathematical equations for implementation. This would enable considering non-constant wear-out failure rates, corrective maintenance, and chance failures in a computationally efficient manner. In

the power system modeling block, it was explained how to obtain the power balance in the system by translating the mission profiles into the generation capacity and by modeling the generation and storage units. The goal of this block was to model the output power of all the converters in the system, which would pave the way for calculating the consequences of converter failures in terms of lost energy and outage duration at any given instant. In the scenario generation block, the details of adopting and training the GAN for generating mission profiles scenarios was discussed. This was done to accommodate the considerable generation uncertainty existing in the renewable-based PEPS. Finally, at the state enumeration and index calculation block, the application of the outputs of previous blocks for calculating the system-level reliability indices were explained.

Chapter 5
Application of the proposed framework and analysis of the system-level reliability results

5.1. Background

In this chapter, the applications and advantages of the proposed reliability assessment framework will be demonstrated by analyzing of the system-level reliability in several case studies. First, it will be shown that how using constant failure rates can introduce significant errors to the system-level reliability assessment. Next, the performance of the proposed availability modeling method (explained in the previous chapter) will be compared with existing approaches in terms of accuracy and computational burden. Moreover, the system-level reliability indices for a case study will be calculated by using the proposed framework. Further, the results will be analyzed to showcase the superiority of the proposed framework in quantifying reliability for benchmarking the PEPSs and assisting the system-level design. It will be shown that the time-dependent and probabilistic outcomes of the framework are more informative and accurate, which consider mission profiles, converter wear-out failures, chance failures, repairs, generation uncertainty, penetration level of renewables. The case studies have been selected based on the systems used in [C3] and [J1]. Furthermore, another case study has been introduced, incorporating larger numbers of power electronic units, which allows performing a more thorough analysis and demonstrating the applications of the proposed framework.

5.2. Using Constant Versus Non-Constant Failure Rates (Case Study I)

In the first case study, which was also presented in [C3], the effect of using constant failure rates (as it is the common assumption in PS reliability studies) on the reliability assessment of the PEPS is investigated. Fig. 5.1. shows the schematics of the case study and the Load Duration Curve (LDC) used for it. Also, the generation uncertainty is not modeled here as the focus of the [C3] has been on modeling the effect of converter wear-out failure on the system-level reliability indices. As a result, it is assumed that the converter output power is constant. Also, the chance failures are ignored, and only wear-out failures are considered, which are described by a Weibull distribution with the shape and scale parameter of β and η. The converter rated power as well as β and η, and μ, the repair rates used in this case study are presented in Table 5.1.

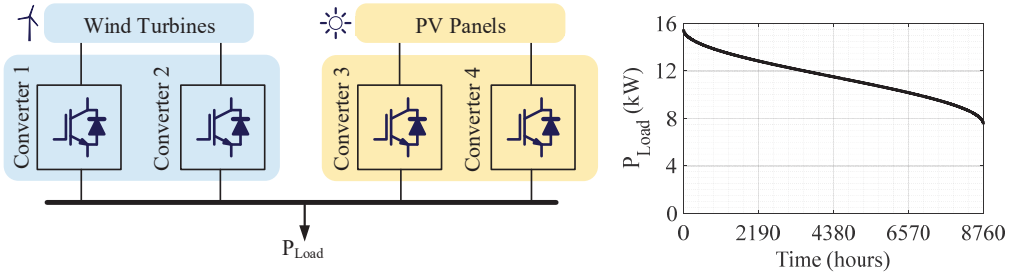

Fig. 5.1. (a) Representation of the case study I, a power electronic-based power system including two photovoltaic converters and two wind turbine converters (b) Probabilistic load modeling as a Load Duration Curve (LDC) [C3].

Table 5.1. Rated power, Weibull parameters for wear-out failures, and repair rate of the converters used in the case study I (Fig. 5.1 (a)) [C3]

	Rated Power (kW)	Weibull parameters		Repair Rate [r/y]
		β	η [y]	
Converter 1	5	3	8.5	150
Converter 2	5	3	8.5	150
Converter 3	4	3.3	10.9	100
Converter 4	4	3.3	10.9	100

As a special case of Weibull distribution with shape and scale parameter of β and η, When $\beta = 1$, the Weibull distribution becomes an exponential distribution, where the failure rate is equal $1/\eta$. The *EENS* (Expected Energy Not Supplied) index of the above system is calculated and shown in Fig. 5.2, once considering a Weibull distribution with the parameters in Table 5.1 and once using the constant failure rate of $1/\eta$. Also, the results have been validated by comparing them with the Monte Carlo simulation result, where the details have been presented in [C3].

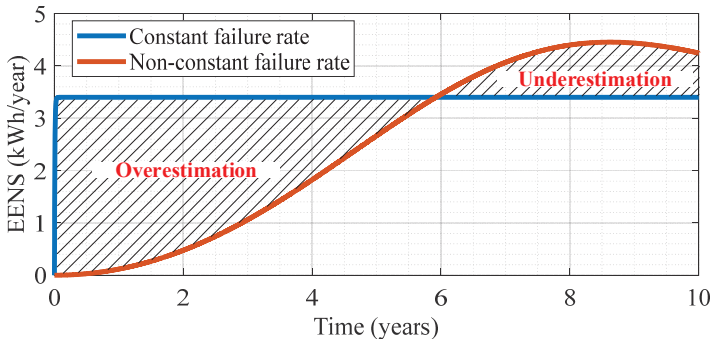

Fig. 5.2. Comparing the *EENS* (Expected Energy Not Supplied) index of the case study I (Fig. 5.1) considering constant and non-constant failure rates for the case study shown in Fig. 5.1 [C3].

As Fig. 5.2 shows, the *EENS* in the non-constant failure rate case reaches its steady-state limit very fast and remains constant afterwards. When non-constant failure rates are used, the value is small at the beginning, while it gradually increases as the time passes. This is reasonable considering that the converter wear-out failure rates increase over time due to the aging. From Fig. 5.2, it can be concluded that using non-constant failure rates results in the overestimation of the reliability in the short term. Also, it leads to the underestimation of the reliability in the long run.

5.3. Availability Modeling of Power Converters Considering Non-Constant Failure Rates (Case Study II)

As discussed before, there are several methods for availability modeling for systems with aging and non-constant failure rates. These methods are as follows: PieceWise Approach (PWA), Method of Device of Stages (MDS), Semi Markov Approach (SMA), and Monte Carlo Simulation (MCS). Each of these methods have limitations in terms of accuracy and computation time. As a result, in this part, the accuracy and computation time of these methods will be compared with the proposed availability modeling method. To do so, the time-dependent *EENS* of a case study will be calculated and compared by using the above methods. The case study is a modified version of the Roy Billinton Test System (RBTS), which is a popular test system for reliability studies [55], [87]. Fig. 5.3 shows the schematics of the case study incorporating a wind farm and three HVDC connections. The capacity factor of the wind farm is 0.49 and other parameters are presented in Table 5.2. Moreover, failure and repair data, including the shape and scale parameter of Weibull, chance failure rate, and repair rates, are listed in Table 5.2 [88], [89].

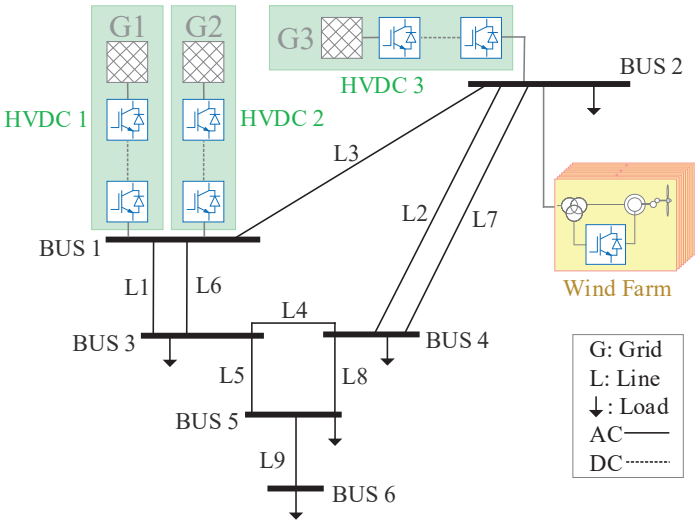

Fig. 5.3. Diagram of the case study II, a power electronic-based power system used for benchmarking the converter availability modeling methods [55], [87], [J1].

Table 5.2. Capacity of units as well as the failure and repair data for the case study II (shown in Fig. 5.3) [55], [88], [89], [J1]

Unit converters	**Capacity [MW]**	**Wear-out failures (Weibull distribution)**		**Rate of chance failures [f./yr]**	**Repair time [hr]**
		Shape factor	**Scale factor [yr]**		
HVDC 1	50	3	8	0.04	163
HVDC 2	60	3	10	0.08	151
HVDC 3	50	2.6	7	0.08	123
Wind farm	160	3	12	0.18	57

Based on the above information, the *EENS* is calculated for the case study by using six different methods as shown in Fig. 5.4. Furthermore, the computational burden and the accuracy of these methods are compared with each other in Table 5.3, where computation time, steady-state error, and Root Mean Square Error (RMSE) of the *EENS* are compared. The details of obtaining these results have been explained in detail in [J1].

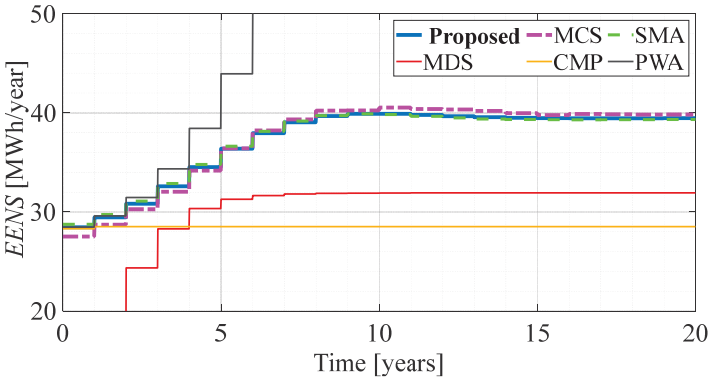

Fig. 5.4. The *EENS* (Expected Energy Not Supplied) index of the case study II (Fig. 5.3) as a function of time – comparison of the results calculated from six different approaches (including the proposed, MCS: Monte Carlo Simulation, SMA: Semi-Markov Approach, MDS: Method of Device of Stages, CMP: Continuous Markov Process, PWS: PieceWise Approach) [J1].

Table 5.3. Comparison of the proposed method with the state-of-the-art methods in terms of computation time and error [J1]

Method	**Computation time [s]**	**Steady-state error [%]**	**RMSE [MWh/yr]**
SMA	5220	0.37	0
MCS	273	0.74	0.6697
MDS	0.3	19.12	8.6806
CMP	0.9	27.75	22.1234
PWA	0.2	> 100	> 150
Proposed	3.6	0.07	0.1913

From Fig. 5.4 and Table 5.3, it can be seen that, for small time frames, e.g., $t < 4$ [y], the PWA has good accuracy, while offering a low computation time. However, for longer time frames, it results in large errors as it diverges from the correct value. Form Table 5.3, it can be also seen that the MDS has a low computational burden, while it does not have an acceptable accuracy. This is reasonable because the MDS approximates the failure rate of a unit by a set of Exponential distributions. Nevertheless, for the PEPS, the failure rate is a combination of Weibull and Exponential distributions, which cannot be properly modeled with the assumption used in MDS.

From Fig. 5.4 and Table 5.3, the MCS and SMA offer the highest accuracy, similar to the proposed availability modeling method in [J1]. However, the computation time of the SMA is substantial, which makes it impractical for reliability assessment of larger systems. Also, the proposed method in [J1] excels the MCS in terms of computation time, while it offers a similar accuracy. Notable, the computation time of the proposed method, MCS, and SMA are 3.6, 273, and 5220 [s], respectively.

5.4. Benchmarking the Power Electronic-based Grids and Analysis of the System-Level Reliability by Using the Proposed Framework (Case Study III)

In this section, the proposed framework will be used to assess the system-level reliability of a PEPS. Moreover, the results will be analyzed to investigate the impact of several factors on the system-level reliability, including, converter failures, generation uncertainty, and the penetration level of renewables.

5.4.1. Case Study Description

The schematics of the case study is shown in Fig. 5.5. Also, the capacity and number of units in each power generation and storage plant are presented in Table 5.4. Converter topologies used in the case study for the photovoltaic systems, wind turbines, and battery storage units (e.g., in PV1, PV2, WT, BT1, and BT2 in Fig. 5.5) are shown in Fig. 5.6 to Fig. 5.8, respectively. The battery units, BT1 and BT2, are identical, where their capacity is equal to 350 [kWh] each, which is selected based on the guidelines provided in [90], [91]. In addition, the corresponding specifications and electrical parameters for the above-mentioned converter units and the grid are presented in Table 5.5 and Table 5.6. Furthermore, cut-in, rated, and cut-out speeds of wind turbines, and G for the PV system are given in Table 5.7 and Table 5.8. Since the purpose of the case study is to demonstrate the system-level framework, for wear-out modeling, only the wear-out of IGBTs in PV, WT, and BT units are considered and modeled here, without the loss of generality. Besides, the repair rates and chance failure rates for the units used in this case study are presented in Table 5.9.

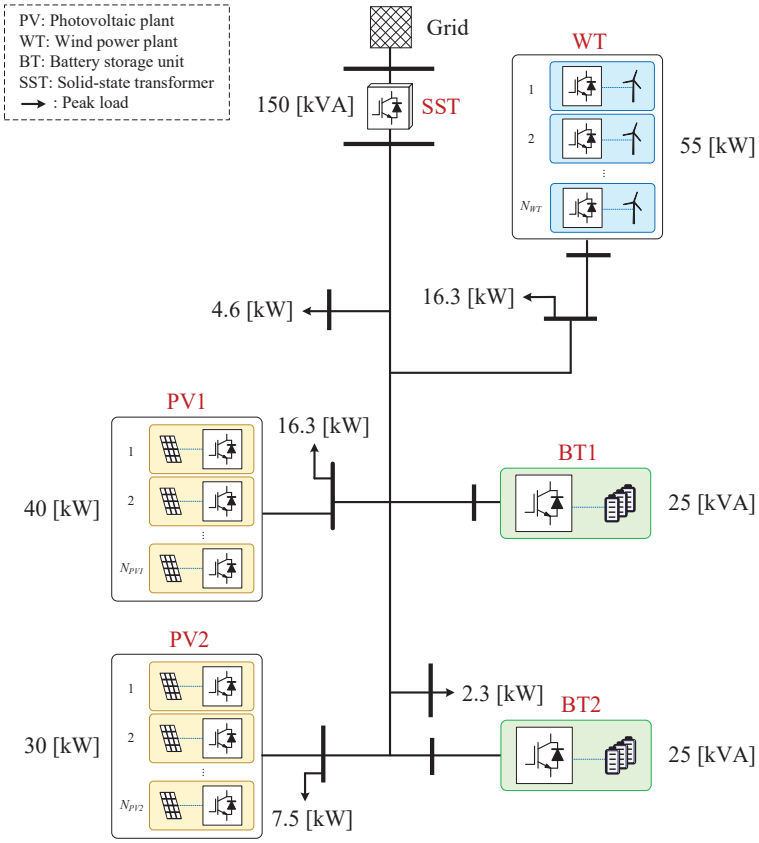

Fig .5.5. Overall schematic of the case study III, a power electronic-based power system, including photovoltaic (PV), wind turbine (WT), and battery storage converter units (BT), and a solid-state transformer (SST), inspired from the CIGRE low-Voltage benchmark network [92].

Table 5.4. Specification of the power system elements in the case study III shown in Fig. 5.5

Power System Element	Number of units	Capacity of each unit [kW]
PV1	10	4
PV2	10	3
WT	10	5.5
BT1	1	25
BT2	1	25
SST	1	150
Aggregated peak load	-	47

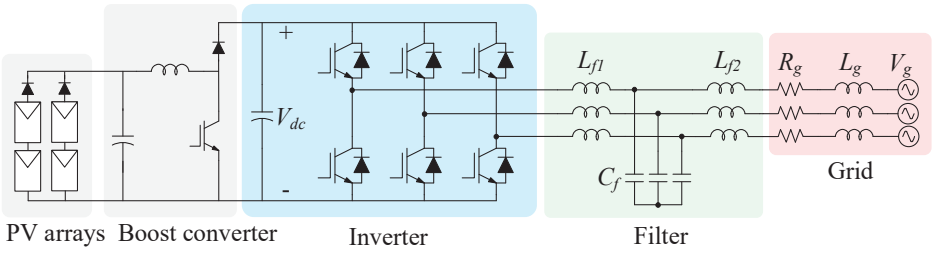

Fig. 5.6. Diagram of the converter structure used in each unit of PV1 and PV2 plants in Case study III (Fig. 5.5).

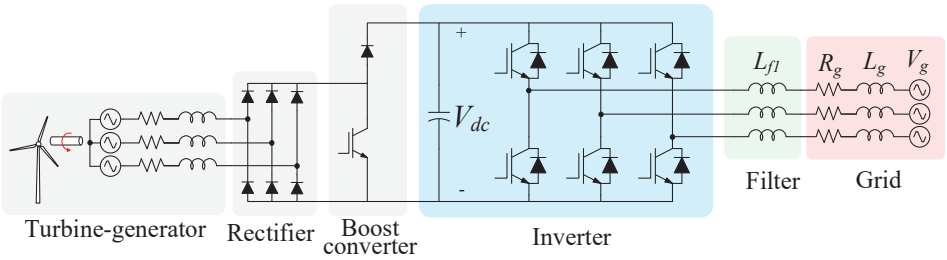

Fig. 5.7. Diagram of the converter structure used in each unit of WT plant in Case study III (Fig. 5.5).

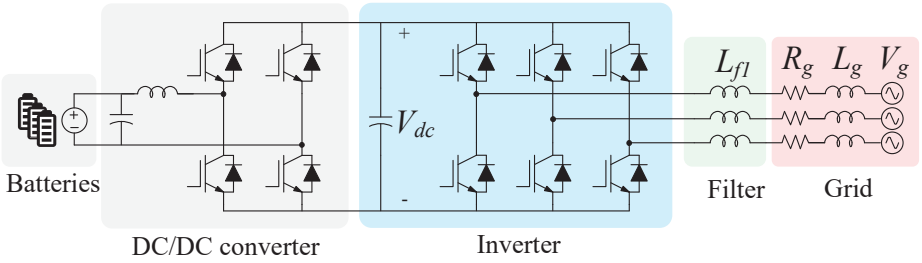

Fig. 5.8. Diagram of the converter structure used in BT1 and BT2 units in in Case study III (Fig. 5.5).

Table 5.5. Electrical parameters of the power electronic units used in the Case study III, according to the diagrams shown in Fig. 5.5 to Fig. 5.8 [93]–[95]

Parameter	Value for *PV1*	Value for *PV2*	Value for *WT*	Value for *BT1* and *BT2*
f_{sw} [kHz]	5	10	10	10
V_{dc} [V]	800	750	400	800
C_{dc} [µF]	56	47	82	47
L_{f1} [mH]	5	7	4	1
L_{f2} [mH]	1	1.1	-	-
C_f [µF]	2.6	0.7	-	-
Selected IGBT	F3L25R12W1T4_B27	F3L25R12W1T4_B27	FS20R06W1E3_B11	FF450R12KT4

Table 5.6. Grid parameters at the point of interconnection of power converters in Fig. 5.5 to Fig. 5.8

Parameter	Value
L_g [mH]	1
R_g [Ω]	0.5
f_g [Hz]	50
$V_{g,rms}$ [V]	230

Table 5.7. Specification of wind turbines used in the WT plant in Fig. 5.5

Parameter	Value
P_r [kW]	5.5
V_c [m/s]	3
V_r [m/s]	12
V_f [m/s]	25

Table 5.8. Specification of photovoltaic units used in the PV1 and PV2 plants in Fig. 5.5

Parameter	Value for *PV1*	Value for *PV2*
P_r [kW]	4	3
G [m^2]	5	3.75

Table 5.9. Repair rates (μ) and chance failure rates (λ) of the units in case study III (Fig. 5.5) [19], [96]–[99]

Units in the power system element	λ [f/y]	μ [r/y]
PV1	0.06	100
PV2	0.06	100
WT	0.15	100
BT1	0.05	100
BT2	0.05	100
SST	0.01	25

5.4.2. Mission Profiles Uncertainty

The solar irradiance profile for years 2007, 2009, and 2014 at Las Vegas, NV at week #30 can be seen in Fig. 5.9 [76]. As Fig. 5.9 shows, although the daily profiles bear some temporal patterns, the exact value of solar irradiance is highly uncertain and varies from hour to hour and year to year. A similar argument holds for the wind speed profiles, although the temporal patterns might be stronger from season to season rather than daily. As a result, unlike the conventional power systems, where the generation capacity could be controlled as desired at any time, the generation profile in renewable-based power systems is uncertain and will vary from time to time. This fact complicates the reliability assessment of renewable- and PE-based PSs compared to the conventional ones. In other words, not only the probabilistic properties of the generation capacity and unit availabilities must be considered in the analysis, but also their temporal patterns must be incorporated. To consider all these factors simultaneously, a hybrid framework was proposed in Chapter 4, where the scenario generation by the Generative Adversarial Network (GAN) was done to handle the generation uncertainty in parallel with availability modeling of the converters to model the converter outages. Notably, the GAN was able to capture all the temporal and probabilistic properties of the real profiles – i.e., it could reconstruct the same time-probability distributions and emulate real generation profiles. Therefore, the GAN was implemented and trained, and subsequently, 200 unique solar irradiance and wind speed scenarios were generated by using it to model the generation uncertainties. It is worth mentioning that the number of scenarios meets the condition stated in (4.38). The GAN-generated mission profile scenarios were shown and evaluated in Chapter 3 in terms of the Cumulative Distribution Function (CDF), Power Spectral Density (PSD), and their first moment. From the comparison, it was shown that the GAN-generated profiles could successfully capture all the temporal and probabilistic properties of the real scenarios. Therefore, the GAN is used here as

well to generate diverse and realistic scenarios, emulating potential real scenarios, to assist the reliability assessment by taking the generation uncertainty into account.

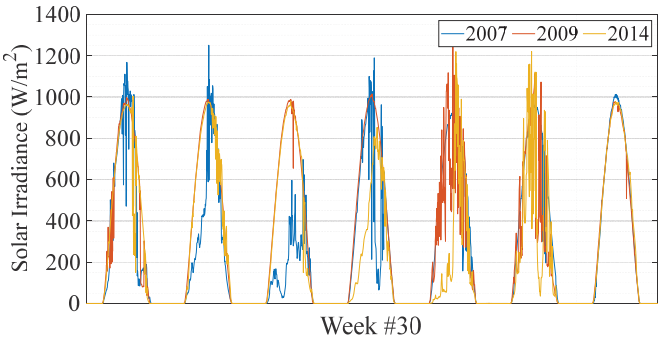

Fig. 5.9. Uncertainty of historical solar irradiance profiles, demonstrated at a specific week in three different years at Las Vegas, NV [C2].

5.4.3. Time-Dependency of the Reliability Indices

In Fig. 5.10, the solar irradiance and wind speed profile for 2007 are shown [76]. Depending on the solar irradiance and wind speed and based on whether the converters are healthy or faulty, the system can be in various states in terms of generating capacity. The output power of PV1, PV2, WT, BT1, and BT2, in a given state of $j = 31$, which means that the SST is down, are shown in Fig. 5.11 to Fig. 5.14. Notably, in this state, the system will operate analogous to an islanded microgrid. It should be mentioned that when calculating the final reliability index, not only this state, but also all other possible unreliability events are considered. In Fig. 5.11 to Fig. 5.14, the output power profile for the PV1 and PV2 plants are calculated based on (4.17) and Fig. 4.3 by using the mission profiles of Fig 5.10. Similarly, the output power of the wind turbine converters in WT is calculated according to (4.19) and Fig. 4.3. Accordingly, the output power of the battery converters in BT1 and BT2 can be obtained from (5.25).

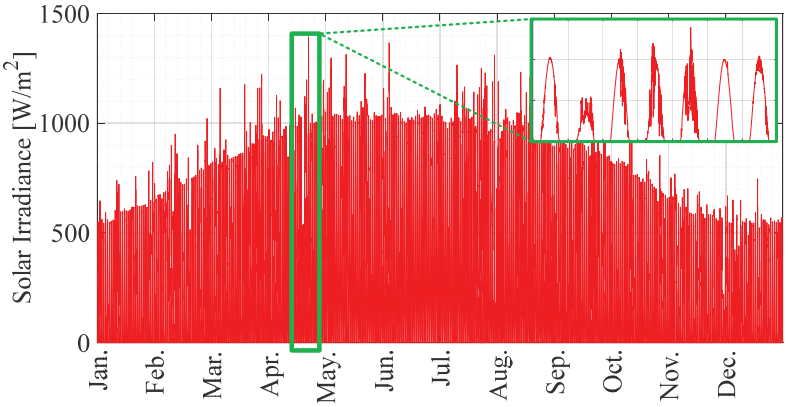

(a)

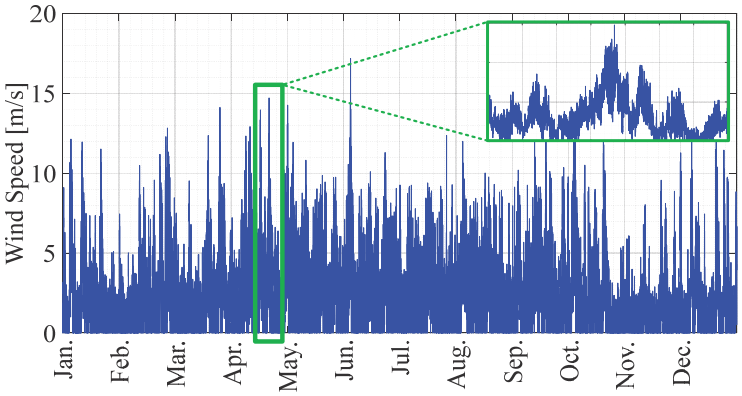

(b)

Fig. 5.10. Annal mission profiles used for demonstration of time series results for the system shown in Fig. 5.5: (a) solar irradiance, (b) wind speed.

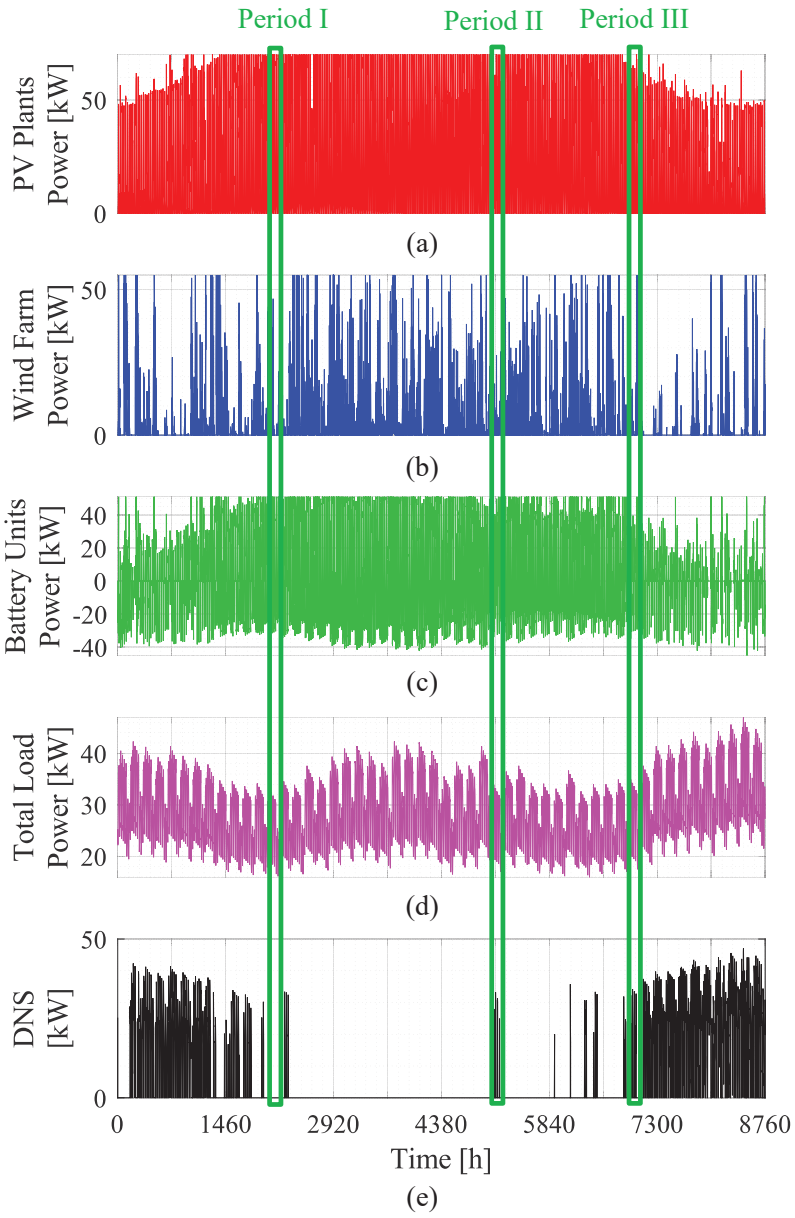

Fig. 5.11. Time series of the Case study III (Fig. 5.5) obtained by using the proposed framework, showing the output power of different converter units at a given system state (i.e., $j = 31$) where the SST is down: (a) photovoltaic inverter units, aggregating PV1 and PV2, (b) wind converter units in WT, (c) battery units aggregating BT1 and BT2 (d) load profile time

series, (e) DNS (Demand Not Supplied), from (4.35), indicating the load power that cannot be supplied in this state.

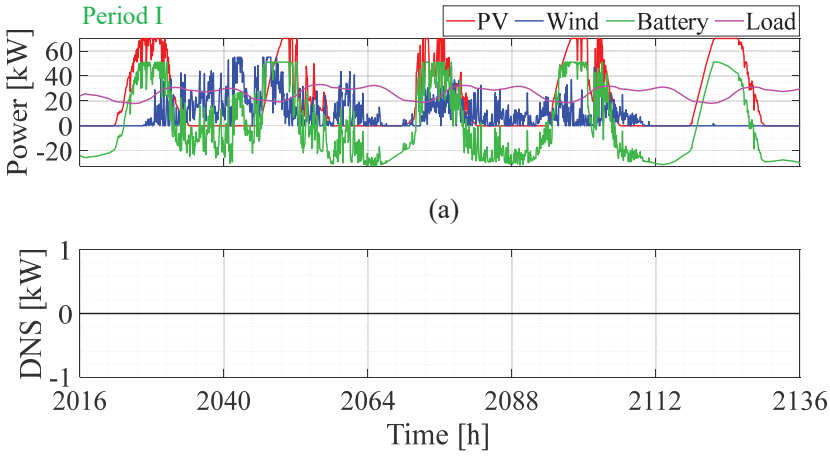

Fig. 5.12. Time series of the Case study III (shown in Fig. 5.5) in period I (shown in Fig. 5.11): (a) the output power of PV1+PV2, WT, and BT1 = BT2 in Fig. 5.5, (b) DNS (Demand Not Supplied) indicating the load power that cannot be supplied from (4.35).

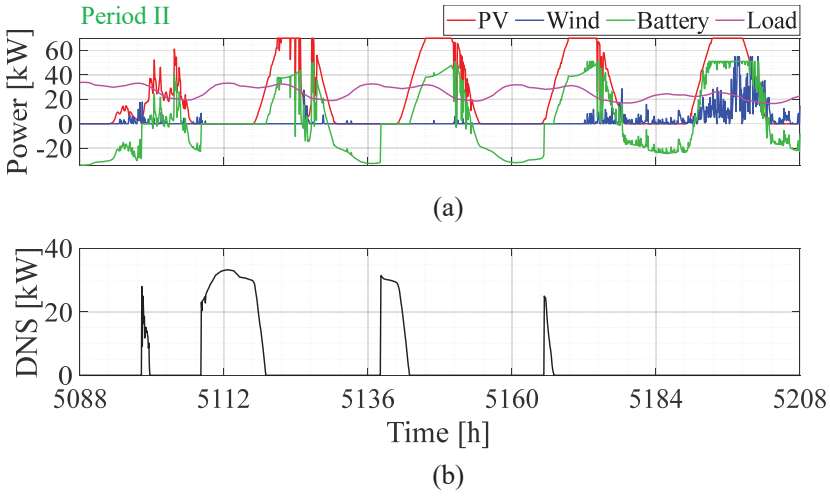

Fig. 5.13. Time series of the Case study III (shown in Fig. 5.5) in period II (shown in Fig. 5.11): (a) the output power of PV1+PV2, WT, and BT1 = BT2 in Fig. 5.5, (b) DNS (Demand Not Supplied) indicating the load power that cannot be supplied from (4.35).

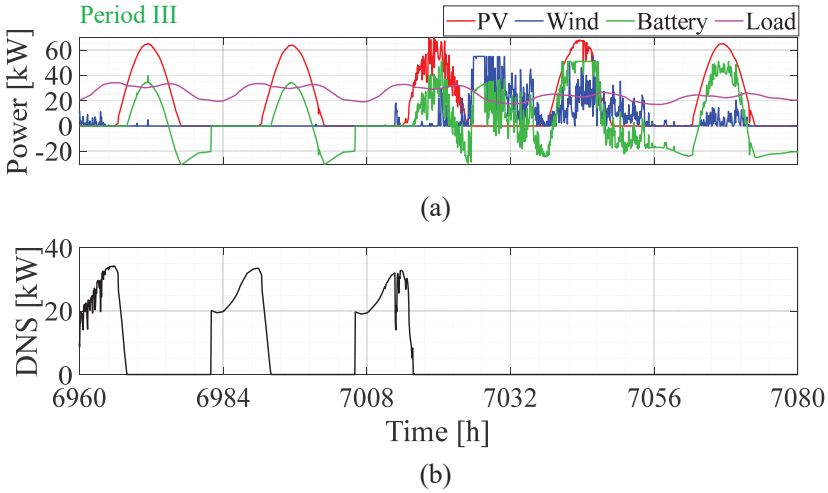

Fig. 5.14. Time series of the Case study III (shown in Fig. 5.5) in period III (shown in Fig. 5.11): (a) the output power of PV1+PV2, WT, and BT1 = BT2 in Fig. 5.5, (b) DNS (Demand Not Supplied) indicating the load power that cannot be supplied from (4.35).

By obtaining the converter availabilities and knowing the converter output profiles, the system-level reliability indices such as *ENS* and *LOL* can be calculated based on Fig. 4.3 and from (4.37) and (4.40). Notably, the *ENS* can be calculated based on the *DNS* according to (4.35), and thereby acquiring the *EENS* from (4.41). It is worth pointing out that, in Fig. 5.11 to Fig. 5.14, the *DNS* indicates the "consequence" of the above-mentioned state ($j = 31$, which can be translated into the failure of SST), in terms of energy lost.

In this regard, one of the main advantages of the proposed framework is employing the factor of "time" besides the "probability" – not only in the modeling but also in providing the output results. In other words, from the results of the framework, it can be known that, at which periods of the year, more severe outages are expected, and more preventive measures should be taken. For instance, Fig. 5.15 shows that the *EENS* is considerably higher throughout December and November compared to other months, while this number is zero for June, July, and August. In contrast, in the conventional methods, the value of the *EENS* would be the same for all months of the year, as they are based on purely probabilistic approaches and cannot distinguish time-related properties. Therefore, conventional reliability indices (which provide only a static number for the entire year) do not reveal such insightful information when compared to the results of the proposed framework.

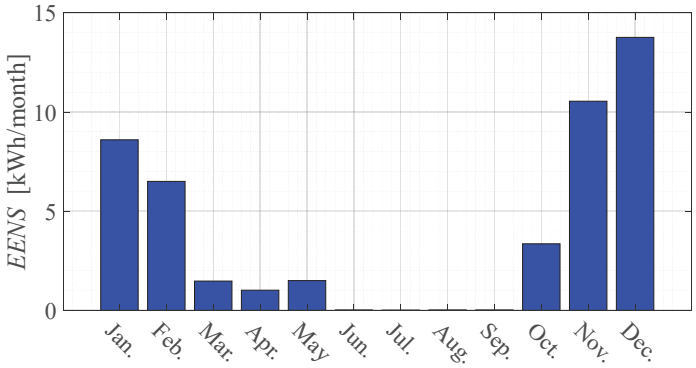

Fig. 5.15. Comparing the variation of the monthly *EENS* (Expected Energy Not Supplied) index for different months within one year.

5.4.4. Generation Uncertainty and Mission Profile-Dependency of the Reliability Indices

The above analyses were done, given that the converters are new – that is, when the system age = 1 [y]. When the converters age, their reliability metrics, and subsequently their availabilities are worsened. Therefore, it is expected that the system reliability indices follow the same trend. Thus, when the system age = 20 [y], the same analysis can be repeated with regards to changes in the converter availabilities. As a result, a new value for the reliability indices can be obtained. In Table 5.10, for the historical mission profiles happened in 2007, the value of the *EENS* and *LOLE* have been presented for two different system ages that is age = 1 [y] and age = [20] years. A similar analysis has been performed given the historical mission profiles of 2015, and the results for the *EENS* and *LOLE* are reported in Table 5.10.

Table 5.10. Comparison of the EENS (Expected Energy Not Supplied) and LOLE (Loss Of Load Expectation) for two different system ages, and when two different years of mission profiles (same location) are used

	***EENS* [kWh/y] at age = 1 [y]**	***EENS* [kWh/y] at age = 20 [y]**	***LOLE* [h/y] at age = 1 [y]**	***LOLE* [h/y] at age = 20 [y]**
2007 mission profile	41.10	117.41	1.55	4.44
2015 mission profile	50.08	142.96	1.91	5.46

According to Table 5.10, for the system age =1 [y], the value of *EENS* would be 22% larger if the mission profile of 2015 is used instead of the 2007. This considerable difference is justifiable with respect to the intermittent nature of renewables and the uncertainty in the generation profiles. Therefore, by using different years of mission profiles, a different number will be obtained for the *EENS*. Thus, the calculated reliability index is highly sensitive to the year of the mission profile, which is available for the study, and thereby introducing significant errors. As a result, due to various uncertainties, the reliability index will follow a probability distribution, as opposed to a static number (which is considered in the conventional reliability assessment methodologies).

For the above reason, the proposed framework suggests using the PDF of the reliability index as an output result, which can provide more practical information compared to a static value. To reconstruct the distribution of the reliability indices, the GAN is trained and used to generate 200 (according to Algorithm 4.1) realistic mission profile scenarios to account for the generation uncertainties. Other uncertainties were already handled in the reliability and availability modeling blocks as elaborated in Chapter 3 and Chapter 4. Although unique and distinct, the GAN-generated profiles capture the probabilistic and temporal properties of the real profiles. Therefore, they can represent the potential scenarios that the system will be exposed to in terms of generation capacity. For each scenario n, SC_n the procedure depicted in Fig. 4.3 is done and a value is calculated for the indices such as ENS_n and LOL_n. When the process is repeated for all scenarios, and ENS_n and LOL_n are calculated for $1 \leq n \leq N_{scenarios}$, the PDF of the indices can be calculated.

Moreover, the value of the *EENS* and *LOLE* by using different years of mission profiles are shown in Fig. 5.16 and Fig. 5.17. As Fig. 5.16 and Fig. 5.17 show, the obtained values for the *EENS* and *LOLE* can be noticeably different for various years. Furthermore, Fig. 5.18 and Fig. 5.19 show the PDF of the *ENS* and the *LOL* for the Case study III in Fig 5.5 with the parameters in Table 5.4 to Table 5.9. In addition, the values of the *ENS*, provided that only the profile of 2007 or only the profile of 2015 are used, are pointed out in the Fig. 5.18 and Fig. 5.19. As it can be seen in Fig. 5.18 and Fig. 5.19, the obtained values for the reliability indices can be different, such that the obtained value for the *LOL* and *ENS* considering the 2007 profile would be 23% and 22% larger when the 2015 profile is used. Hence, using the GAN-generated profiles, and subsequently extracting the PDF of the *ENS* and *LOL*, will be more realistic and provide a better understanding of the distribution and uncertainties of the indices.

For a better comparability of the results, the acquired PDFs can be characterized by approximating them with a Normal distribution considering the mean (μ) and standard deviation (σ), i.e., $N(\mu,\sigma)$, as provided in Fig. 5.18 and Fig. 5.19. It is worth pointing out that μ can be used as an indicator for the *expected value* of the index, while σ can be an indicator for the *uncertainty* of the index.

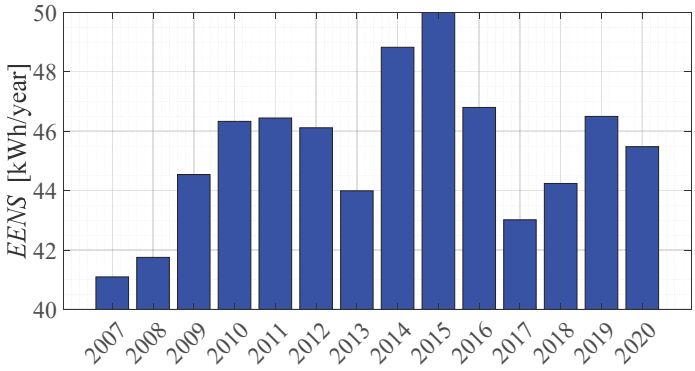

Fig. 5.16. Comparison of the *EENS* (Expected Energy Not Supplied) for Case study III, when only one year of mission profile is used, demonstrating that the generation uncertainty can lead to a noticeable error in calculating the reliability indices.

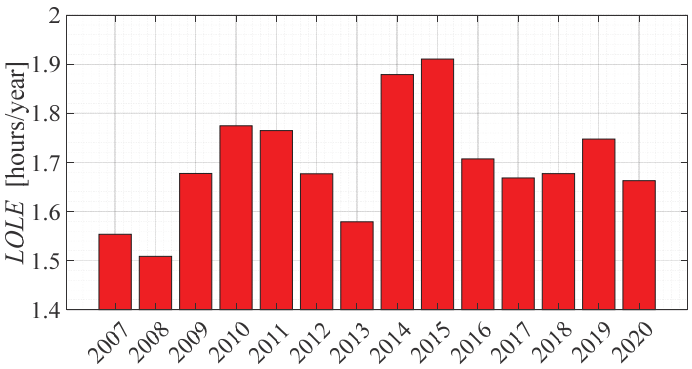

Fig. 5.17. Comparison of the *LOLE* (Loss Of Load Expectation) for Case study III, when only one year of mission profile is used, demonstrating that the generation uncertainty can lead to a noticeable error in calculating the reliability indices.

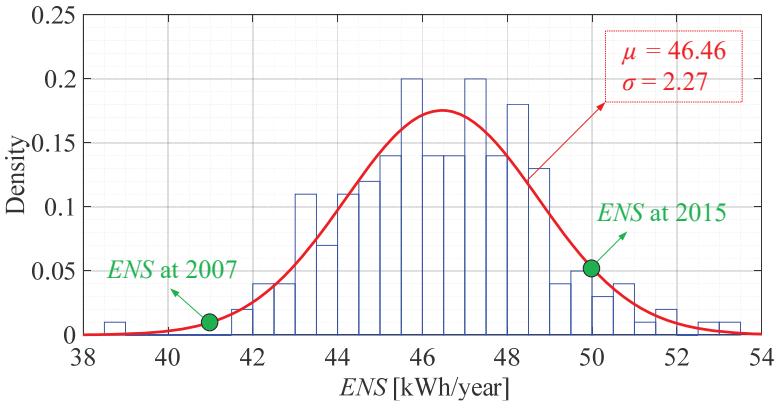

Fig. 5.18. Probability Density Function (PDF) of *ENS* (Energy Not Supplied) index for Case study III, indicating the distribution of outage severity in terms of lost energy, where generation uncertainty is demonstrated by pointing out the results of historical data from 2007 and 2015.

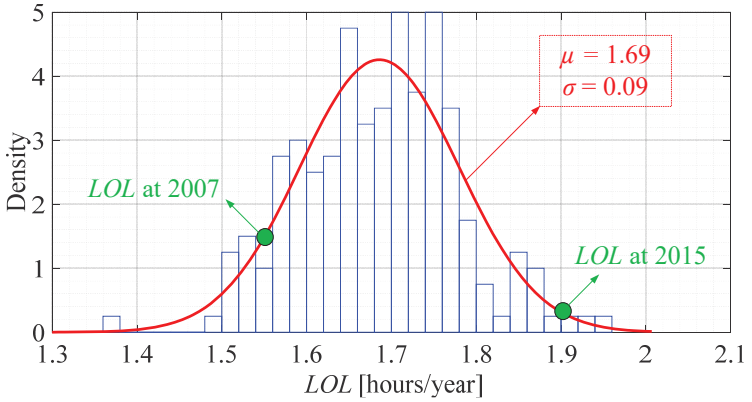

Fig. 5.19. Probability Density Function (PDF) of *LOL* (Loss Of Load) index for Case study III, indicating the distribution of overall outage duration, where generation uncertainty is demonstrated by pointing out the results of historical data from 2007 and 2015.

5.4.5. Impact of Power Electronic Components Aging on the System-Level Reliability

Another advantage of the developed framework is that not only the current performance of the system can be evaluated, but also the future performance can be predicted. The previous analysis was for the case where the converters were new – that is, the system age = 1 [y]. When the converters age, their failure rate increases due to wear-out failures, and thereby decreasing the reliability. Thus, in this part, the effect of converter aging on the system-level indices will be investigated. To do so, the PDF of the *LOL* and *ENS* are obtained for different system ages by using the proposed framework. Notably, for three different system ages – namely, age = 1 [y], age = 10 [y], and age = 20 [y] – the PDFs are shown in Fig. 5.20 for *LOL,* and in Fig. 5.21 for *ENS*. Moreover, for these three cases, the PDFs are approximated by a Normal distribution, $N(\mu,\sigma)$, whose parameters are also shown in Fig. 5.20 and Fig. 5.21. As it can be seen from Fig. 5.20 and Fig. 5.21, as the converter age increases, both μ and σ increase. In other words, both the expected value (μ) and the uncertainty (σ) of the reliability indices increase when the converter age increases. Hence, by using the proposed framework, the effect of converter aging on the system-level reliability indices can be studied quantitatively, as illustrated in Fig. 5.22.

Moreover, the variation of *EENS* in terms of the system age is shown in Fig. 5.23 in the form of a box plot, where the median, max, min as well as the first and third quartile are depicted. It is worth reminding that in the conventional methods, only one number will be reported as *EENS* for all system ages. Also, the *EENS* itself has some uncertainties, which cannot be reflected in one number, while it can be quantified by using the proposed framework as shown in Fig. 5.23.

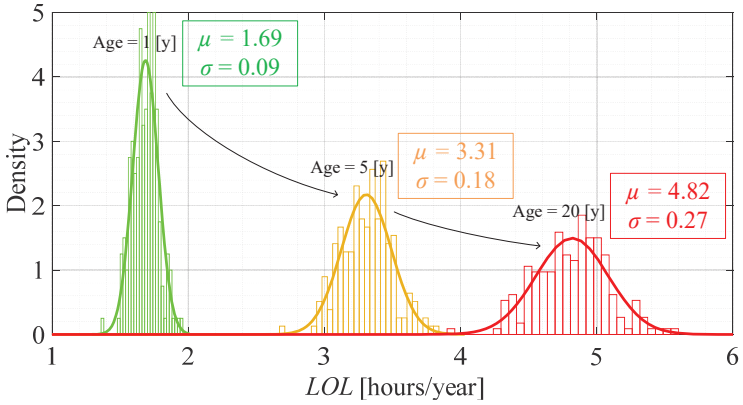

Fig. 5.20. Comparison of the PDFs of *LOL* for three different system ages (i.e., $y = 1$, 5, and 20 [years]), demonstrating how the converter aging and wear-out failures affects the system-level reliability indices in terms of outage durations.

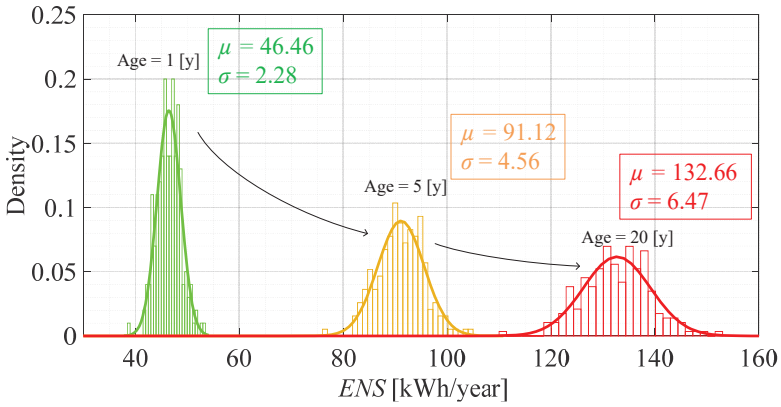

Fig. 5.21. Comparison of the PDFs of *ENS* for three different system ages (i.e., $y = 1$, 5, and 20 [years]), demonstrating how the converter aging and wear-out failures affects the system-level reliability indices in terms of the energy not supplied.

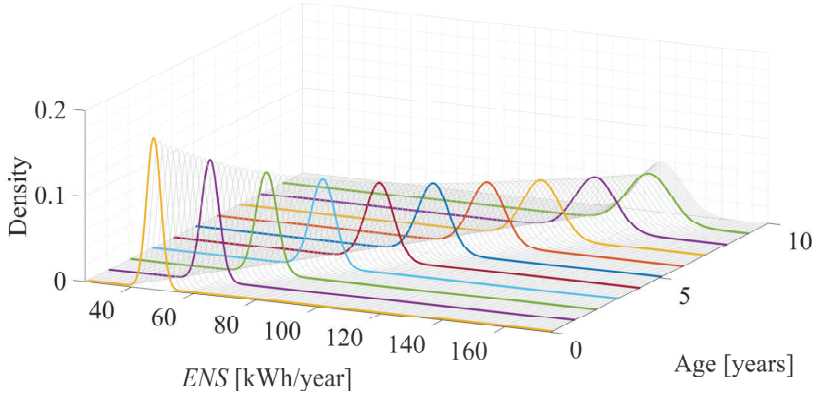

Fig. 5.22. Variation of the system *ENS* index (Energy Not Supplied) as a function of system age (which can be interpreted as an illustration of how the system-level strength of a power electronic-based power system degrades with converter aging).

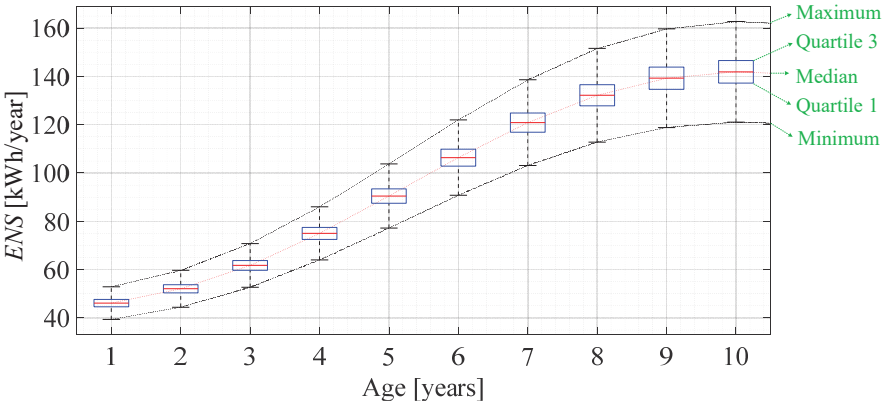

Fig. 5.23. Variation of the system *ENS* index (Energy Not Supplied) and its uncertainty as a function of system age.

Since, in the proposed framework, the wear-out failures are modeled accurately considering the mission profiles and physics of failure (refer to Fig. 3.1 and Fig. 4.7 flow chart of reliability modeling), the effect of aging on the *EENS* is evident as can be seen from Fig 5.23. However, in the conventional system-level reliability assessment methodologies, wear-out failures are neglected, and the failure rate of converters are approximated with a constant value, which is time-independent. Therefore, this oversimplification results in a constant value over time for the reliability indices (e.g., *EENS*), while the actual value of the index increases over time due to converter aging. Accordingly, considering the constant failure rates for converters and neglecting wear-out failures can introduce error to the estimated reliability, which can, in turn, lead to an unreliable or overdesigned system.

5.4.6. System-Level Design for Reliability and Benchmarking

In this part, the proposed framework will be used to benchmark the Case study III and ensure that it will meet its short- and long-term reliability targets. The parameters of the case study were already presented in Table 5.4 to Table 5.9. Accordingly, the PDF of *LOL* is calculated for two different cases with age = 1 [y] and age = 20 [y] and shown in Fig. 5.24. As discussed before, for the *LOL*, a target value is set for the system designers, where it is required that the overall value of the *LOL* must not exceed this limit. For some European countries, the value of this target is between LOL_{target} = 4 to 8 [h/y]. As it can be seen in Fig. 5.24, the system passes the above requirement when age = 1 [y], given that the LOL_{target} = 4 [h/y]. However, when the converters age, i.e., age = 20 [y], the PDF of *LOL* exceeds the limits, indicating that the system will fail to meet its target *LOL* over time. Many approaches can be adopted to tackle this problem, e.g., changing the converter-level designs and maintenance.

Another approach, which will be used here, is to consider a larger design margin at the system-level, by incorporating more generation resources at the beginning. By doing so, the loss of generation due to power electronics degradation and failures will be covered by having more generatio capacity in the system. To demonstrate this, PV3, a 30-kW power plant (with identical specifications as PV2 in Table 5.4 to Table 5.9 and Fig. 5.5 and Fig. 5.9) was added to the system.

Subsequently, the PDF of *LOL* at age = 20 [y] was calculated in two cases – before and after adding the PV3. The PDF of *LOL* in these tow cases as well as the LOL_{target} are shown in Fig. 5.25. As it can be seen in Fig. 5.25, after adding the PV3, the system will meet its LOL_{target} requirement, even though the converters failure rates have increased over time. As a result, with such an analysis, the system designers have a quantitative tool to benchmark their designs and assess the viability of different options, to make sure that they meet the reliability requirements.

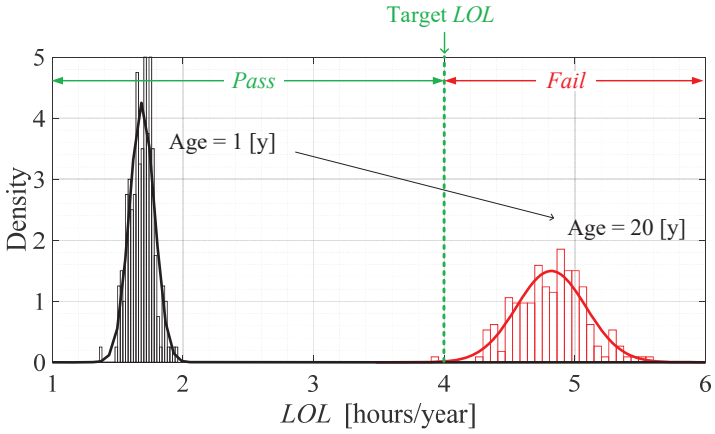

Fig. 5.24. Illustration of the design requirement of LOL_{target} = 4 [h/y] as well as the PDF of *LOL* for two different system ages, where the system fulfills the requirement when its age = 1 [y], while it fails to meet the requirement when the age = 20 [y].

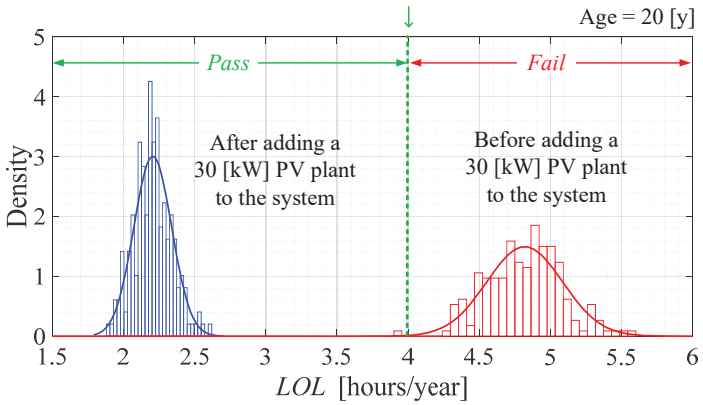

Fig. 5.25. PDF of *LOL* at age = 20 [y] before and after adding a 30-kW photovoltaic plant, illustrating how increasing the generation capacity influences the system-level indices and ensures that the reliability requirements are met even in the long run.

5.4.7. Impact of Renewable Penetration Level

In this part, the effect of increasing the renewables on the system-level reliability indices will be investigated. To study the impact of penetration of renewables, another version of the case study with 10% penetration of renewables are considered. It is worth mentioning that the definition of penetration level used here indicates the percentage of the load energy that is supplied from the renewable-generated power [100]. The capacity and number of units for this version of the case study can be seen in Table 5.11. Also, it should be noted that the penetration level for the first version of the case study, which was presented in Table 5.4 was 80%.

Table 5.11. Specification of the power system elements in a modified version of the Case study III (Fig. 5.5), where the renewables penetration level is 10%

Power System Element	Number of units	Capacity of each unit [kW]
PV1	1	4
PV2	1	3
WT	1	5.5
BT1	1	25
BT2	1	25
SST	1	150
Aggregated peak load	1	47

On the one hand, when more renewables are integrated into the grid, some converters, e.g., battery converters, experience higher loading and longer operating times. The resulted overstress leads to the decrease of reliability at the converter level, which will be demonstrated here for battery units by comparing the converter-level reliability for two cases of high- and low-penetration levels of renewables. On the other hand, by adding more renewables to the grid, the generation capacity increases, which can potentially increase the system-level reliability. Considering these two factors, it cannot be easily predicted that whether the overall system reliability decreases or increases. Therefore, to study the effect of renewable penetration, the system-level reliability indices are calculated, by using the proposed framework, for two different versions of the case study with 80% and 10% renewable penetration (refer to Table 5.4 and Table 5.11), so that a quantitative comparison is possible. Also, the rating of SST is the same in both cases.

Converter-level reliability:

Acquiring the converter-level reliability metrics was explained in Chapter 3. Also, it was noted that the mission profiles play a key role in the reliability of converters. In this regard, the output power profile for the battery converters for two version of the case study is shown in Fig. 5.26 to Fig. 5.29. Furthermore, the failure rate and availability of the battery converters in those two cases are shown in Fig. 5.30 and Fig. 5.31, respectively. Since, the batteries are charged from the renewable-generated power, in the case study with higher penetration of renewables, the battery converter experiences a higher power profile as can be seen in Fig. 5.26 to Fig. 5.29. Generally, higher power profile means that the converters components undergo a higher thermal stress, which can be translated into a lower expected lifetime and subsequently a lower reliability. The curves shown in Fig. 5.30 represent the failure rate due to wear-out of the components of the converters. Accordingly, the converter availability can be calculated by considering the chance failures (failures which have their root-causes in external factors) and the maintenance (i.e., repair rate). As a result, the converter availability for two versions of the case study (10% (Table. 5.11) and 80% (Table 5.4) energy-based penetration level) are shown in Fig. 5.31. Moreover, it should be noted that, due to the aging of components, the availability of converters decreases over time for any given mission profile as Fig 5.31 shows. Hence, it is expected that the reliability indices at the system-level will be aggravated as the time passes.

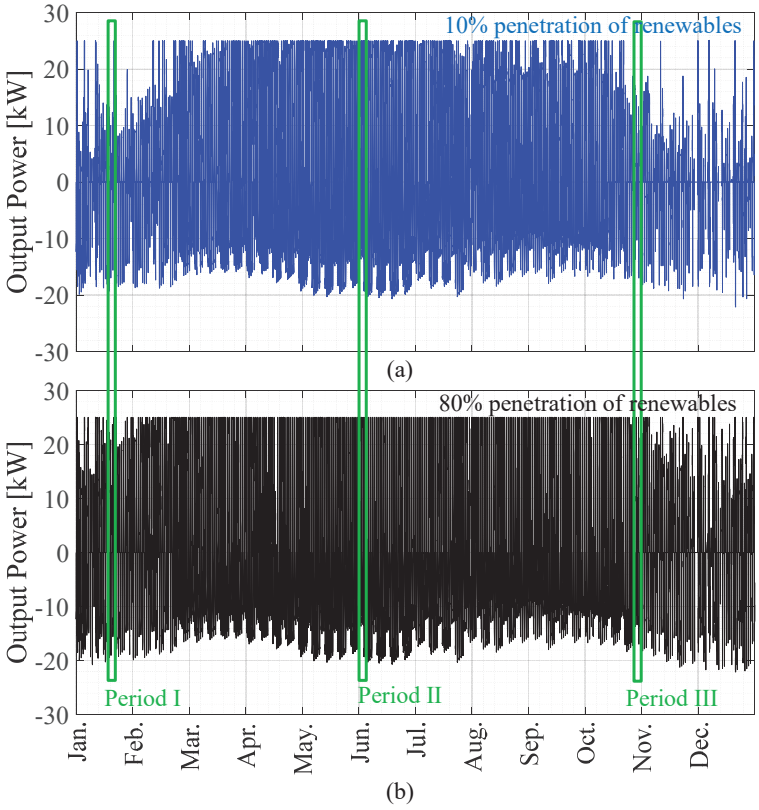

Fig. 5.26. Time series of the output power of the battery units (BT1 = BT2) in Fig. 5.5: (a) 10% penetration level of renewables with Table 5.11 parameters, (b) 80% penetration level of renewables with Table 5.4 parameters,

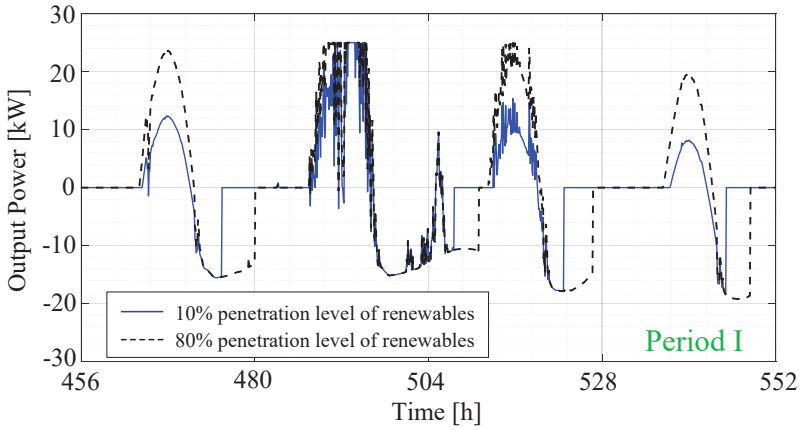

Fig. 5.27. Time series of the output power of the battery units (BT1 = BT2 in Fig. 5.5), for period I (shown in Fig. 5.26), considering two cases with 10% and 80% penetration level of renewables, demonstrating how the increase of the renewables penetration level increases the stress on the battery converters in the case study.

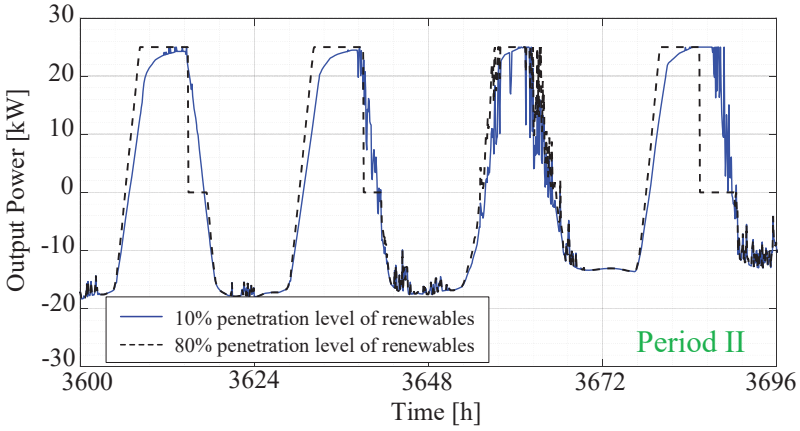

Fig. 5.28. Time series of the output power of the battery units (BT1 = BT2 in Fig. 5.5), for period II (shown in Fig. 5.26), considering two cases with 10% and 80% penetration level of renewables, demonstrating how the increase of the renewables penetration level increases the stress on the battery converters in the case study.

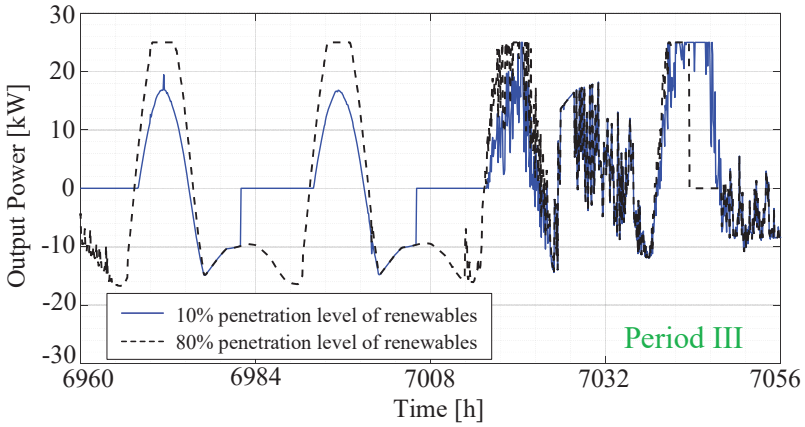

Fig. 5.29. Time series of the output power of the battery units (BT1 = BT2 in Fig. 5.5), for period III (shown in Fig. 5.26), considering two cases with 10% and 80% penetration level of renewables, demonstrating how the increase of the renewables penetration level increases the stress on the battery converters in the case study.

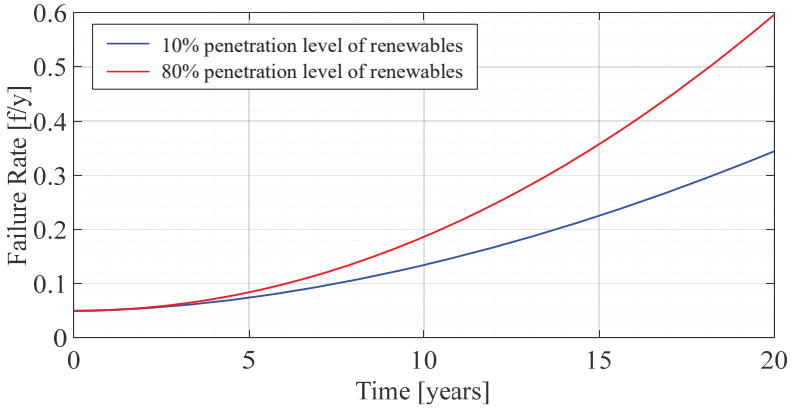

Fig. 5.30. Comparison of the failure rate of the battery converter units (BT1 and BT2 in Fig. 5.5) over time, for two cases of 10% (blue) and 80% (red) penetration level of renewables.

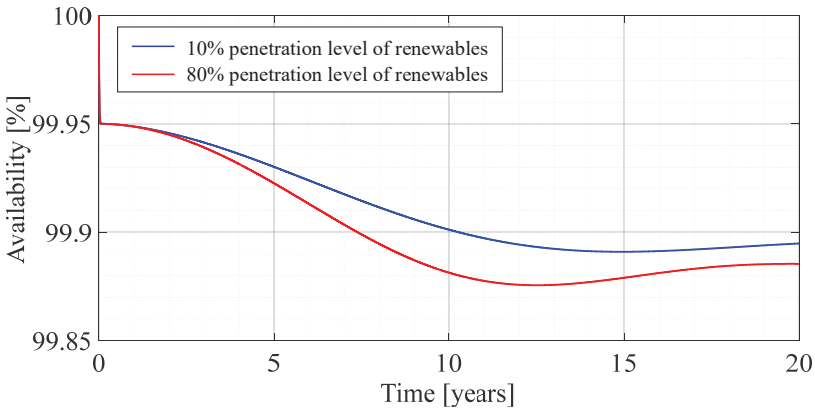

Fig. 5.31. Comparison of the availability of the battery converter units (BT1 and BT2 in Fig. 5.5) over time, for two cases of 10% (blue) and 80% (red) penetration level of renewables.

System-level reliability:

The PDF of *ENS* is shown in Fig 5.32, for 80% and 10% penetration level cases. As it can be seen in Fig 5.32, increasing the generation capacity by adding more renewables to the grid was helpful in increasing the system-level reliability, even though it put stress on some converters and increased their failure rate (Fig. 5.30).

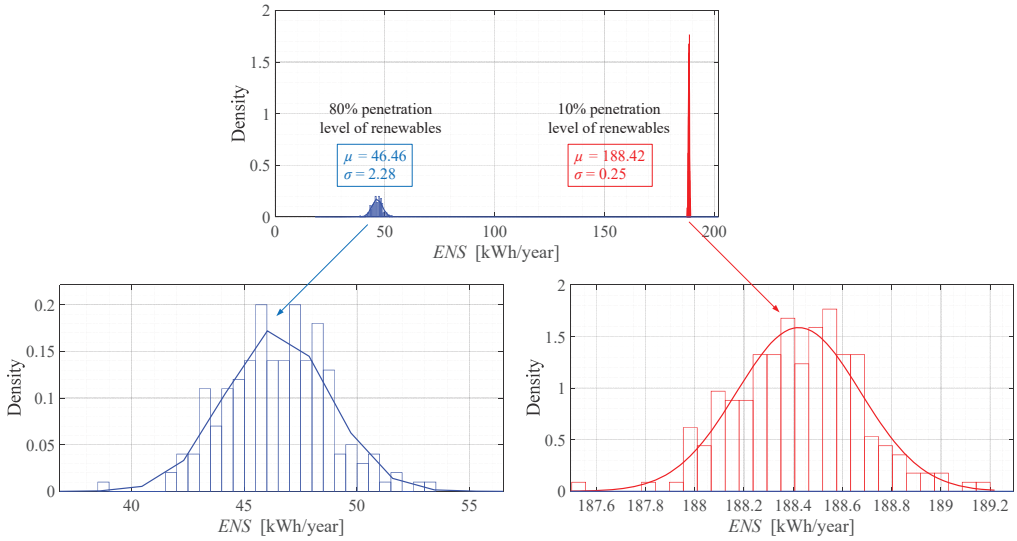

Fig. 5.32. Comparison of the PDF of *LOL* index for two cases of 10% and 80% penetration level of renewables, where μ decreases and σ increases as the penetration level increases.

Also, from the analysis, it was found out that the *ENS* is affected more significantly in contrast to the *LOL*. This can be interpreted such that the overall duration of outages is not influenced considerably when the penetration level of renewables changes. However, the decrease of *ENS* suggests that the severity of the outages is much less when more renewables added to the system generation units. Also, μ and σ of the PDFs are given in Fig 5.32. In this regard, when the penetration level increases, μ of the *ENS* decreases, indicating that the system experiences less severe outages, while σ increases, which is reasonable due to the more uncertainty introduced by the renewable generation.

5.5. Summary

In this chapter, the merits of the proposed framework as a system-level quantitative reliability assessment tool were demonstrated by using it for assessing the reliability of several case studies. In these case studies, the errors introduced by using the constant failure rates were discussed. Also, the proposed availability modeling method was explained by comparing its results with conventional methods in terms of computational efficiency. Further, the effect of several factors (i.e., mission profiles, wear-out failure and aging of power converters, generation uncertainty, temporal patterns of renewable resources as well as their penetration level) on the system-level reliability of a PEPS was investigated, where the results were analyzed and discussed. The above results are some examples of how using the developed framework can assist the system level reliability assessment used for planning of the PEPS. There are more potentials, which are not shown here. Furthermore, since the framework is model-based, the effect of many parameters on the system-level reliability could be studied. For example, any changes in the converter-level design, could be modeled, where the wear-out failure rate would change accordingly - and the impact on the system can be seen immediately.

Chapter 6
Conclusion

In this chapter, the conclusions and key findings of this PhD project will be summarized. Furthermore, the main contributions will be highlighted, and the potentials future works will be discussed.

6.1. Summary

As discussed before, the main objective of this PhD project was to develop a methodology to enable the system-level reliability assessment of modern power systems considering the power electronics failures. This incorporation caused several challenges, which resulted in the introduction of new concerns when assessing the reliability of a Power Electronic-based Power System (PEPS). On the other hand, conventional power system reliability assessment methodologies were unable to consider and model these new considerations. Therefore, new methodologies must have been developed to tackle these challenges and incorporate those considerations.

Thus, in Chapter 1, these research gaps were analyzed and explained in detail. Given these shortcomings, the motivation of this PhD project was discussed, where several research tasks were defined accordingly to tackle the existing challenges. Based on these research tasks, the research questions and project objectives were formulated, and a roadmap to address them was presented. Also, the limitations and assumptions of this project were clarified.

In Chapter 2, the fundamentals of reliability assessment in power systems were discussed to provide a better understating of the concepts, including the hierarchical levels, different system classifications, and application of probabilistic and deterministic methods. Then, the reliability indices in power systems were discussed, where famous indices were explained and the principles of calculating them were demonstrated. There, it was explained that the “probability” and “consequence” of failure events are the main information needed to calculate any reliability index in the power systems. Next, the conventional approach for outage modeling of synchronous generators was discussed. Subsequently, the main mathematical methods (that are frequently used in power system reliability studies) for calculating the state probabilities were elaborated upon. These methods included Portability Convolution method, Markov method, State Enumeration technique, and Monte Carlo simulation. Notably, the mathematical details for implementation of these methods, as well as the merits and demerits of them, and when to use each method were also discussed. Further, the Capacity Outage Probability Table (COPT) was explained, aggregating the probability and consequence of failure states. Accordingly, it was demonstrated how to form the COPT and Load Duration Curve (LDC), and subsequently, how to use its information to calculate the reliability indices. Finally, the impact of non-power

electronic failures on the power system reliability was discussed by providing an example of outage modeling of a wind turbine circuit breaker.

In Chapter 3, the fundamentals of reliability modeling in power electronics, particularly wear-out failure modeling were highlighted. First, the conventional reliability analysis by handbooks were discussed, where the limitations of this approach were explained. Next, the overall reliability assessment process, from component-level up to the converter-level were presented, where all the necessary steps were explained. These steps included the electrothermal modeling, damage calculation using lifetime models, uncertainty handling using Monte Carlo simulation, and calculating converter reliability by using the reliability block diagrams, where they were demonstrated by implementing them on a PhotoVoltaic (PV) inverter example. Afterwards, the issue of mission profile uncertainty was investigated and demonstrated with detailed examples. Furthermore, the solution to this problem was presented, which included generating realistic mission profile scenarios by using the Generative Adversarial Networks (GANs). The GAN-generated scenarios were compared with historical scenarios in terms of PSD (Power Spectral Density), their first moment, and CDF (Cumulation Distribution Function). It was shown that the GAN-generated scenarios are analogous to historical profiles, which makes them suitable for mission profile scenario emulation. Further, it was shown that how using this approach can reduce the converter reliability estimation error, which were caused due to mission profile uncertainties.

In Chapter 4, the proposed framework for the PEPS system-level reliability assessment was presented, where different blocks of the framework were explained in detail. This framework was model-based and considered various factors in the PEPS reliability assessment (e.g., mission profiles, physics of failures, were-out modeling, aging of power electronic converters, chance failures, maintenance, and generation uncertainty). The overall block diagram and interconnection between the blocks, as well as flowcharts for the computer implementation of the proposed framework were presented. In this regard, each block was introduced and their role in incorporating the above factors were clarified. These blocks included the converter availability modeling, power system modeling, scenario generation, state enumeration, and index calculation. Regarding the availability modeling block, the process to calculate the converter availability given the wear-out models, chance failures, and repair rates were provided. Since in PEPSs, non-constant failure rates must be used, conventional availability modeling methods, such as Markov process, could not be used. Therefore, a new method was presented, which could give a high accuracy while significantly lowering the computation time. Furthermore, the mathematical details for the computer implementation of the proposed method were presented. Concerning the power system modeling block, the main goal was to formulate the output power of all the converters in the PEPS. By doing so, it would be possible to evaluate the consequences of any failures of any converters. This included modeling the generating units (i.e., PV and Wind Turbine (WT) units), by translating the mission profiles into output power, which were discussed. Also, the output power of battery storage units considering their energy management scheme and the balance of energy between

demand and supply were modeled. Regarding the scenario generation block, the fundamentals of scenario generation by using the GANs were explained, where all the mathematical details for its computer implementation were also provided. In the state enumeration and index calculation blocks, the combination of data from previous blocks was discussed, where it was shown how to calculate the reliability indices accordingly. It was also pointed out that the outcomes of the proposed framework are time-dependent Probability Density Functions (PDFs), as opposed to static (time-independent) values in conventional approaches. By doing so, the effect of power electronics wear-out failures on the system-level reliability indices could be studied. Furthermore, the uncertainty of the index itself is reflected in that PDF.

In Chapter 5, the results obtained by using the above methods were applied on different systems and the results were analyzed. In other words, the reliability indices for several case studies were calculated by using the proposed approaches, and the effect of various factors on the system-level reliability were investigated to provide insights and demonstrate the superiority of the proposed methods.

In the first part, it was shown that using constant failure rates could result in the underestimation of the reliability in the short term. Similarly, it was shown that it could result in the overestimation of the reliability in the long term. Hence, it was concluded that using the non-constant failure rates is a must for PEPS reliability assessment.

Next, to use these non-constant failure rates, a new availability modeling method was used, where its performance in terms of computational efficiency was compared with the state-of-the-art approaches. These approaches included PWA (piecewise Approach), MDS (Method of Device of Stages), SMA (Semi Markov Approach), MCS (Monte Carlo Simulation), which were evaluated by applying them to calculate the reliability indices of a case study. It was shown that using the PWA and MDS can introduce significant errors to the system-level reliability indices, due to inaccurate modeling of the converter availability. On the other hand, the MCS and SMA demonstrated a high accuracy, while suffered from a high computation time. In contrast, the proposed availability modeling approach, had a high accuracy similar to that of SMA and MCS, while the computation time was significantly lower. Notably, the computation time of the proposed method, MCS, and SMA were 3.6, 273, and 5220 [s], respectively. This is important because in larger PEPSs where the availability of many power converters must be modeled, the computation time of the availability modeling block determines whether the entire framework would be feasible or not.

Moreover, the performance of the comprehensive framework for system-level reliability assessment was evaluated by using it for a new case study. First, the case study was described, where all necessary the system-level and converter-level specifications, as well as failure and repair data were presented.

Further, by using the proposed framework, the LOL (Loss Of Load) and ENS (Energy Not Supplied) indices were calculated for the case study. It was demonstrated that the outcomes of the proposed framework are mission profile-dependent, where a

change in the converter mission profile led to a change in the converter failure rate and availability, which was consequently reflected on the system-level indices.

Also, since the time series of the results were available in the proposed framework, more information were deductible from the results, which will be explained more here. From the analysis of the time series, it was shown that the ENS was zero in July, while it was the highest in December. This provides more useful information for the PEPSs with higher penetration of renewables (which are non-dispatchable units and highly depend on climate conditions). Therefore, It helps the system planners and operator be aware of the vulnerabilities that changes in different time scales. Nevertheless, in the conventional PS studies, only one constant number is reported for an entire year for the ENS. Therefore, the above information was not possible to be deducted from a single yearly value provided in the conventional approaches. However, this was justifiable for conventional synchronous generators that were considered as dispatchable units.

Furthermore, the effect of generation uncertainty on the system-level reliability indices was investigated by using the proposed framework. By using a few diagrams, it was shown that the reliability indices might change from year to year due to the volatile nature of renewables, such that the ENS could vary 23% from 2007 to 2015. Therefore, using purely probabilistic approaches or using only one year of mission profiles can cause noticeable error in the calculated reliability indices. The above behavior of the reliability indices was reasonable because they are caused not only by converter failures but also due to generation uncertainty. As a result, the outcomes of the proposed framework are PDFs, and not only a static value (like conventional approaches). By doing so, the uncertainty of the index itself can also be obtained and studied.

Moreover, the effect of components wear-out failures and converter aging on the system-level reliability was studied quantitatively. Hence, time-dependent PDFs were calculated for reliability indices, where the PDFs' characteristics change with time because of converter aging. In other words, since the converter availability and reliability degrade with time and they are modeled into the framework, it is automatically reflected on the system-level indices. For example, the LOLE changed form 1.7 [h/y] to 4.8 [h/y] for the presented case study, when the system age changed from 1 [y] to 20[y]. Therefore, it was possible to investigate the impact of converter aging on not only the average value of the reliability index, but also on its worst-case and best-case scenarios. It was also concluded that the proposed framework enables not only the evaluation of the current performance of the system, but also the prediction of its future performance.

It was also demonstrated how the comprehensive framework can be used to benchmark the system and assist the design for reliability at the system level. In this regard, in a case study, it was shown that the system could meet its LOL_{target} requirement when the system age = 1 [y], while it violated its LOL_{target} requirement at age = 20 [y]. In other words, by using the proposed framework, the system was benchmarked to identify the unreliable design. Therefore, it can help the system designers to check their system-level designs and ensure that a specific design will

meet its reliability requirements in the long run. The above design problem was fixed by adding a new PV pant to the system (i.e., increasing the design margin) and recalculation of the reliability index. Subsequently, it was shown that that the new design will meet its LOL_{target} requirements even in the long term.

Also, the impact of the penetration level of the renewables on the system reliability was studied. Two case studies were compared where the energy-based penetration level was 10% and 80%, respectively. It was shown that the converter-level reliability of battery inverters decreased as the penetration level of renewables increased. This was reasonable because the power profile of the battery converter increases due to more available power in the system, which means a higher stress on them, and therefore, a lower converter-level reliability. However, the system-level reliability improved when the penetration level increased. Given that the PDF of reliability indices are characterized by a normal distribution with mean and standard deviation of $N(\mu , \sigma)$, it was shown that, as the penetration level increases, μ decreases, while σ increases. When μ decreases, it means that the expected value of the unreliability decreases. This is reasonable because more generation capacity is added to the system, as more renewables are integrated into the grid. In contrast, an increase in σ means that the uncertainty of the index has increased. This is also reasonable since, the volatile nature of renewables dominates the system as the penetration level increases.

6.2. Main Contributions of the Thesis

The key contributions of this PhD thesis are as follows.

A comprehensive understanding of the power system reliability: The prerequisite of developing models for the PEPS reliability assessment is to understand the conventional power system reliability assessment methods and to be able to implement them. This has been done in chapter 2, where a comprehensive review of the methods has been presented, and relevant concepts and principles have been discussed in detail.

Implementing a simplified way of converter-level reliability modeling: This has been done by leveraging the analytical equations for electrothermal mapping, which was explained in chapter 3. Further, the comparison of the results with accurate simulation models were presented for validation.

A solution for mission profile uncertainty handling in converter-level reliability modeling: This has been done in chapter 3, where the usage of the machine learning concept of GAN was suggested to generate mission profiles. Furthermore, the idea was implemented and verified by providing several test results. Furthermore, the improvement of the reliability estimation results after using the GANs was demonstrated in chapter 3.

A new availability modeling method with a high computational efficiency: Since the conventional method such as Markov were unable to model the availability with non-

constant failure rates, a new method was proposed in chapter 4. Furthermore, in chapter 5, it was shown that, compared to complicated mathematical approaches, this method results in a high accuracy with a significantly lower computation time.

A comprehensive framework for system-level reliability assessment of the PEPS: This model-based framework is developed according to the V-shaped modeling approach, which incorporates the system-level down to the converter-level and component-level reliability and vice versa. It provides a tool for system-level designers to check the reliability of the design options, benchmark them, and guarantee their long-term reliability, which has the following advantages.

- This means that every factor that has a physical model (e.g., physics of failure) can be integrated into the framework, and its impact on the system-level reliability can be investigated. Since it is a model-based approach, the consequences of any changes in the parameters at the component and converter levels can be studied on the system level reliability indices.
- Moreover, the role of mission profiles is highlighted in the developed framework as they influence both converter failures and generation capacity.
- Further, it is a hybrid "muti-timescale" and "probabilistic" approach, as it was explained. When doing electro-thermal modeling for component reliability modeling, very small timescales in the order of milliseconds are considered. To evaluate the consequence of converter failures, time series with the resolutions in the order of 1 to 5 minutes are used. In contrast, the availability of the converters varies with a 1-year time step. Finally, the overall study time horizon typically deals with cases in 10- to 30-year time frames.
- The output of the proposed framework are time-dependent PDFs for each reliability index, as opposed to a constant (i.e., time-independent) value in traditional approaches. The characteristics of the PDFs change every year due to the converter aging and the increase of wear-out failures. As a result, the effect of converter aging on the system-level reliability indices can be studied quantitatively. In other words, the comprehensive frameworks enable the designers to not only evaluate the current performance of the system in terms of reliability, but also predict its future and long-term performance.
- Furthermore, the PDF reflects the generation uncertainty, which is translated into the index uncertainty, where the designer can obtain a worst-case, best-case, and average scenario for the reliability index and make better-informed decisions.
- Also, chance failures and corrective maintenance are also considered in the developed framework.
- All in all, it provides a tool for system designer to benchmark their system-level design, ensure that it meets its long-term reliability goals, and compare various design options with each other in terms of reliability.

6.3. Future Works and Research Perspectives

Although, in this PhD project, it was tried to address as many research gaps as possible, there are still numerous interesting challenges to be studied. Tackling these challenges in the future works will improve the outcomes of the current work and make the reliability assessment of the PEPS more mature, realistic, and efficient. Some of the areas that can be considered for future studies are as follows:

- In this PhD project, only the failure of components due to the thermal-induced stress was studied. Nevertheless, several recent research works have suggested the noticeable contribution of other factors such as humidity and cosmic rays. As a result, modeling these phenomena physically and statically, and incorporating them into the developed framework will enhance the accuracy of the outcomes. Further, it would be interesting to investigate how these factors influence the system-level reliability indices.
- In this research work, DC power flow method was adopted to model the power balance in the system, as the focus was to develop the framework itself. Nevertheless, using this approach results in ignoring the reactive power. In the future works, more advance power flow methods can be adopted, to also consider the reactive power impact in the model. By doing so the contribution of active and reactive power on the system-level unreliability can be separated and investigated.
- The reliability studies only targeted the hierarchical level I – that is, only generation and storage units were considered in the models. In other words, the transmission lines, their limits, their failures, and their impact on power balance in the system was ignored. Therefore, if these factors can also be integrated into the framework – that is the hierarchical level II analysis be added - more comprehensive results will be obtained. Further, the contribution of the generation and transmission facilities in the unreliability can be separated, which can shed light on the importance of each hierarchical level and help identifying the weakest links.
- Only wear-out failures of power semiconductors and capacitors were modeled and used. Nevertheless, there are many other components in a power electronic converter that can fail. So, by adding failures models for other components, the accuracy of the results will improve.
- The main focus of the project was to develop an assessment tool for the PEPS. It would be worthwhile to use the outcomes of this tool to realize the system-level design for reliability. In other words, a future work can be done to apply the developed framework in improving and maintaining the reliability of the PEPS in the long run.
- In this PhD project, the wear-out and chance failures were modeled and considered for system-level assessment. It could be interesting to model and consider the early failures and infant mortalities by studying their impact on the system-level reliability indices.

References

[1] P. S. R. Murty, "*Power Systems Analysis,*" 2nd editio. Cambridge, MA: Butterworth-Heinemann, 2017.

[2] B. Alves, "Net Electricity Consumption Worldwide in Select Years from 1980 to 2019," *Statistia*, 2022. [Online]. Available: https://www.statista.com/statistics/280704/world-power-consumption/. [Accessed: 19-Aug-2022].

[3] The U.S. Department of Energy, "Department of Energy Report Explores U.S. Advanced Small Modular Reactors to Boost Grid Resiliency," 2018. [Online]. Available: https://www.energy.gov/ne/articles/department-energy-report-explores-us-advanced-small-modular-reactors-boost-grid#:~:text=of Nuclear Energy-,Department of Energy Report Explores U.S. Advanced,Reactors to Boost Grid Resiliency&text=The U.S. Department of. [Accessed: 19-Aug-2022].

[4] European Commission, "Study on the Quality of Electricity Market Data of Transmission System Operators, Electricity Supply Disruptions, and Their Impact on the European Electricity Markets," Brussels, Belgium, 2018.

[5] The World Bank, "Underutilized Potential : The Business Costs of Unreliable Infrastructure in Developing Countries," 2019.

[6] IVA Electricity Crossroads project, "Reliability in Sweden's Electricity System: A Project Report," Stockholm, Sweden, 2017.

[7] C. Growitsch, R. Malischek, S. Nick, and H. Wetzel, "The Costs of Power Interruptions in Germany - an Assessment in the Light of the Energiewende," Institute of Energy Economics at the University of Cologne (EWI), Köln, 2013.

[8] BBC, "Energy Firms to Pay £10.5m over August Power Cut," 2022. [Online]. Available: https://www.bbc.com/news/business-50971717. [Accessed: 19-Aug-2022].

[9] M. S. Johannes Reichl, Jed J. Cohen, Klaus Moeltner, "Electricity Supply Security, Service Valuation, and Public Perception of Energy Infrastructure," in *Protecting Electricity Networks from Natural Hazards*, Vienna, Asutria: Organization for Security and Co-operation in Europe (OSCE), 2016, p. 124.

[10] Electricity Consumers Resource Council (ELCON), "The Economic Impacts of the August 2003 Blackout," Washington, DC, USA, 2004.

[11] IEA, "World Energy Outlook 2021," Paris, 2021.

[12] U.S. Energy Information Administration. (IEA), “International Energy Outlook 2021,” Washington, DC, 2021.

[13] Y. Lin, J. Eto, B. Johnson, J. Flicker, R. Lasseter, H. Villegas Pico, G.-S. Seo, B. Pierre, and A. Ellis, “Research Roadmap on Grid-Forming Inverters,” Golden, CO (United States), Nov. 2020.

[14] EPRI, “Enhancing Energy System Reliability and Resiliency in a Net-Zero Economy,” Palo Alto, CA, 2022.

[15] P. Hacke, S. Lokanath, P. Williams, A. Vasan, P. Sochor, G. TamizhMani, H. Shinohara, and S. Kurtz, “A Status Review of Photovoltaic Power Conversion Equipment Reliability, Safety, and Quality Assurance Protocols,” *Renew. Sustain. Energy Rev.*, vol. 82, pp. 1097–1112, Feb. 2018.

[16] A. Golnas, “PV System Reliability: An Operator’s Perspective,” *IEEE J. Photovoltaics*, vol. 3, no. 1, pp. 416–421, Jan. 2013.

[17] I. Lillo-Bravo, P. González-Martínez, M. Larrañeta, and J. Guasumba-Codena, “Impact of Energy Losses Due to Failures on Photovoltaic Plant Energy Balance,” *Energies*, vol. 11, no. 2, p. 363, Feb. 2018.

[18] “PV System Component Fault and Failure Compilation and Analysis,” Sandia National Laboratory, Albuquerque, NM, and Livermore, CA (United States), 2018, pp. 1-38.

[19] D. C. Jordan, B. Marion, C. Deline, T. Barnes, and M. Bolinger, “PV Field Reliability Status—Analysis of 100 000 Solar Systems,” *Prog. Photovoltaics Res. Appl.*, vol. 28, no. 8, pp. 739–754, Aug. 2020.

[20] E. Artigao, S. Martin-Martinez, A. Ceña, A. Honrubia-Escribano, and E. Gomez-Lazaro, “Failure Rate and Downtime Survey of Wind Turbines Located in Spain,” *IET Renew. Power Gener.*, vol. 15, no. 1, pp. 225–236, Jan. 2021.

[21] K. Fischer, K. Pelka, S. Puls, M.-H. Poech, A. Mertens, A. Bartschat, B. Tegtmeier, C. Broer, and J. Wenske, “Exploring the Causes of Power-Converter Failure in Wind Turbines Based on Comprehensive Field-Data and Damage Analysis,” *Energies*, vol. 12, no. 4, p. 593, Feb. 2019.

[22] Y. Lin, L. Tu, H. Liu, and W. Li, “Fault Analysis of Wind Turbines in China,” *Renew. Sustain. Energy Rev.*, vol. 55, pp. 482–490, Mar. 2016.

[23] “Portfolio Review 2016; System Performance, Availability and Reliability Trend Analysis,” SPARTA, London, 2017, pp. 1-9.

[24] Energinet, “Security of Electricity Supply Report 2020,” Fredericia, Denmark, 2020.

[25] S. Peyghami and F. Blaabjerg, “Availability Modeling in Power Converters

Considering Components Aging," *IEEE Trans. Energy Convers.*, vol. 35, no. 4, pp. 1981–1984, Dec. 2020.

[26] A. Gupta, O. P. Yadav, D. DeVoto, and J. J. Major, "A Review of Degradation Behavior and Modeling of Capacitors," *ASME 2018 Int. Tech. Conf. Exhib. Packag. Integr. Electron. Photonic Microsystems*, 2018, pp. 1-10.

[27] H. Wang and F. Blaabjerg, "Reliability of Capacitors for DC-Link Applications in Power Electronic Converters—an Overview," *IEEE Trans. Ind. Appl.*, vol. 50, no. 5, pp. 3569–3578, Sep. 2014.

[28] N. Dornic, A. Ibrahim, Z. Khatir, N. Degrenne, S. Mollov, and D. Ingrosso, "Analysis of the Aging Mechanism Occurring at the Bond-Wire Contact of IGBT Power Devices during Power Cycling," *Microelectron. Reliab.*, vol. 114, p. 113873, Nov. 2020.

[29] S. Song, S. Munk-Nielsen, and C. Uhrenfeldt, "How Can a Cutting-Edge Gallium Nitride High-Electron-Mobility Transistor Encounter Catastrophic Failure within the Acceptable Temperature Range?," *IEEE Trans. Power Electron.*, vol. 35, no. 7, pp. 6711–6718, Jul. 2020.

[30] S. E. De León-Aldaco, H. Calleja, F. Chan, and H. R. Jiménez-Grajales, "Effect of the Mission Profile on the Reliability of a Power Converter Aimed at Photovoltaic Applications—a Case Study," *IEEE Trans. Power Electron.*, vol. 28, no. 6, pp. 2998–3007, Jun. 2013.

[31] V. Najmi, J. Wang, R. Burgos, and D. Boroyevich, "Reliability-Oriented Switching Frequency Analysis for Modular Multilevel Converter (MMC)," in *2015 IEEE Energy Conversion Congress and Exposition (ECCE)*, 2015, pp. 5554–5559.

[32] Y. Miao, W. Lei, S. Li, X. Lv, B. Li, P. Wang, J. Xu, and H. Li, "Influence of Inverter DC Voltage on the Reliability of IGBT," in *AIP Conference Proceeding*, 2018, p. 020023.

[33] M. Abarzadeh, S. Peyghami, K. Al-Haddad, N. Weise, L. Chang, and F. Blaabjerg, "Reliability and Performance Improvement of PUC Converter Using a New Single-Carrier Sensor-Less PWM Method with Pseudo Reference Functions," *IEEE Trans. Power Electron.*, vol. 36, no. 5, pp. 6092–6105, May 2021.

[34] J. Jiang, S. Peyghami, C. Coates, and F. Blaabjerg, "A Decentralized Reliability-Enhanced Power Sharing Strategy for PV-Based Microgrids," *IEEE Trans. Power Electron.*, vol. 36, no. 6, pp. 7281–7293, Jun. 2021.

[35] S. Peyghami, P. Davari, and F. Blaabjerg, "System-Level Reliability-Oriented Power Sharing Strategy for DC Power Systems," *IEEE Trans. Ind. Appl.*, vol. 55, no. 5, pp. 4865–4875, May 2019.

[36] Electronic Components and Systems Division (ZVEI), "*Handbook for Robustness Validation of Automotive Electrical/Electronic Modules.*" Frankfurt, Germany: ZVEI - Zentralverband Elektrotechnik- und Elektronikindustrie e. V., 2013.

[37] E. Laloya, O. Lucia, H. Sarnago, and J. M. Burdio, "Heat Management in Power Converters: From State of the Art to Future Ultrahigh Efficiency Systems," *IEEE Trans. Power Electron.*, vol. 31, no. 11, pp. 7896–7908, Nov. 2016.

[38] J. Kuprat, C. H. van der Broeck, M. Andresen, S. Kalker, M. Liserre, and R. W. De Doncker, "Research on Active Thermal Control: Actual Status and Future Trends," *IEEE J. Emerg. Sel. Top. Power Electron.*, vol. 9, no. 6, pp. 6494–6506, Dec. 2021.

[39] S. Peyghami, Z. Wang, and F. Blaabjerg, "A Guideline for Reliability Prediction in Power Electronic Converters," *IEEE Trans. Power Electron.*, vol. 35, no. 10, pp. 10958–10968, Oct. 2020.

[40] I. Bazovsky, "*Reliability Theory and Practice.*" Prentice-Hall, 1961.

[41] W. Li, Ed., "*Risk Assessment of Power Systems.*" Hoboken, NJ, USA: John Wiley & Sons, Inc., 2014.

[42] E. S. I. G. (ESIG), "Design Study Requirements for a U.S. Macrogrid: A Path to Achieving the Nation's Energy System Transformation Goals," Reston, VA, 2022.

[43] S. Peyghami, P. Palensky, and F. Blaabjerg, "An Overview on the Reliability of Modern Power Electronic Based Power Systems," *IEEE Open J. Power Electron.*, vol. 1, pp. 34–50, 2020.

[44] "*Military Handbook MIL-HDBK-217F: Reliability Prediction of Electronic Equipment.*" Washington, DC, USA, 1995.

[45] International Electrotechnical Commission (IEC), "*IEC 61709 (2017): Electric Components - Reliability - Reference Conditions for Failure Rates and Stress Models for Conversion.*" International Electrotechnical Commission, 2017.

[46] "A Methodology for Components Reliability, FIDES," 2010. [Online]. Available: https://www.fides-reliability.org/. [Accessed: 11-Nov-2019].

[47] P. Tu, S. Member, S. Yang, and S. Member, "Reliability- and Cost-Based Redundancy Design for Modular Multilevel Converter," *IEEE Trans. Ind. Electron.*, vol. 66, no. 3, pp. 2333–2342, 2019.

[48] H. Wang, M. Liserre, F. Blaabjerg, P. de Place Rimmen, J. B. Jacobsen, T. Kvisgaard, and J. Landkildehus, "Transitioning to Physics-of-Failure as a

Reliability Driver in Power Electronics," *IEEE J. Emerg. Sel. Top. Power Electron.*, vol. 2, no. 1, pp. 97–114, Mar. 2014.

[49] W. Liu, D. Zhou, F. Iannuzzo, M. Hartmann, and F. Blaabjerg, "Separation and Validation of Bond-Wire and Solder Layer Failure Modes in IGBT Modules," *IEEE Trans. Ind. Appl.*, vol. 58, no. 2, pp. 2324–2331, Mar. 2022.

[50] Y. Song and B. Wang, "Survey on Reliability of Power Electronic Systems," *IEEE Trans. Power Electron.*, vol. 28, no. 1, pp. 591–604, Jan. 2013.

[51] E. Suhir, "To Burn-in, or Not to Burn-in: That's the Question," *Aerospace*, vol. 6, no. 3, p. 29, Mar. 2019.

[52] A. Davoodi, S. Peyghami, Y. Yang, T. Dragicevic, and F. Blaabjerg, "A Preventive Maintenance Planning Approach for Wind Converters," in *2020 5th IEEE Workshop on the Electronic Grid (eGRID)*, 2020, pp. 1–8.

[53] R. Billinton and R. N. Allan, "*Reliab. Eval. Power Syst.*" Boston, MA: Springer US, 1996.

[54] S. Peyghami, M. Fotuhi-Firuzabad, and F. Blaabjerg, "Reliability Evaluation in Microgrids with Non-Exponential Failure Rates of Power Units," *IEEE Syst. J.*, vol. 14, no. 2, pp. 2861–2872, Jun. 2020.

[55] S. Peyghami, F. Blaabjerg, and P. Palensky, "Incorporating Power Electronic Converters Reliability into Modern Power System Reliability Analysis," *IEEE J. Emerg. Sel. Top. Power Electron.*, pp. 1–1, 2020.

[56] H. Wang, K. Ma, and F. Blaabjerg, "Design for Reliability of Power Electronic Systems," in *IECON 2012 - 38th Annual Conference on IEEE Industrial Electronics Society*, 2012, pp. 33–44.

[57] R. Billinton and R. N. Allan, "*Reliab. Eval. Eng. Syst.,*" 2nd ed. Boston, MA: Springer US, 1992.

[58] K. Ma, U.-M. Choi, and F. Blaabjerg, "Prediction and Validation of Wear-out Reliability Metrics for Power Semiconductor Devices with Mission Profiles in Motor Drive Application," *IEEE Trans. Power Electron.*, vol. 33, no. 11, pp. 9843–9853, Nov. 2018.

[59] T. K. Vrana and E. Johansson, "Overview of Power System Reliability Assessment Techniques," in *Proc. of CIGRE International Symp. Recife,* 2011.

[60] P. Zhang, K. Meng, and Z. Dong, "Probabilistic vs Deterministic Power System Stability and Reliability Assessment BT - Emerging Techniques in Power System Analysis," Z. Dong and P. Zhang, Eds. Berlin, Heidelberg: Springer Berlin Heidelberg, 2010, pp. 117–145.

[61] M. Milligan, "Methods to Model and Calculate Capacity Contributions of

Variable Generation for Resource Adequacy Planning (IVGTF1-2)," Princeton, NJ, 2011.

[62] "IEEE Guide for Electric Power Distribution Reliability Indices," *IEEE Std 1366-2012 (Revision IEEE Std 1366-2003)*, pp. 1–43, 2012.

[63] M. Rausand and A. Høyland, "Markov Processes," in *System Reliability Theory: Models, Statistical Methods, and Applications*, 2008, pp. 301–360.

[64] A. Janssen, D. Makareinis, and C.-E. Solver, "International Surveys on Circuit-Breaker Reliability Data for Substation and System Studies," *IEEE Trans. Power Deliv.*, vol. 29, no. 2, pp. 808–814, Apr. 2014.

[65] P. Slade and R. Smith, "Electrical Switching Life of Vacuum Circuit Breaker Interrupters," in *Electrical Contacts - 2006. Proceedings of the 52nd IEEE Holm Conference on Electrical Contacts*, 2006, pp. 32–37.

[66] H. Jia-min, F. Xing-ming, Z. Xin, H. Zhi-chao, Z. Qi-tao, L. Cong, and S. Wei-jian, "VCB Contact System Electrical Endurance On-Line Condition Monitoring Technology and Its Application," in *2012 25th International Symposium on Discharges and Electrical Insulation in Vacuum (ISDEIV)*, 2012, pp. 513–516.

[67] P. Industries, "Contact Erosion in Circuit Breaker Vacuum Interrupters 01.4TB.142," Powell Industries, 2019.

[68] International Electrotechnical Commission (IEC), "IEC TR 62380: Reliability Data Handbook-Universal Model for Reliability Prediction of Electronics Components, PCBs and Equipment," 2006.

[69] T. Dragicevic, P. Wheeler, and F. Blaabjerg, "Artificial Intelligence Aided Automated Design for Reliability of Power Electronic Systems," *IEEE Trans. Power Electron.*, vol. 34, no. 8, pp. 7161–7171, Aug. 2019.

[70] M. Nadia, H. Lassad, Z. Abderrahmen, and C. Abdelkader, "Influence of Temperature and Irradiance on the Different Solar PV Panel Technologies," *Int. J. Energy Sect. Manag.*, vol. 15, no. 2, pp. 421–430, Mar. 2021.

[71] M. H. Albadi and E. F. El-Saadany, "Wind Turbines Capacity Factor Modeling—a Novel Approach," *IEEE Trans. Power Syst.*, vol. 24, no. 3, pp. 1637–1638, Aug. 2009.

[72] A. Wintrich, N. Ulrich, T. Werner, and T. Reimann, "*Application Manual Power Semiconductors.*" Ilmenau, Germany: SEMIKRON International GmbH, 2015.

[73] J. W. Kolar and S. D. Round, "Analytical Calculation of the RMS Current Stress on the DC-Link Capacitor of Voltage-PWM Converter Systems," *IEE Proc. - Electr. Power Appl.*, vol. 153, no. 4, pp. 535–543, 2006.

[74] “Infineon AN2019-05: PC and TC Diagrams,” Munich, Germany: Infineon Technologies AG, 2019, pp. 1–15.

[75] “IEEE Guide for Selecting and Using Reliability Predictions Based on IEEE 1413,” *IEEE Std 1413.1-2002*, pp. 1–97, 2003.

[76] A. Andreas and T. Stoffel, “NREL Report No. DA-5500-56509,” University of Nevada (UNLV), Las Vegas, Nevada, 2006.

[77] M. Arjovsky, S. Chintala, and L. Bottou, “Wasserstein Generative Adversarial Networks,” *34th Int. Conf. Mach. Learn. ICML 2017*, vol. 1, pp. 298–321, 2017.

[78] Y. Chen, Y. Wang, D. Kirschen, and B. Zhang, “Model-Free Renewable Scenario Generation Using Generative Adversarial Networks,” *IEEE Trans. Power Syst.*, vol. 33, no. 3, pp. 3265–3275, May 2018.

[79] A. Lisnianski and G. Levitin, “*Multi-State System Reliability,*” vol. 6. WORLD SCIENTIFIC, 2003.

[80] M. Jooshaki, A. Abbaspour, M. Fotuhi-Firuzabad, M. Moeini-Aghtaie, and M. Lehtonen, “Incorporating the Effects of Service Quality Regulation in Decision-making Framework of Distribution Companies,” *IET Gener. Transm. Distrib.*, vol. 12, no. 18, pp. 4172–4181, Oct. 2018.

[81] R. A. P. Franco and F. H. T. Vieira, “Analytical Method for Extraction of the Single-Diode Model Parameters for Photovoltaic Panels from Datasheet Data,” *Electron. Lett.*, vol. 54, no. 8, pp. 519–521, Apr. 2018.

[82] A. Sangwongwanich, Y. Yang, D. Sera, F. Blaabjerg, and D. Zhou, “On the Impacts of PV Array Sizing on the Inverter Reliability and Lifetime,” *IEEE Trans. Ind. Appl.*, vol. 54, no. 4, pp. 3656–3667, Jul. 2018.

[83] F. Blaabjerg, Y. Yang, D. Yang, and X. Wang, “Distributed Power-Generation Systems and Protection,” *Proc. IEEE*, vol. 105, no. 7, pp. 1311–1331, Jul. 2017.

[84] J. M. Morales, R. Mínguez, and A. J. Conejo, “A Methodology to Generate Statistically Dependent Wind Speed Scenarios,” *Appl. Energy*, vol. 87, no. 3, pp. 843–855, Mar. 2010.

[85] Y. Rubner, C. Tomasi, and L. J. Guibas, “The Earth Mover’s Distance as a Metric for Image Retrieval,” *Int. J. Comput. Vis.*, vol. 40, no. 2, pp. 99–121, 2000.

[86] M. Bicher, M. Wastian, D. Brunmeir, and N. Popper, “Review on Monte Carlo Simulation Stopping Rules: How Many Samples Are Really Enough?,” *SNE Simul. Notes Eur.*, vol. 32, no. 1, pp. 1–8, 2022.

[87] R. Billinton, S. Kumar, N. Chowdhury, K. Chu, K. Debnath, L. Goel, E. Khan,

P. Kos, G. Nourbakhsh, and J. Oteng-Adjei, “A Reliability Test System for Educational Purposes-Basic Data,” *IEEE Trans. Power Syst.*, vol. 4, no. 3, pp. 1238–1244, 1989.

[88] J. Carroll, A. McDonald, and D. McMillan, “Failure Rate, Repair Time and Unscheduled O&M Cost Analysis of Offshore Wind Turbines,” *Wind Energy*, vol. 19, no. 6, pp. 1107–1119, Jun. 2016.

[89] M. G. Bennett and L. Crowe, “A Survey of the Reliability of HVDC Systems throughout the World during 2017 - 2018,” in *CIGRE Session 48 - 48th International Conference on Large High Voltage Electric Systems 2020*, 2020.

[90] A. A. Akhil, G. Huff, A. B. Currier, B. C. Kaun, D. M. Rastler, S. B. Chen, A. L. Cotter, D. T. Bradshaw, and W. D. Gauntlett, “DOE/EPRI 2013 Electricity Storage Handbook in Collaboration with NRECA,” Albuquerque, New Mexico, 2013.

[91] “Handbook on Battery Energy Storage System,” Manila, Philippines, Dec. 2018.

[92] C. international des grands réseaux électriques. Comité d’études C6 and I. C. on Large Electric Systems, “*Benchmark Systems for Network Integration of Renewable and Distributed Energy Resources: Task Force C6.04*.” CIGRÉ, 2014.

[93] M. Castilla, J. Miret, A. Camacho, J. Matas, and L. G. de Vicuna, “Reduction of Current Harmonic Distortion in Three-Phase Grid-Connectedphotovoltaic Inverters via Resonant Current Control,” *IEEE Trans. Ind. Electron.*, vol. 60, no. 4, pp. 1464–1472, Apr. 2013.

[94] R. Cisneros, F. Mancilla-David, and R. Ortega, “Passivity-Based Control of a Grid-Connected Small-Scale Windmill with Limited Control Authority,” *IEEE J. Emerg. Sel. Top. Power Electron.*, vol. 1, no. 4, pp. 247–259, Dec. 2013.

[95] J. Han, X. Zhou, S. Lu, and P. Zhao, “A Three-Phase Bidirectional Grid-Connected AC/DC Converter for V2G Applications,” *J. Control Sci. Eng.*, vol. 2020, p. 8844073, 2020.

[96] S. Baschel, E. Koubli, J. Roy, and R. Gottschalg, “Impact of Component Reliability on Large Scale Photovoltaic Systems’ Performance,” *Energies*, vol. 11, no. 6, p. 1579, Jun. 2018.

[97] F. Spertino, A. Amato, G. Casali, A. Ciocia, and G. Malgaroli, “Reliability Analysis and Repair Activity for the Components of 350 KW Inverters in a Large Scale Grid-Connected Photovoltaic System,” *Electronics*, vol. 10, no. 5, p. 564, Feb. 2021.

[98] K. Fischer, K. Pelka, A. Bartschat, B. Tegtmeier, D. Coronado, C. Broer, and J. Wenske, “Reliability of Power Converters in Wind Turbines: Exploratory Analysis of Failure and Operating Data from a Worldwide Turbine Fleet,” *IEEE Trans. Power Electron.*, vol. 34, no. 7, pp. 6332–6344, Jul. 2019.

[99] “Transformer Reliability Survey,” CIGRE working group A2.37, Paris, 2015, pp. 1-122.

[100] D. Q. Hung, N. Mithulananthan, and K. Y. Lee, “Determining PV Penetration for Distribution Systems with Time-Varying Load Models,” *IEEE Trans. Power Syst.*, vol. 29, no. 6, pp. 3048–3057, Nov. 2014.

ISSN (online): 2446-1636
ISBN (online): 978-87-7573-775-8

AALBORG UNIVERSITY PRESS